UNIVERSITEIT GENT

Vrije Universiteit Brussel

INTERUNIVERSITY PROGRAMME MASTER OF SCIENCE IN PHYSICAL LAND RESOURCES

Universiteit Gent
Vrije Universiteit Brussel
Belgium

Integration of detailed borehole core measurements and pump test data from the aquifers below the Boom Clay in the groundwater flow model

June 2014

Promoter:
Prof. Dr. ir. Marijke Huysmans

Mentors:
Dr. Bart Rogiers
Dr. Katrijn Vandersteen

Master dissertation in partial fulfilment of the requirements for the Degree of **Master of Science in Physical Land Resources**

by: **George Bennett**

Acknowledgement

First I would like to thank the Belgian Nuclear Research Centre, SCK•CEN for giving me the opportunity to perform this master thesis.

Secondly, I wish to thank my promoter Prof. Dr. ir. Marijke Huysmans, my mentors Dr. Bart Rogiers and Dr. Katrijn Vandersteen for their continuing support and constructive contributions to this research.

I also like to thank Ms. Lisa Potums, who helped me in the characterization of the borehole cores with a handheld air permeameter.

Finally, I wish to thank my parents for their support and encouragement throughout my study.

Abstract

For more than three decades now, the Belgian Nuclear Research Centre (SCK•CEN) has been investigating the possibility of using the Boom Clay in north-eastern Belgium (Campine area) as the host rock for high-level and/or long-lived radioactive waste disposal. Since then several studies on characterization and modelling of groundwater flow for the aquifers above and below the Boom Clay have been carried out for better understanding of water and solutes transport in this area as this is important for demonstrating feasibility and safety of such a radioactive waste disposal. According to Vandersteen et al. (2012), the detailed hydrogeological characterization of the aquifers below the Boom Clay especially Oligocene and Ledo-Paniselian-Brusselian aquifers is of high importance for reducing the uncertainty of the current groundwater flow model for the aquifers below the Boom Clay. However the amount of available hydraulic conductivity data for these aquifers is limited and has not yet been used for the model parameterization. To continue with characterization and modelling of groundwater flow for the aquifers below the Boom Clay this study used data from a portable air permeameter to estimate saturated hydraulic conductivities for the Oligocene and Bartoon aquifer system (Potums, 2014). The up-scaled saturated hydraulic conductivity estimates together with pumping test data from the Oligocene and Ledo-Paniselian-Brusselian aquifers are integrated into the current groundwater flow model for the aquifers below the Boom Clay. Small-scale air permeameter-based measurements are important as they incorporate real-world aquifer heterogeneity into the model hence improve the conceptual model, and potentially model performance.

Results show that on average the Ledo-Paniselian-Brusselian (LPB) aquifer is approximately 30 times more permeable than the Oligocene aquifer. The average horizontal hydraulic conductivity value for this aquifer is 13.10 m/d. Because of its higher conductivity, people will preferably pump from the LPB aquifer and not from the Oligocene aquifer. Also, because of the low transmissivity of the Oligocene aquifer, pumping effects in this aquifer are likely to remain local, while for the LPB aquifer (which has a higher transmissivity), there are regional effects of pumping. Moreover, mathematical equations describing the depth-dependency for hydraulic conductivities for the Zelzate formation in the Oligocene aquifer have been established.

The integration of the air permeameter-based data and pumping test data from the Oligocene and LPB aquifers into the current groundwater flow model for the aquifers below the Boom Clay makes the model parameterization more data-based on realistic.

Table of contents

List of figures

List of tables

List of symbols and SI units

K_s: saturated hydraulic conductivity

k_a: air permeability

K_h: horizontal hydraulic conductivity

K_v: vertical hydraulic conductivity

m: meter

mD: millidarcy

m/d: metre per day

m/s: metre per second

Abbreviations

SCK•CEN:	Studiecentrum voor kernenergie/Centre d'étude de l'énergie nucléaire
HCOV:	Hydrogeologische Codering van de Ondergrond van Vlaanderen (Hydrogeological coding of the subsurface of Flanders)
TAW:	Tweede Algemene Waterpassing (The Second General Levelling is the reference height against which height in Belgium are expressed. A TAW-height of 0 m is equal to the average sea level at low tide at Ostend)
VANI:	Vertical anisotropy
LPB:	Ledo-Paniselian-Brusselian

1 Introduction

1.1 Background and general context

In Belgium, the Belgian Nuclear Research Centre (SCK•CEN) for more than 35 years now has been investigating the possibility of using the Boom Clay in north-eastern Belgium (Campine area) as the host rock for high-level and/or long-lived radioactive waste disposal (Vandersteen et al., 2012; Vandersteen and Gedeon, 2013). For safety assessment of radioactive waste disposal and precaution for any leakage to the biosphere, detailed hydrogeological characterization of the aquifers above and below the Boom Clay formation (Figure 1) is of high importance in order to have accurate groundwater flow and solute transport models which predict the flow of water and transport of solutes at high precision. A geological profile in the Campine area showing the major geological formations is given in Figure 1.

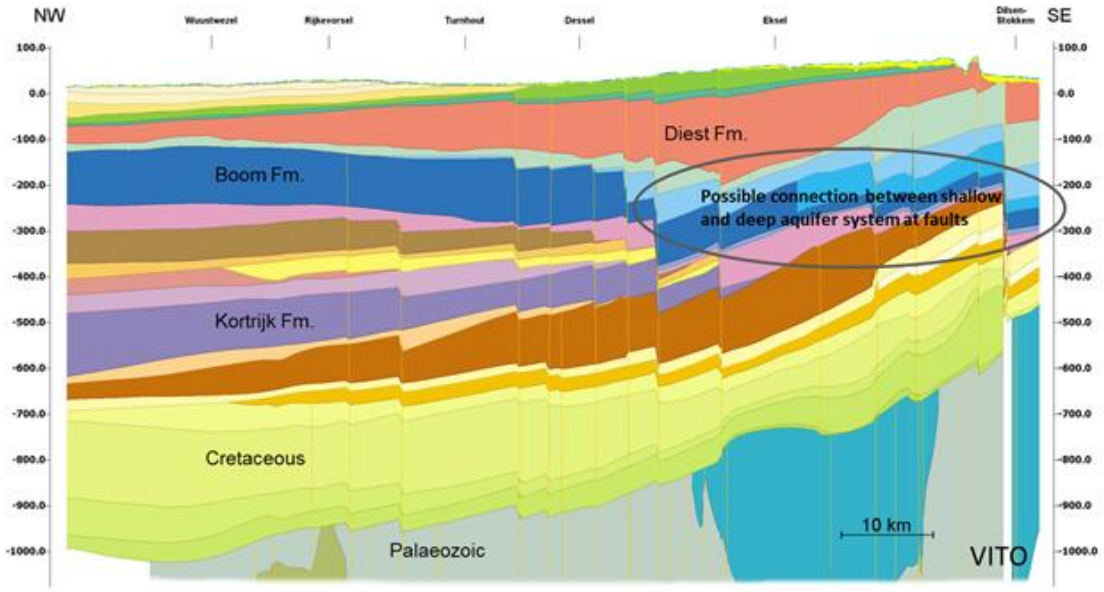

Figure 1. A geological cross section showing the major geological formations in the Campine area (from Vandersteen et al., 2013).

One of the most important parameters determining groundwater flow and contaminant transport in both unsaturated and saturated porous media is saturated hydraulic conductivity (K_s). In aquifers, K_s is spatially varying due to presence of small-scale sedimentary heterogeneity (Huysmans et al., 2008; Possemiers et al., 2012). Incorporation of the spatial variability of this parameter in simulations of groundwater flow and contaminant transport models is of great need for accurate model predictions (Huysmans & Dassargues, 2009; Rogiers et al., 2014).

The detailed hydrogeological characterization of the aquifers below the Boom Clay can be advanced by comparing and up-scaling small-scale hydraulic conductivity values from borehole core measurements with large-scale hydraulic conductivity values from pump test data before integrating them into the current groundwater flow model for the aquifers below the Boom Clay. The relatively cheap, fast and easy way of measuring small-scale hydraulic conductivity from borehole core is by using a portable air permeameter (Winters, 2012; Rogiers et al., 2014).

The transient deep aquifer pumping model (DAP – **D**eep **A**quifer **P**umping model) (Gedeon & Wemaere, 2009, modified by Vandersteen et al. (2012)) is the current groundwater flow model for the aquifers below the Boom Clay. The current DAP model was calibrated but no hydraulic conductivity data was used. The integration of the air permeameter-based data and pumping test data into the current DAP model will make the model parameterization more data-based on realistic.

1.2 Problem Statement

In the framework of the research at SCK•CEN concerning the Boom Clay as a host-formation for the disposal of radioactive waste, it is necessary to perform detailed characterization of the aquifers above and below the Boom clay. To continue this area of research, this study focuses on the characterization of the aquifers below the Boom Clay, especially the Oligocene and Bartoon aquifer system and the Ledo-Paniselian-Brusselian aquifer. Currently the amount of available hydraulic conductivity data for these aquifers is limited and has not yet been used for parameterization of the DAP model.

This study is going to use air permeameter-based measurements from Potums (2014) to estimate saturated hydraulic conductivities for the Oligocene and Bartoon aquifer system. In a recent study by Rogiers et al. (2014), it has been shown that the use of a handheld air permeameter is very efficient for the high-resolution characterization of borehole cores. These detailed measurements are very informative, but their spatial representativity (or support volume) is rather limited.

The study also is going to analyse the available pumping test data from the Oligocene aquifer and the Ledo-Paniselian-Brusselian aquifer. The air permeameter-based data will be compared with larger-scale hydraulic conductivity values from pumping tests, and an up-scaling approach will be invoked before integrating these data in the current DAP model.

1.3 Objectives and Scope

1.3.1 General objective

The main purpose of this research is to integrate detailed borehole core measurements and pump test data from the aquifers below the Boom Clay into the current DAP model (Vandersteen et al., 2012).

1.3.2 Specific objectives

i. To use air permeameter-based measurements from Potums (2014) to estimate saturated hydraulic conductivities for the Oligocene and Bartoon aquifer system.
ii. To compare the obtained air permeameter-based data to available pumping test data, and develop an up-scaling approach.
iii. To integrate all available data in the current DAP model.
iv. To recalibrate the current DAP model and do some research on the results of the new versus the old model.

2 Literature review

2.1 Air permeametry

The author of this thesis assisted in the data collection of air permeameter-based measurements in the framework of Potums (2014) Bachelor thesis. It has been shown by Rogiers et al. (2014) that the hand-held air permeameter is a very efficient cost-effective tool to obtain high-resolution information on variability of K_s from borehole core slabs. The same device also was used in several successful studies (Huysmans et al., 2008; Rogiers et al., 2011, 2013a; Possemiers et al., 2012).

The centimetre-scale air permeability measurements on borehole core slabs from the aquifers below the Boom Clay (Potums, 2014) were taken by using the TinyPerm II device (New England Research & Vindum Engineering, 2013). The TinyPerm II device (Figure 2) consists of a vacuum cylinder, pressure transducer, handle and plunger, and a microprocessor and control unit.

Figure 2. A picture of the TinyPerm II Portable Permeameter (Source: www.azom.com).

Measurements are taken by pressing the permeameter tip against the borehole core material, and pressing the plunger to create a vacuum causing air to flow from the unsaturated porous medium into the device where the gas flow rate and pressure are monitored by the pressure transducer and analysed by the microprocessor unit. Using signal processing algorithms, the unsteady state response function is computed and related to the sample air permeability (k_a). The exact value of k_a (in mD) can be determined by an equipment specific calibration curve (New England Research and Vindum Engineering 2013).

As implemented by Huysmans et al. (2008), also in this study, a custom made metallic screen was fitted at the outlet of the equipment to prevent loose sand debris being sucked into the device. Hence the relationship developed by Huysmans et al. (2008) between k_a (mD) and TinyPerm II value for the device equipped with a filter is used to convert the obtained TinyPerm II value into k_a value (Equation 2.1).

$$\boldsymbol{k_a = 10^{\left(\frac{12.967 - \ TinyPerm\ II\ value}{0.8386}\right)}} \qquad (2.1)$$

The device has an inner tip diameter of 9 mm, and an outer diameter of 21 mm, resulting in an investigation depth of ~11 mm for 95% of the spatial weighting function, and ~19 mm for 99%, allowing for a very detailed small-scale analysis on the core slabs that have a maximum material depth of ~30 mm (Rogiers et al., 2014). According to Goggin et al. (1988) and Jensen et al. (1994), the volume of sediment involved in a permeameter measurement for isotropic porous media is defined by a hemisphere two to four times the internal radius of the tip seal. Measurements in permeable sands take a few seconds, less permeable samples take up to a few minutes and clays might take several dozens of minutes (Huysmans et al., 2008; Rogiers et al., 2014).

Empirical equations have to be used to convert the obtained k_a values into K_s estimates because it is hard to obtain totally dry sediment conditions under field conditions, and because of the polar characteristics of water and gas slippage effects (Rogiers et al., 2013c, 2014). Therefore, the empirical equation proposed by Loll et al. (1999) is used in this study for the initial K_s estimates based on obtained ka values (Equation 2.2).

$$\boldsymbol{K_s = 10^{(1.27\ x\ log_{10}(k_a\ x\ 9.87\ x\ 10^{-16})+14.11)}} \qquad (2.2)$$

where k_a is expressed in mD and K_s in m/d. More details can be find in Potums (2014).

2.2 Hydrostratigraphy of the study area

A hydrostratigraphic unit can be defined as a formation, part of a formation, or group of formations in which there are similar hydraulic characteristics allowing for grouping into water bearing (aquifers) or water retarding (aquitards) (Harding ESE Inc., 2001; Mukherjee, 2011). Delineation of hydrostratigraphy of the study area is a very important step towards groundwater flow modelling since it gives the basis for setting flow boundary conditions and model parameterization.

The study area in this research is the Campine area, north-eastern Belgium, and more specifically the extent of the current DAP model (Figure 3).

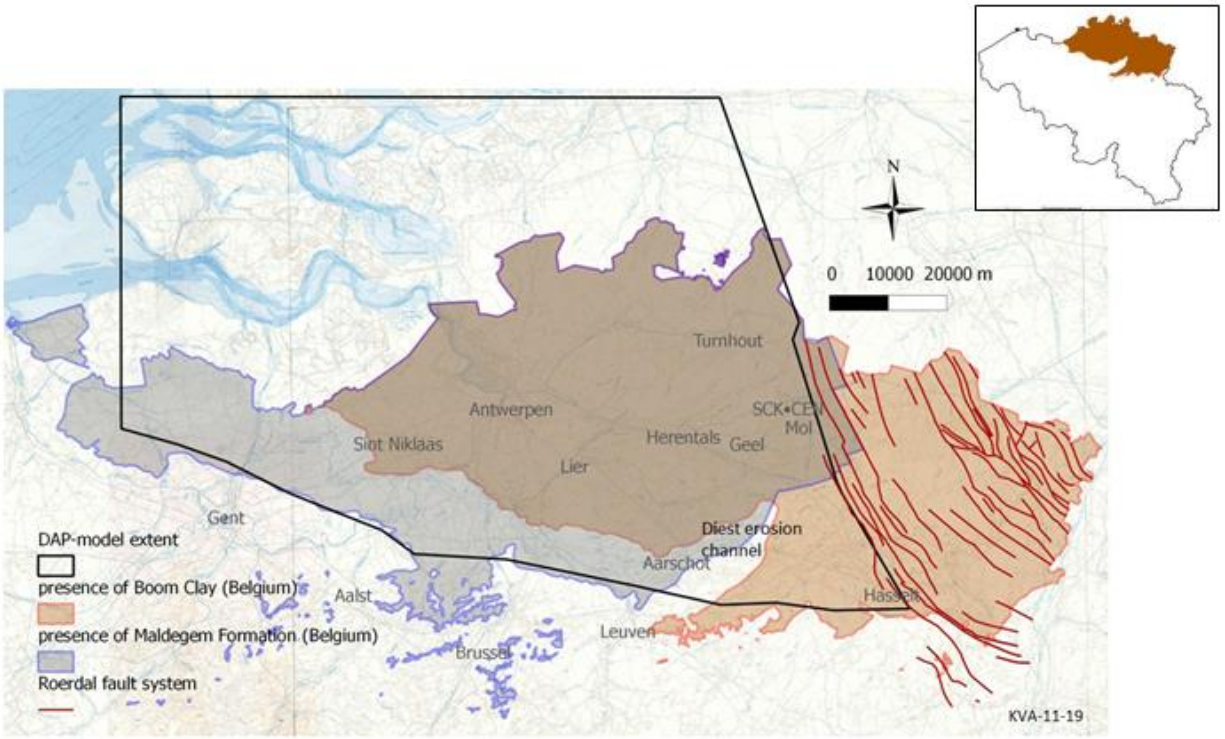

Figure 3. Extent of the DAP model (in black) in relation to the presence of Boom Clay, Asse/Ursel Clay and the fault system of the Roer Valley Graben (from Vandersteen et al., 2012). A map of Belgium with the location of the Boom Formation is shown in the upper right corner (from Vandersteen et al., 2014).

In this study, the hydrogeological units division is based on the HCOV (Hydrogeologische Codering van de Ondergrond van Vlaanderen) system developed by Meyus et al. (2000). The hydrogeological units of the study area from top to bottom can be categorized into three main parts; these are aquifers above the Boom Clay, the Boom aquitard, and aquifer and aquitard systems below the Boom Clay. The Boom Clay is considered as a low-permeable barrier (Vandersteen et al., 2012, 2013, 2014).

The aquifers above the Boom Clay comprise two units, from top to bottom; the Quaternary Aquifer Systems (HCOV 0100) and the Campine Aquifer System (HCOV 0200). The Boom Aquitard (HCOV 0300) comprises sub-units of very low-permeable clay layers. While the aquifer and aquitard systems below the Boom Clay from top to bottom comprise the Oligocene Aquifer System (HCOV 0400), the Bartoon Aquitard System (HCOV 0500), the Ledo-Paniselian-Brusselian Aquifer System (HCOV 0600), the Paniselian Aquitard (HCOV 0700), the

Ypresian Aquifer (HCOV 0800), the Ypresian Aquitard System (HCOV 0900), the Paleocene Aquifer System (HCOV 1000), the Cretaceous Aquifer System (HCOV 1100), Jurassic-Triassic-Permian units (HCOV 1200) and the Basement rocks (HCOV 1300).

In this study, emphasis is given to the aquifer and aquitard systems just below the Boom Clay. These are the Oligocene Aquifer System (HCOV 0400), the Bartoon Aquitard System (HCOV 0500) and the Ledo-Paniselian-Brusselian Aquifer System (HCOV 0600). Also the Miocene Aquifer (HCOV 0250) which lies just above the Boom Clay and the Boom Clay itself (Boom Aquitard (HCOV 0300)) are discussed since they are included in the current DAP model.

The Miocene aquifer (HCOV 0250)

This is the lowest part of the Campine Aquifer System (HCOV 0200). Ten metres of the lower part of this system are included in the deep aquifer pumping model only to provide the upper boundary conditions to the system (Vandersteen et al., 2012, 2013). For a detailed subdivision of this unit, see Table 1.

Boom aquitard (HCOV 0300)

The Boom Clay consists of very low-permeable clays of marine origin. It is subdivided into four main stratigraphic units (Table 1), and it subcrops in the entire Campine area. It dips to the north-east. Its base reaches a maximum depth of about -400 mTAW near the northern Belgian border whereas in the Roer Valley Graben (Figure 3) the base can locally reach more than -1000 mTAW. The thickness is between 20 and 50 metres in the outcrop zone, reaching more than 130 metres towards the northern Belgian border. This formation has been eroded in the Diestian erosion channel hence being filled with marine sands from the Diest Formation (Vandersteen et al., 2012, 2013, 2014). The Boom aquitard is included in the DAP model for its role in groundwater seepage from the shallow aquifer system.

Oligocene aquifer system (HCOV 0400)

This system is quite heterogeneous consisting of sandy clay, clayey sands and sand with, in between, thin discontinuous clay layers (Table 1), hence it has low hydraulic conductivity values. The base of this system dips to the north reaching a maximum depth of approximately -450 mTAW near the northern Belgian border. Towards the east of the Campine, this formation is disturbed by north-west - south-east oriented faults, causing a vertical downward shift of the

aquifer system. Faults also cause an increase in the thickness of the sediments which reaches up to 50 metres here, while the overall thickness of the sediments is restricted to a few tens of meters in the western part (Vandersteen et al., 2012, 2013, 2014).

Bartoon aquitard (HCOV 0500)

The Bartoon aquitard is formed by low permeable clay layers alternated with higher permeable sandy layers of the Maldegem Formation (Table 1). This aquitard is absent in the province of Limburg. The base dips to the north reaching a maximum depth of more than -450 mTAW, and it has maximum thickness of about 50 metres (Vandersteen et al., 2012, 2013, 2014).

Ledo-Paniselian-Brusselian aquifer system (HCOV 0600)

This is one of the main aquifers in the North-East Belgium, with numerous pumping wells located south of the rivers Demer and Dijle. The water becomes too salty to be used as drinking water as you move towards the north and west, this is due to the influence of the former marine environment. It is present in the central and western part of the Campine, but it is absent in the largest part of the province of Limburg. The base of this system dips to the north reaching a maximum depth of approximately -500 mTAW. It has a fairly constant thickness of approximately 50 metres and mainly consists of fine to coarse glauconitic and calcareous sands, containing limestone benches and locally thin marl and clay lenses (Vandersteen et al., 2012, 2013, 2014). For a detailed subdivision of this unit, see Table 1.

Table 1. Detailed hydro- and lithostratigraphy for the aquifers above and below the Boom Clay in the Campine area (modified after Vandersteen et al., 2012, 2013, 2014).

HYDROSTRATIGRAPHY			**LITHOSTRATIGRAPHY**		
HCOV coding			**FORAMATION**		**Main**
Main unit	**Sub-unit**	**Basic-unit**	**+ code**	**Member + code**	**lithology**
Campine Aquifer System (0200)	Miocene Aquifer (0250)	Kattendijk Sands and/or lower sands of Lillo (0251)	DIEST Di		sand
		Diest Sands (0252)		Deurne DiDn	sand
				Dessel DiDe	
		Bolderberg Sands (0253)	BOLDERBERG Bb	Opitter BbOp	sand
				Genk BbGe	
				Houthalen BbHo	
		Berchem and/or Voort Sands (0254)	BERCHEM Bc	Antwerpen BcAb	sand
			VOORT Vo	Voort VoVo	sand
		Veldhoven Clay (0255)		Veldhoven VoVe	clay
		Eigenbilzen Sands (0256)	EIGENBILZEN Eg		sand
Boom Aquitard (0300)		Clayey part of Eigenbilzen (0301)	BOOM Bm	Boeretang BmBo	clay
		Putte Clay (0302)		Putte BmPu	
		Terhagen Clay (0303)		Terhagen BmTe	
		Belsele-Waas Clay (0304)		Belsele Waas BmBw	
Oligocene Aquifer (0400)	Kerniel Sand (0410)		BILZEN Bi	Kerniel BiKe	sand
	Kleine-Spouwen Clay (0420)			Kleine Spouwen BiKs	clay
	Ruisbroek-Berg Aquifer (0430)	Berg Sands (0431)		Berg BiBe	sand
		Kerkom Sands (0432)	BORGLOON Bo	Kerkom BoKe	sand
		Alden Biesen Clayey Sands (0433)		Alden Biesen BoOb	
		Boutersem Sands (0434)		Boutersem BoBt	
		Ruisbroek Sands (0435)		Ruisbroek ZzRu	
	Tongeren Aquitard (0440)	Henis Clay (0441)	ZELZATE Zz	Henis BoHe	clay
		Watervliet Clay (0442)		Watervliet ZzWa	
	Lower-Oligocene Aquifer System (0450)	Neerrepen Sands (0451	St. H. HERN Sh	Neerrepen ShNe	sand
		Grimmertingen Sand-Clay (0452)		Grimmertingen ShGr	sand
		Bassevelde Clay Sand (0453)		Bassevelde ZzBa	
Bartoon Aquitard (0500		Onderdijke Clay (0501)	MALDEGEM Ma	Onderdijke MaOd	clay
		Buisputten Sand (0502)		Buisputten MaBu	sand
		Zomergem Clay (0503)		Zomergem MaZo	clay
		Onderdaele Sand (0504)		Onderdaele MaOn	sand
		Ursel and/or Asse Clay (0505)		Ursel MaUr /Asse MaAs	clay
				Wemmel MaWe	sand
Ledo-Paniseliaan Brusseliaan Aquifer (0600)	Wemmel-Lede Aquifer (0610)		LEDE Ld		sand
	Brussel Sands (0620)		BRUSSEL Br		
	Upper Paniselian deposits (0630)		AALTER Aa		sand, sand clay
	Lower Paniselian sandy deposits (0640)		GENTBRUGGE Ge	Vlierzele GeVl	Sand

2.3 Current groundwater model for the deep aquifers in North-East Belgium

The transient deep aquifer pumping model (DAP – **D**eep **A**quifer **P**umping model) (Gedeon & Wemaere, 2009, modified by Vandersteen et al. (2012)), for the aquifers lying below the Boom Clay is used in this study. Figure 4 illustrates the vertical cross-section of the conceptual DAP model.

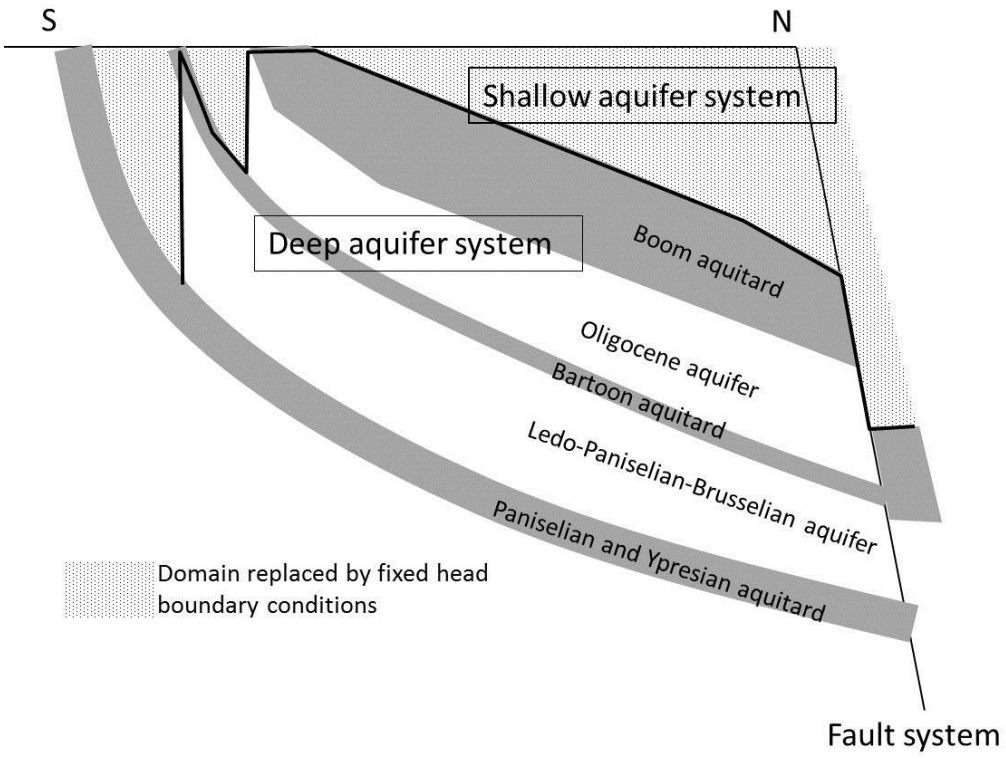

Figure 4. Vertical cross-section of the conceptual DAP model (Gedeon & Wemaere, 2009; Vandersteen et al., 2012, 2013).

The DAP model represents the confined and unconfined parts of the groundwater system in the Campine region. This includes the Miocene aquifer, the Boom aquitard and, confined and unconfined parts of the Oligocene aquifer, the Bartoon aquitard system and the Ledo-Paniselian-Brusselian aquifer. The confined parts of the Oligocene aquifer, the Bartoon aquitard and the Ledo-Paniselian-Brusselian aquifer are called the deep aquifer system (Figure 4) (Vandersteen et al., 2012, 2013).

Since the deep aquifer system is confined by very low-permeable Boom Clay, groundwater sources here are very limited and the system in its natural form is characterised by slow, low rate groundwater flow. The natural groundwater flow here is mainly affected by human induced

groundwater extraction. This has been confirmed by Labat (2011) that for more than 30 years of piezometric records there is a gradual decrease in groundwater levels in this system due to the considerable pumping in combination with a limited recharge. The system is continuously recharged at its outcrop areas, also little recharge is provided through the Boom Clay at areas with high elevation. Artesian water levels occur in the lowly-situated discharge areas having a low pumping influence (Vandersteen et al., 2012, 2013).

In the horizontal direction (Figure 3), the DAP model has dimensions of 95 km x 140 km. It extends to the south as far as the outcrops of the major aquitards: the Maldegem Formation (Asse/Ursel Clay of the Bartoon aquitard system), confining the Ledo-Paniselian-Brusselian aquifer and the Boom Clay, confining the Oligocene aquifer system. The northern and western boundaries of the model are chosen arbitrarily and go towards the north nearly as far as the Oosterschelde River and towards the west as far as Zeeland (The Netherlands). The eastern boundary is placed at the fault system of the Roer Valley Graben in the northeast of the Campine (Vandersteen et al., 2012).

In the horizontal schematization of the DAP model (Figure 5), cell dimensions (row length and column width) ranging from 500 to 4000 m. The most detailed representation (500 m x 500 m) is at locations with a high density of pumping wells and in the area around the Mol site, since this site is currently chosen as the reference site (Vandersteen et al., 2012).

In the vertical direction (Figure 6), the model contains 11 numerical layers. Since the hydrogeologic-unit flow (HUF) package (Anderman and Hill, 2000) of MODFLOW-2005 was used in the current DAP model, the numerical grid was defined independently of the hydrostratigraphic unit geometry. However the hydrostratigraphic unit geometry was used as a guidance to define the numerical layer geometry. The numerical layer geometry was created by interpolation of the processed hydrostratigraphic unit geometry from a cell size of 100 m × 100 m to the irregular modelling grid (Vandersteen et al., 2012). The description of the way these layers are defined is given in Table 2.

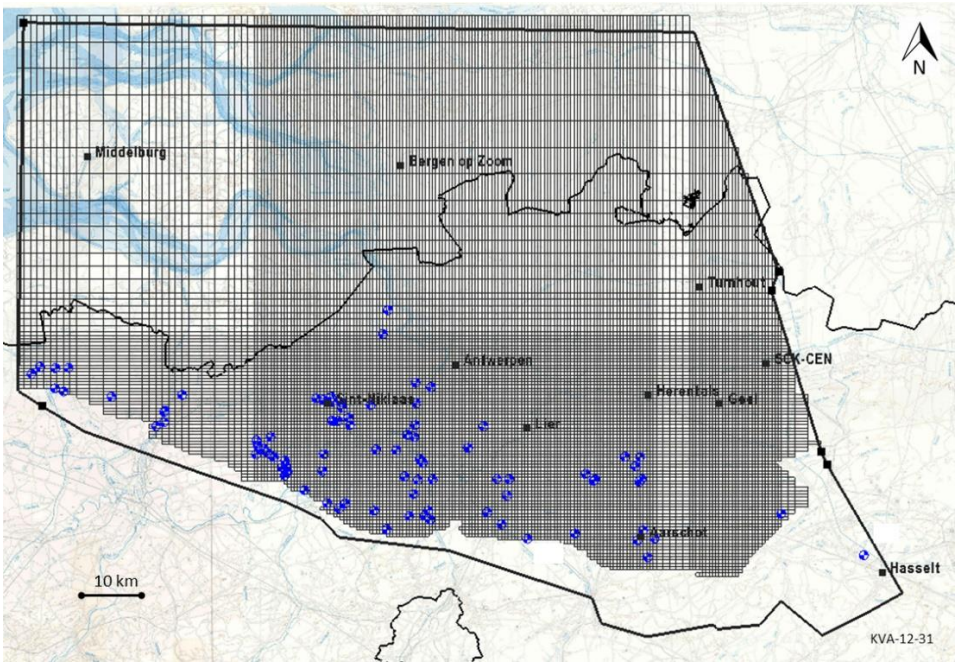

Figure 5. Horizontal schematization of the DAP model (example for the 11th numerical layer). Cell dimensions are ranging from 500 to 4000 m. The most detailed representation is at locations with a high density in pumping wells (in blue) and in the area around the Mol site (from Vandersteen et al., 2012).

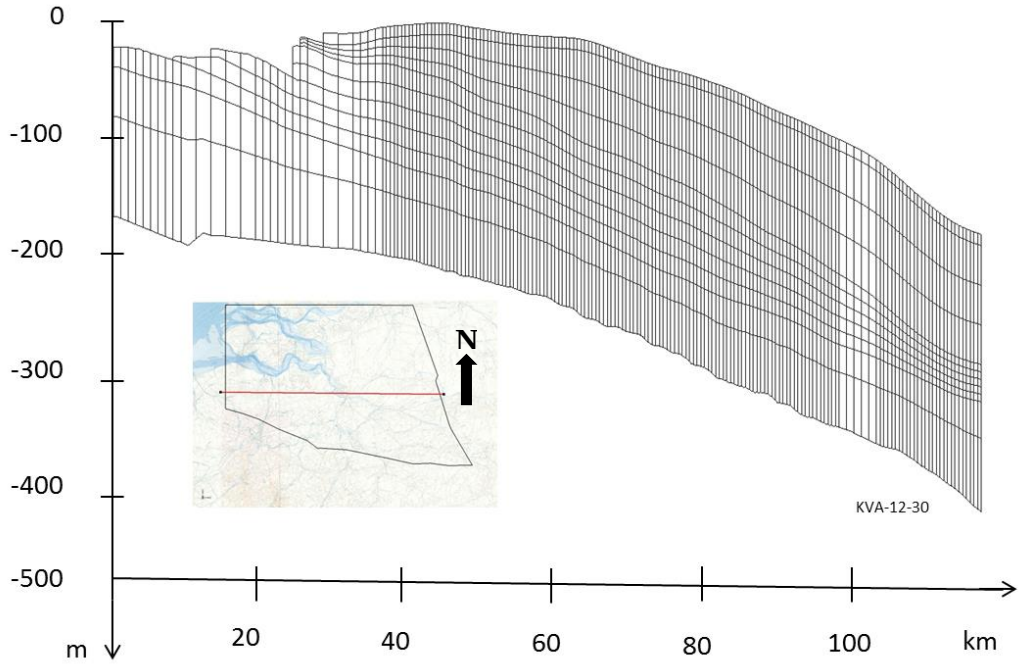

Figure 6. Vertical schematization of the DAP model showing the subdivision in 11 numerical layers (from Vandersteen et al., 2012).

Table 2. Definition of the numerical layers in relation to the hydrostratigraphy (modified after Vandersteen et al., 2012).

Layer	Description
1	Representing the 10 metres of the lower part of the Miocene aquifer.
2, 3, 4	Layers of the members of Boom Formation and the Bilzen Formation. The top of layer 2 and bottom of layer 4 correspond to the top and bottom of the Boeretang Member and the Belsele-Waas Member respectively. The boundaries between are defined by dividing the total thickness of the Boom Formation into 3 equal parts.
5, 6, 7,8,9	Layers of the members of the Oligocene aquifer and Bartoon aquitard. The top of layer 5 and bottom of layer 9 correspond to the bottom and top of the Boom Formation and the Ledo-Paniselian-Brusselian aquifer respectively. The boundaries between are defined by dividing the total thickness of the Oligocene aquifer and Bartoon aquitard into 5 equal parts.
10,11	Layers of the Ledo-Paniselian-Brusselian aquifer. The top of layer 10 and the bottom of layer 11 corresponds to the top and bottom of the Ledo-Paniselian-Brusselian aquifer respectively. While 1/3 and 2/3 of the total thickness of the Ledo-Paniselian-Brusselian aquifer correspond to the thickness of the 10^{th} and 11^{th} layer respectively.

In the current DAP model, three types of boundary conditions are applied. Fixed head boundary condition is assumed in the ten metres of the lower part of the Miocene aquifer. Also fixed head boundary condition is assumed in the unconfined parts of the Oligocene aquifer, Bartoon aquitard and Ledo-Paniselian-Brusselian aquifer in the southern part of the model (Figure 7). Fixed head boundary conditions are applied in these parts because they are not significantly influenced by pumping from deep aquifers, and are dominated by close-to-surface hydrological processes with heads fluctuating seasonally without any apparent long-term trend. Zero flux boundary condition is assumed at the model bottom due to the presence of the Paniselian and Ypresian aquitard system which act as a barrier. Also zero flux boundary condition is applied at the eastern model boundary (Figure 7) in the layers below the Boom Clay because of the vertical Boom Clay position shift by the fault system causing hydraulic isolation from the north-east. General head conditions are assumed at the western and northern model boundaries where the outflow is towards the sea (Figure 7) (Vandersteen et al., 2012).

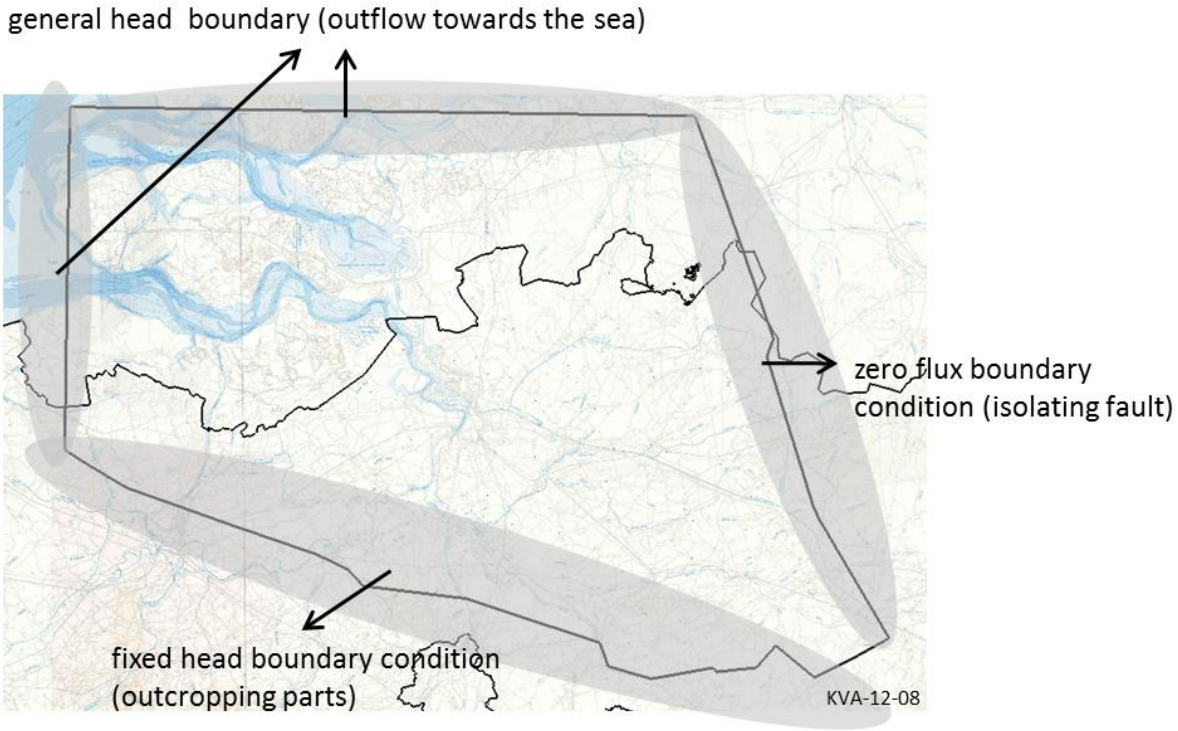

Figure 7. Schematic representation of the current DAP-boundary conditions under the Boom Clay (from Vandersteen et al., 2012).

Sediments of the deep aquifer system dip from their outcrop area towards the north-east, reaching depths of several hundred meters. This deepening leads to increased compaction of the sediments due to the increase of overburden thickness resulting in lower permeability at greater depths, towards the north. Hence the current DAP model assumes that the permeability of the Oligocene Aquifer System, Bartoon Aquitard System and Ledo-Paniselian-Brusselian Aquifer System decreases with increasing depth according to the following exponential relationship (Vandersteen et al., 2012):

$$\boldsymbol{K_{depth} = K_{surface} 10^{-\lambda d}} \quad (2.3)$$

where K_{depth} is the horizontal hydraulic conductivity at depth d [m/d], $K_{surface}$ is the hydraulic conductivity projected to a reference surface in [m/d], d is the depth below the reference surface [m] and λ is the depth-dependence coefficient [m^{-1}].

The current DAP model has four different depth dependency parameters for the hydraulic conductivity, one for the Putte-Terhagen Member of the Boom Clay, one for the Ledo-

Paniselian-Brusselian aquifer, one for the sandy part of the Oligocene aquifer and one for the clayey part of the Oligocene aquifer and the Bartoon aquitard. According to Vandersteen et al. (2012), implementation of these parameters in MODFLOW 2005 was accomplished through the use of the hydraulic-conductivity depth-dependence (KDEP) capability (Anderman and Hill, 2003), which is an addition to the hydrogeologic-unit flow (HUF) package (Anderman and Hill, 2000).

Also the current DAP model assumes that the specific storage coefficient of the sandy layers of the Oligocene Aquifer System, Bartoon Aquitard System and Ledo-Paniselian-Brusselian Aquifer System are depth-dependent according to the formula of van der Gun (van der Gun, 1979), derived for sandy aquifers:

$$S_s = 1.8\,x\,10^{-6} + 2.59\,x\,10^{-4}.d^{-0.7} \quad (2.4)$$

where S_s is the specific storage coefficient [m^{-1}] and d the depth of the sediment [m].

Since the depth-dependency feature is not included in the HUF package for the specific storage parameters, it was implemented through the use of multiplier arrays (Harbaugh, 2005). Each multiplier array contains values of the storage coefficient for every cell in the layer. A single parameter was then included in the model, representing a scaling factor for the multiplier arrays (Vandersteen et al., 2012).

In the current DAP model, the Ledo-Paniselian-Brusselian aquifer system is presented in three hydraulic conductivity zones corresponding to the various stratigraphic members. The DAP model assumes isotropic hydraulic conductivities for the Ledo-Paniselian-Brusselian (LPB) aquifer system and for the sand layers of the Oligocene and Bartoon (OB) formations system.

Moreover, the current DAP model contains one single well multiplication factor (WELL_MLT) for all pumping rates. This parameter was introduced in order to take into account the uncertainty on the exact pumping rates, it is kept constant in time. The well multiplication factor is used to assess the global effect of pumping rates on the simulated heads, rather than an effect of a particular pumping well (Vandersteen et al., 2012).

Initial parameter values for the hydrostratigraphic units in the current DAP model either come from previous modelling work (Gedeon & Wemaere, 2003, 2009), or from borehole measurements. Parameter names and corresponding hydrostratigraphic units in the current DAP model are given in Table 3.

Table 3. Parameter names and corresponding hydrostratigraphic units in the current DAP model (from Vandersteen et al., 2012). The explanation of the symbols used in the parameter name is given below the table.

Parameter name	Hydrostratigraphic unit		Material type
HK_mio	Miocene		sand
VANI_mio			
HK_BmBo	Boom – Boeretang		clay
VANI_BmBo			
HK_BmPuTe	Boom – Putte		clay
VANI_BmPuTe	Boom – Terhagen		
KD_BmPuTe			
HK_Bmbw	Boom – Belsele Waas / Bilzen – Berg		clay/sand
VANI_Bmbw			
HK_OB_sand	Borgloon Ruisbroek Neerrepen Bassevelde Buisputten Onderdaele		sand
VANI_OB_sand			
KD_OB_sand			
HK_OB_clay	Watervliet Onderdijke Zomergem Ursel Asse		clay
VANI_OB_clay			
KD_OB_clay			
HK1_LPB	Vlierzele-Aalter	Zone1	sand
HK2_LPB	Brussel	Zone2	
HK3_LPB	Wemmel-Lede	Zone3	
VANI_LPB	Ledo-Paniselian-Brusselian		
KD_LPB			
SS_sand (scaling factor)	All sandy units		sand
SS_clay	All clayey units		clay
Well_mlt	-		-

HK: hydraulic conductivity; VANI: vertical anisotropy; KD: depth-dependence parameter; SS: specific storage; WELL_MLT: well multiplication factor

The calibration of the current DAP model was conducted by comparing the simulated head values to the observed ones at the observation points. The observation points used for the calibration of the model are listed in Table 4. There are 16 piezometers in the Oligocene aquifer and 21 in the LPB aquifer. A subset of the observation points representing longer data series (shown in bold in Table 4) was used for the manual calibration. Every observation was assigned a weight of one except for the SCK-18b and SCK-18c piezometers which were given a smaller

weight of 1/5 because they are heavily influenced by a large pumping well in the vicinity (Vandersteen et al., 2012).

Table 4. List of observation points used for the calibration of the DAP model. Observation points used only for the manual calibration are given in bold. OL: Oligocene aquifer, L-P-B: Ledo-Paniselian-Brusselian aquifer (from Vandersteen et al., 2012).

Piezometer name	X (m)	Y (m)	bottom screen (m)	top screen (m)	observed period	aquifer
SCK_15b	198409	211736	-278.9	-270.6	1981-2010	OL
SCK_15c	198409	211736	-322.3	-318.4	1981-2010	L-P-B
SCK_18b (low weight)	156020	200694	-61	-57	1983-2010	OL
SCK_18c (low weight)	156020	200694	-108	-104	1983-2010	L-P-B
SCK_19e	160141	227764	-231	-225	1985-2010	OL
SCK_19f	160166	227771	-329	-323	1985-2006	L-P-B
SCK_1c	185001	207740	-195	-191	1985-2010	OL
SCK_20d	175740	236842	-358	-352	1984-2010	OL
SCK_20e	175740	236842	-459	-453	1983-2010	L-P-B
SCK_41c	164455	212040	-131	-129	1984-2010	OL
SCK_41d	164455	212040	-214	-212	1984-2010	L-P-B
SCK_43b	173322	214845	-236	-182.5	1997-2010	OL
SCK_43c	173322	214845	-288.3	-252.6	1997-2010	L-P-B
SCK_44b	175780	225883	-340.5	-269.05	1997-2010	OL
SCK_44c	175780	225883	-374.5	-356.6	1997-2010	L-P-B
SCK_45b	190552	221424	-345	-299	1999-2010	OL
SCK_45c	190552	221424	-404	-362	1997-2010	L-P-B
SCK_47b	142221	224446	-167.5	-161.5	1999-2010	OL
SCK_47c	142221	224446	-241	-235	1999-2010	L-P-B
SCK_51b	175303	202909	-148	-125	2006-2010	OL
SCK_51c	175303	202909	-202	-159.6	2006-2010	L-P-B
SCK_52e	156662	238672	-325	-290	2006-2010	OL
VMM_80207	128900	214430	-42	-47	1992-2010	OL
VMM_80208	128900	214430	-130	-135	1992-2010	L-P-B
VMM_91068	164063	201339	-120	-116	2005-2009	L-P-B
VMM_91071	183057	219988	-336.15	-332.15	2005-2009	L-P-B
VMM_91074	169047	221829	-333	-329	2005-2009	L-P-B
VMM_91083	163722	216014	-174	-169	2006-2009	OL
VMM_91084	163723	216014	-251	-246	2006-2009	L-P-B
VMM_91091	150550	222655	-247	-242	2005-2009	L-P-B
VMM_91095	163620	206993	-110	-102	2006-2009	OL
VMM_91096	163621	206993	-147	-145	2006-2009	OL
VMM_91097	182205	224427	-379.6	-374.6	2005-2009	L-P-B
VMM_91102	189384	196607	-153.5	-151.5	2006-2009	L-P-B
VMM_91104	189388	196607	-125.05	-123.05	2004-2009	OL
VMM_91171	189275	190520	-107	-103	2004-2009	L-P-B
VMM_91321	136891	217532	-165	-163	2005-2009	L-P-B
VMM_91329	133230	218448	-173	-168	2005-2009	L-P-B

The final result of the automatically calibrated DAP model, as obtained by Vandersteen et al. (2012), is shown in Table 5. The plot of observed values against simulated groundwater levels using the automatically estimated parameters is shown in Figure 8.

Table 5. Parameter values and fit statistics for the automatically and manually calibrated DAP model (from Vandersteen et al., 2012).

Parameter name	**Starting value**	**Manually calibrated value[1]**	**Automatically calibrated value**
HK_mio [m/d]	1×10^{-5}	1×10^{-5}	1×10^{-5}
VANI_mio [-]	2×10^{-6}	2×10^{-6}	2×10^{-6}
HK_BmBo [m/d]	3.6×10^{-6}	3.6×10^{-6}	3.6×10^{-6}
VANI_BmBo [-]	6.4	6.4	6.4
HK_BmPuTe [m/d]	1.6×10^{-6}	1.6×10^{-6}	1.6×10^{-6}
VANI_BmPuTe [-]	2.9	2.9	2.9
KD_BmPuTe [1/m]	0.0017	1×10^{-3}	1×10^{-4}
HK_Bmbw [m/d]	0.00016	0.00016	0.00016
VANI_Bmbw [-]	84	84	84
HK_OB_sand [m/d]	0.11	0.0015	0.0015
VANI_OB_sand [-]	1	1	1
KD_OB_sand [1/m]	0.0058	0.001	0.001
HK_OB_clay [m/d]	2.52×10^{-6}	4.52×10^{-6}	4.52×10^{-6}
VANI_OB_clay [-]	4.52	0.5	0.546
KD_OB_clay [1/m]	0.0017	0.005	0.004488
HK1_LPB [m/d]	2	1.2	0.8491
HK2_LPB [m/d]	2	1.7	1.477
HK3_LPB [m/d]	2	0.7	0.6240
VANI_LPB [-]	1	1	1
KD_LPB [1/m]	0.0058	0.006	0.005299
SS_sand (scaling factor) [-]	1	0.03	0.03893
SS_clay [1/m]	1×10^{-4}	1×10^{-5}	3.2×10^{-5}
Well_mlt [-]	1	1	1
Fit statistics			
Sum squared weighted residuals[m^2]		6935.4	1392
Mean residual (ME) [m]		2.52	0.12
Mean absolute residual (MAE) [m]		2.72	1.29
Root mean sq. residual (RMSE)[m]		3.65	1.64
R^2 (measured vs. simulated) [m]		0.97	0.985

[1] The manually calibrated values were used as initial values for the automated calibration.

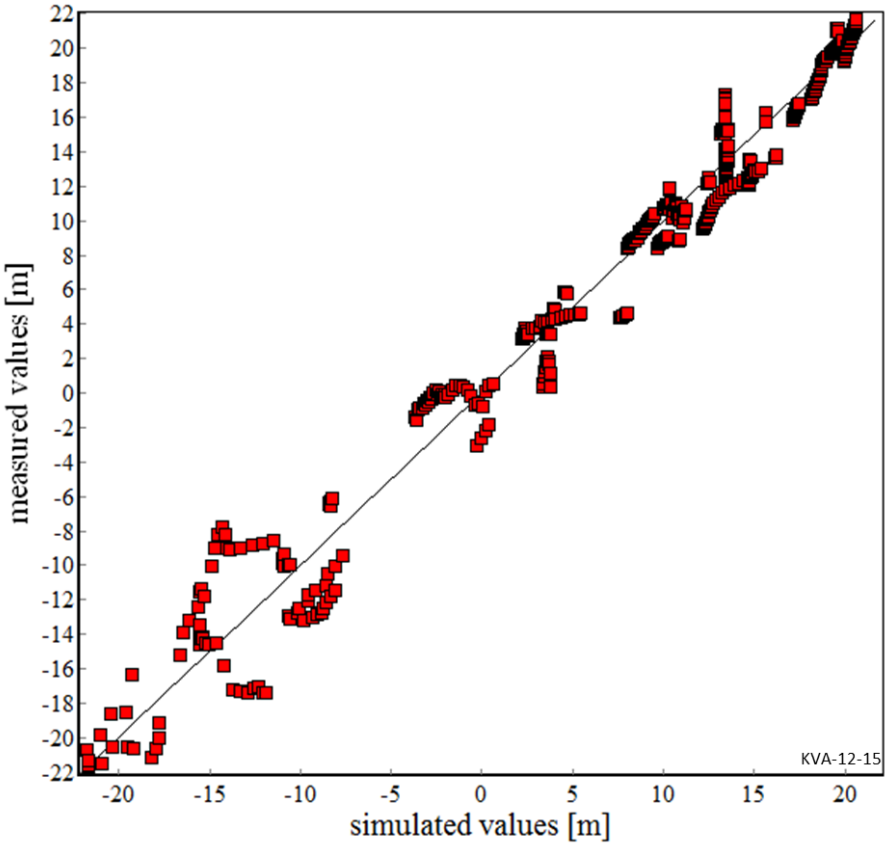

Figure 8. Measured versus simulated groundwater level values in current the DAP-model using the automatically estimated parameters.

3 Methodology

3.1 Characterization of borehole cores from the aquifers below the Boom Clay using the air permeameter

A total of 48 air-dried core slabs from the Essen-1 and Herenthout-1 boreholes containing members of the Oligocene aquifer system and the lowest part of the Boom Clay (Belsele-Waas member) were characterised. Thirty-eight core slabs are from the Essen-1 boreholes while 10 are from Herenthout-1, each with an approximate length of 1 m. Here, the Belsele-Waas member is considered as part of the Oligocene aquifer because the main lithology is dominated by sand with few clay composition. The Belsele-Waas member is combined with the Berg member (Table 1) to form the Belsele-Waas-Berg unit as the upper part of the Oligocene aquifer. The members of the Oligocene aquifers found in the Essen-1 core slabs are Belsele-Waas, Ruisbroek, Wintham

and Watervliet while for Herenthout-1 the members are Belsele-Waas and Ruisbroek. The Ruisbroek, Wintham and Watervliet members all belong to the Zelzate formation. The depth of the investigated core slabs from the Herenthout-1 borehole range from -115.33 mTAW to -128.12 mTAW while for Essen-1 it is from -244 mTAW to -286.48 mTAW. Figure 9 illustrates the depth ranges of the investigated parts of the Oligocene aquifer from these two boreholes.

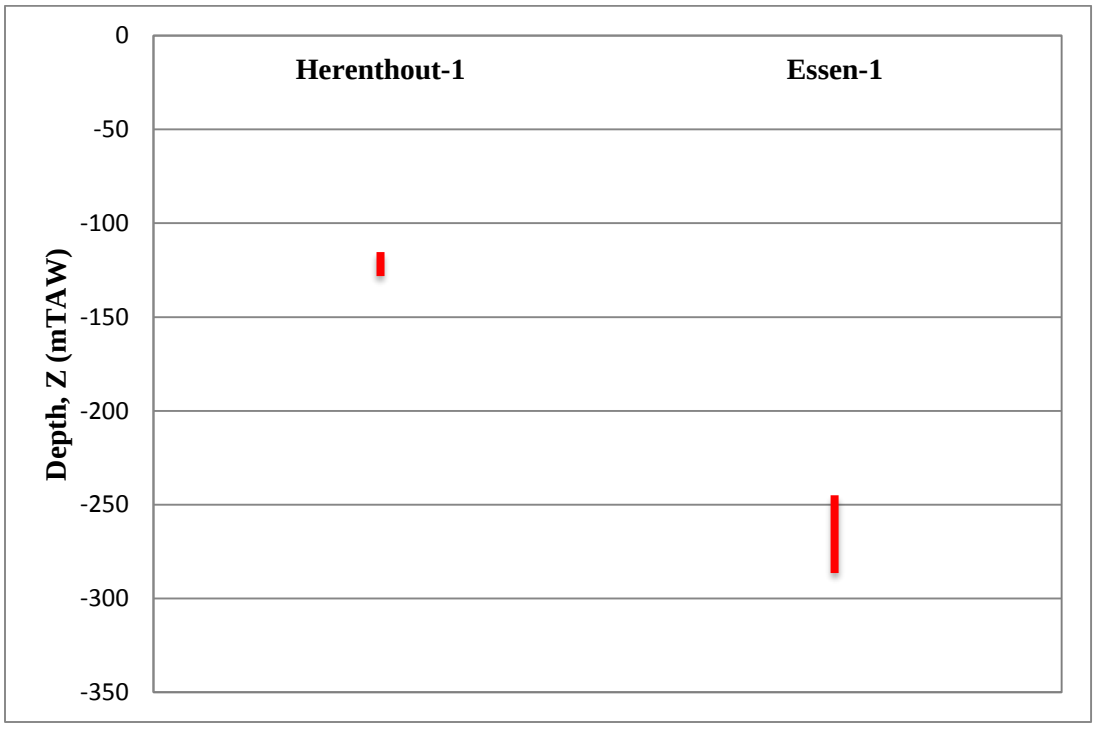

Figure 9. Depth ranges of the investigated parts of the Herenthout-1and Essen-1 boreholes

Measurements of k_a in each core slab were carried out with a spacing of approximately five centimetres. Disturbed sections and/or undulating surfaces were excluded to avoid incorrect measurements caused by air leakage, this resulting in a total of 510 k_a measurements. All measurements were performed within two days, with one person operating the air permeameter, and another one recording the TinyPerm II responses. Since two different air permeameter operators were involved in the measurements, measurements to check their differences were carried out. The results are similar for both operators (Potums, 2014).

3.2 Evaluation of available pumping test data from deep aquifers and comparison to the air permeameter measurements

A total of 67 hydraulic conductivity data from pumping test performed in different locations of the aquifers below the Boom Clay were evaluated. Twenty hydraulic conductivity data are from the Oligocene aquifer (Table 17in Appendix 2) while 47 are from the Ledo-Paniselian-Brusselian aquifer (Table 18 in Appendix 2). For each aquifer the minimum, maximum and average values of hydraulic conductivity were analysed. The variance and standard deviation for each data set were calculated to see how the data are spread out. Comparison between the aquifers is made to gain an understanding on their differences in conductivity and transmissivity (further discussed in section 4.2).

The Oligocene aquifer is the only aquifer below the Boom Clay to be characterised by the air permeameter measurements in this study (section 3.1), for which a comparison with the pumping test data is made. Before up-scaling of the air permeameter-based data, data are compared to get an insight on the difference between large-scale and small-scale measurements in the estimation of the hydraulic conductivity of the aquifer. After up-scaling of the air permeameter-based data the comparison is made to get values which are representative of both methods.

3.3 Up-scaling of the air permeameter-based hydraulic conductivity estimates

Wen & Gómez-Hernández (1996) defined hydraulic conductivity upscaling as a process that transforms a grid of hydraulic conductivities defined at the scale of the measurements, into a coarser grid of block conductivity tensors amenable for input to a numerical flow simulator. The upscaled conductivity is called the (grid) block conductivity because it is spatially constant (homogeneous) within a grid block. But this homogeneous conductivity should represent the heterogeneous conductivity of the grid block as much as possible, hence upscaling replaces a heterogeneous domain with a homogeneous one by ensuring that both domains produce the same response for upscaled boundary conditions (El-Rawy, 2013). The techniques for upscaling range from the simple averaging of the heterogeneous values within the block (e.g. arithmetic and harmonic means), to sophisticated inversions such as the double constraint method (Wen & Gómez-Hernández, 1996; El-Rawy, 2013; Rogiers et al., 2013b).

In hydrogeology, measurements of hydraulic conductivity data either in-situ or in laboratory are usually done at a smaller scale compared to the grid block dimensions of a groundwater flow model. Therefore, upscaling of these data is of major concern in order to produce models with relatively few grid blocks which are simpler to apply, especially when the model has to run many times and/or is used to assimilate time dependent data (El-Rawy, 2013).

In this study, the upscaled parameters were simply obtained by calculating arithmetic and harmonic means from the values measured at each borehole location as follows:

- The upscaled **horizontal conductivity K_h**, per member of each hydrostratigraphic unit and per location was determined as the weighted arithmetic mean of all the samples in the analysed member by using Equation 3.1.

$$K_h = \frac{\sum_{i=1}^{n} k_{ih} D_i}{D} \tag{3.1}$$

  where K_h is the upscaled horizontal conductivity, D is the total thickness of the layer, D_i is the thickness associated with the i_{th} sample and k_{ih} is the horizontal conductivity of the i_{th} layer.

- The upscaled **vertical conductivity K_v**, per member of each hydrostratigraphic unit and per location was determined as the harmonic mean of all the samples in the analysed member by using Equation 3.2.

$$K_v = \frac{D}{\sum_{i=1}^{n} \left(\frac{D_i}{k_{iv}}\right)} \tag{3.2}$$

  where K_v is the upscaled vertical conductivity and k_{iv} is the vertical conductivity of the i_{th} sample.

- The **overall upscaled (regional) conductivity** (both K_h and K_v) per member over all the locations was determined as the geometric mean of the parameters per location by using Equation 3.3.

$$K_{geom} = \sqrt[n]{K_1 K_2 K_3 \ldots\ldots K_n} \tag{3.3}$$

- The **vertical anisotropy** per layer was determined as K_h / K_v (3.4)

3.4 Integration of air permeameter and pumping test data in the current DAP model

The up-scaled air permeameter-based K_h values for the Oligocene aquifer are integrated in the current DAP model by updating the VANI_OB_sand parameter, assuming that $K_h - K_v$ ratio is minimally affected by the sediment expansion in the core slabs (further discussed in section 4.4).
Pumping test data for the Oligocene aquifer are incorporated in the current DAP model by updating the hydraulic conductivity of the sand layers of the Oligocene and Bartoon formations system. This is done by setting its reasonable lower and upper values based on the obtained range. A start value is arbitrarily chosen within the range (further discussed in section 4.4).
In case of the Ledo-Paniselian-Brusselian (LPB) aquifer, pumping test data are incorporated in the current DAP model by using a multiplier file. The multiplier file is used to specify multiplier arrays which can be used to calculate layer variables from parameter values. We account for the depth-dependency directly in the multiplier file by calculating the K_h field for each cell in a spreadsheet. The K_h values in the multiplier file are the starting values for the model updates. A single new parameter named HK_LPB is introduced in the model, representing a scaling factor for the multiplier arrays. This new update removes the following parameters from the current DAP model: HK1_LPB, HK2_LPB, HK3_LPB and KD_LPB (Table 3).
To accomplish this new update in the LPB aquifer, first, mathematical equations describing the K_h depth-dependency in the LPB aquifer were establishing from the measurements. The equations are based on the spatial distribution of the available pumping test data (Figure 10) and on assumption that the available data represent K_h values at the middle of the LPB aquifer thickness.

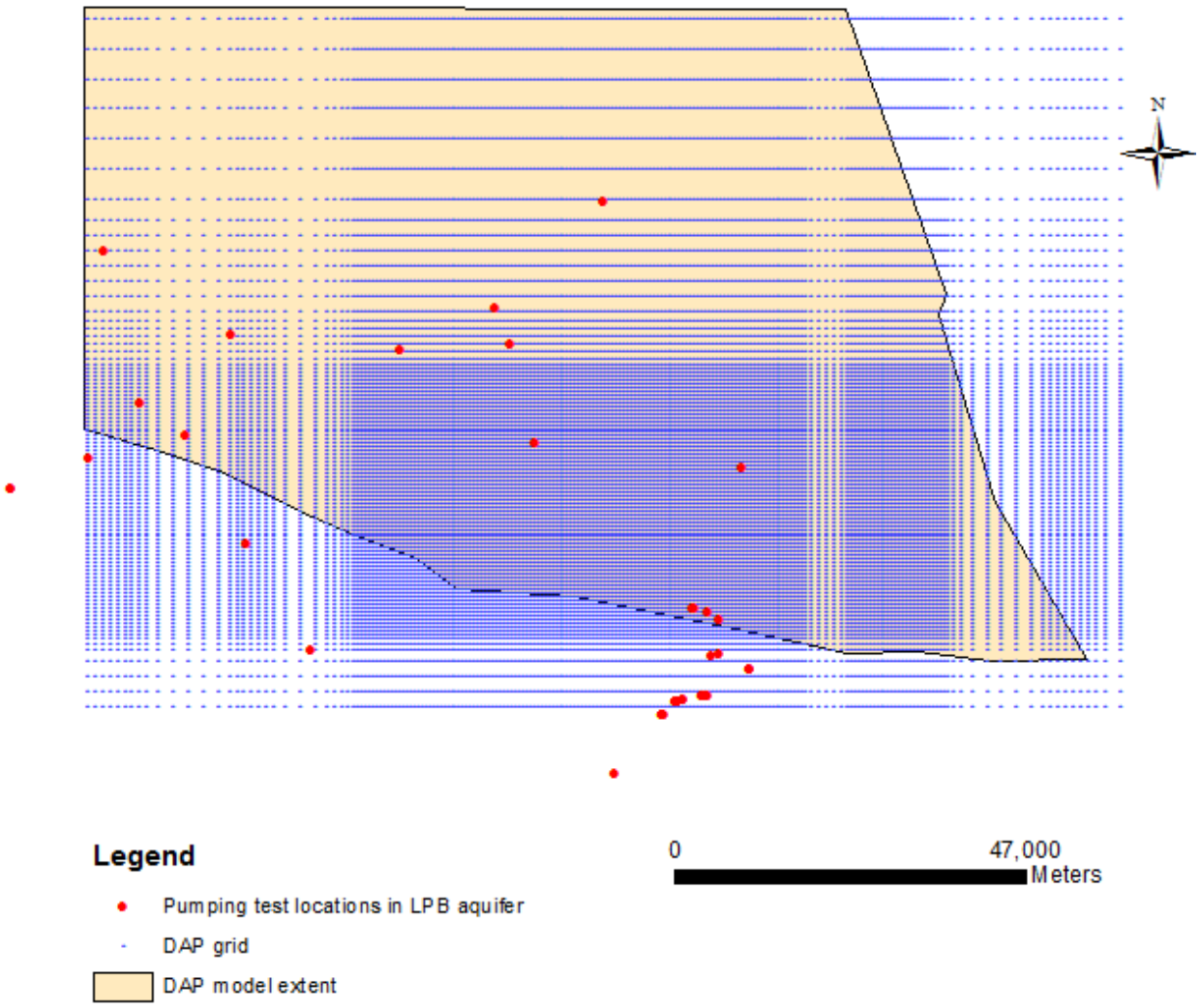

Figure 10. Pumping test locations in the Ledo-Paniselian-Brusselian (LPB) aquifer in reference to the DAP grid nodes.

Figure 11 shows two mathematical equations (Equation 3.5 and Equation 3.6) describing possible trends of the K_h depth-dependency at the middle of the LPB aquifer thickness. Slug test data were included in Figure 11 only to compare the pumping test data at a greater depth, they were not used in establishing the equations.

$$\boldsymbol{logK_h = 0.0063d + 1.0209} \quad (3.5)$$

$$\boldsymbol{logK_h = 1.7629e^{0.0088d} - 0.8} \quad (3.6)$$

where d is the depth below the reference surface expressed in metre, and K_h is in m/d.

In Figure 11(b), the value of 0.8 in the expression $\boldsymbol{y = logK_h + 0.8}$ was basically set as the horizontal asymptote, making it the minimum K_h in the LPB aquifer. Equation 3.6 (Figure 11(b)) shows the best fit than Equation 3.5 (Figure 11(a)). Both equations were used in the analysis for comparison purpose.

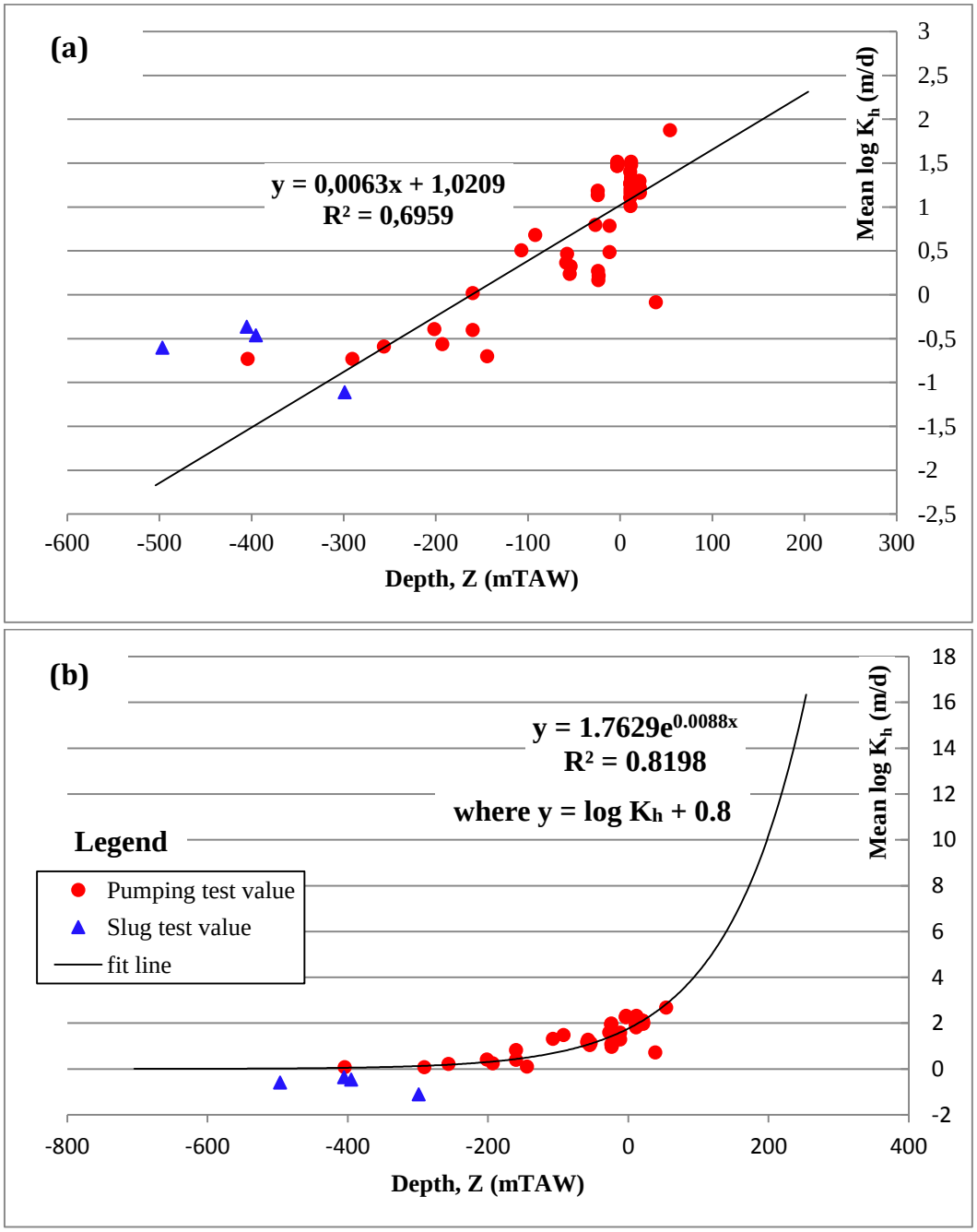

Figure 11. Relationships between mean log Kh and Z (mTAW) in the Ledo-Paniselian-Brusselian (LPB) aquifer, (a) linear relationship (b) exponential relationship.

Equation 3.5 and Equation 3.6 are used to estimate the values of K_h (K_h *estimate*) at each pumping test location and for the entire LPB aquifer. The values of mean log K_h at each pumping test location are obtained through logarithmic transformation of the mean values of the available pumping test data (Table 18 in Appendix 2). The residuals of log K_h at each pumping test location are calculated by using Equation 3.7.

$$\boldsymbol{logK_h\, residual\ = mean\, logK_h - \ logK_h\, estimate} \tag{3.7}$$

The final K_h values for the entire LPB aquifer in reference to the DAP grid are calculated by using Equation 3.8.

$$\boldsymbol{K_h = K_h\, estimate\ + K_h\, residual} \tag{3.8}$$

The residuals obtained in Equation 3.7, which were computed from the available data, are treated as estimates of the model error. To find the value of K_h *residual* parameter in Equation 3.8 an assumption is made that the estimates of the model error at each pumping test location remain the same for the entire LPB aquifer. Therefore the residuals of log K_h at each pumping test location are interpolated in the entire LPB aquifer to get values of the K_h *residual* parameter.
The kriging interpolation method was used in this study. The kriging method interpolates a value of a random field at an unobserved location based on available surrounding measurements. The kriging problem consists of finding the weights $\{\lambda_\alpha\}$, $\alpha = 1, \ldots, n$ such that:

$$Variance\left(\sum_{\alpha=1}^{n(\mathbf{u})} \lambda_\alpha [Z(\mathbf{u}_\alpha) - m(\mathbf{u}_\alpha)] - [Z(\mathbf{u}) - m(\mathbf{u})]\right) \quad \text{is minimum} \tag{3.9}$$

where $\mathbf{u}$ is the location vector for estimation point, $\mathbf{u}_\alpha$ is the location vector for the neighboring point, $Z(\mathbf{u})$ is a generic random function of location u, $Z(\mathbf{u}_\alpha)$ is a generic random function of the neighboring location, $n(\mathbf{u})$ is the number of data points in local neighborhood, $m(\mathbf{u})$ is the expected value (mean) of $Z(\mathbf{u})$, and $m(\mathbf{u}_\alpha)$ is the mean of $Z(\mathbf{u}_\alpha)$.

Two algorithms of the kriging method, Simple Kriging (SK) and Ordinary Kriging (OK) were used in this study for comparison purpose. The simple kriging assumes there is no trend on the data set and the population mean ($m(\mathbf{u})$) is known and constant. This is a rare situation. The ordinary kriging assumes the mean is unknown and the trend is approximately constant within the search neighborhood. This is the predominant case.

The Stanford Geostatistical Earth Modeling Software (SGeMS) was used for running the kriging algorithms. The SGeMS is an open-source geostatistical package for solving problems involving spatially correlated variables (Remy et al., 2009). The kriging interpolation method uses a variogram to describe the spatial structure of random processes. The variogram (γ (h)) is a variance function in a probabilistic field, which is used to express the dispersion of the data (Sakata et al., 2004). It is defined as half of the average squared difference between variable values separated by a lag vector **h** (Deutsch & Journel, 1998):

$$\gamma(\mathbf{h}) = \frac{1}{2N(\mathbf{h})} \sum_{i=1}^{N(\mathbf{h})} (x_i - x_i')^2 \tag{3.10}$$

where N (**h**) is the number of pairs and x_i and x_i' are a data pair separated by **h**.

Variograms are usually modeled with a variogram model. The model used in this study is the Gaussian model (Equation 3.11) (Remy et al., 2009). The estimated surface produced by this model is smooth and continuous, making it suitable for use in an optimizing design (Sakata et al., 2004).

$$\gamma(\mathbf{h}) = C_0 + C\left(1 - \exp\left(\frac{-3\|\mathbf{h}\|^2}{a^2}\right)\right) \tag{3.11}$$

where **h** is the lag distance, C_0 is the nugget effect, C is the sill and a is the practical range.

The input parameters for variogram computation are; number of lags, lag separation, lag tolerance, number of directions, azimuth, dip angle, tolerance and bandwidth (Figure 12).

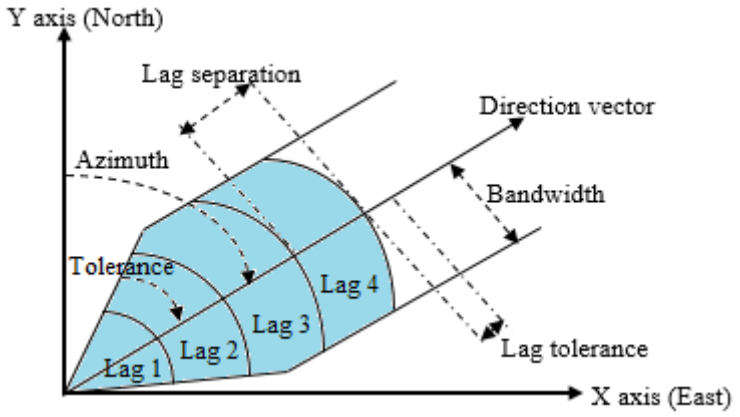

Figure 12. A sketch showing the input parameters for variogram computation.

The number of lags is the number of bins that are calculated. The lag separation is the distance between two paired data point locations. The lag tolerance is the allowable distance on either side of a lag separation to be reported to the same lag. The number of directions specifies the number of directions along which to compute the experimental variograms, each with the same number of lags. The azimuth is the direction along which the property varies the least (i.e. the direction of maximum continuity or minimum anisotropy). The azimuth angle is the first angle of rotation of the vector. The direction of the azimuth is clockwise 180 degrees from North. The dip angle is the second angle of rotation and it represents a downward rotation of the vector from the horizontal plane. The tolerance is used to define an angular tolerance on the major and minor directional azimuths beyond which no data pairs are selected. The maximum tolerance is 90 degrees and is used when computing anisotropic variograms. The bandwidth is the maximum acceptable deviation from the direction vector.

Table 6 shows the input parameter values for the variogram computation. By considering the dimensions of the current DAP model (95 km x 140 km), the value of lag separation times the number of lags is set to be approximately half of the shortest dimension (95 km). In this study the value is 45 km (45000 m). Lag tolerance is half of the lag separation. The criteria are based on the optimization of the variogram computation. A tolerance greater than 90° was chosen to compute omni-directional variogram. The omni-directional variogram was chosen in order to have a clearly interpretable structure because it contains more sample pairs than any directional variogram.

Table 6. Input parameters for variogram computation.

Input parameter	**Value**
Number of lags	9
Lag separation [m]	5000
Lag tolerance [m]	2500
Number of directions	1
Azimuth	0°
Dip	0°
Tolerance	100°
Bandwidth	0

The shape of the variogram is described by the following parameters: nugget effect, sill and range (Figure 13). The nugget represents a discontinuity of the variogram that can be present at the origin. The discontinuity is attributed to micro-scale effects and measurement error. The sill

is the limit of the variogram tending to infinity lag distances. The sill consists of the nugget effect, if present, and the partial sill. The range is the distance in which the difference of the variogram from the sill becomes negligible.

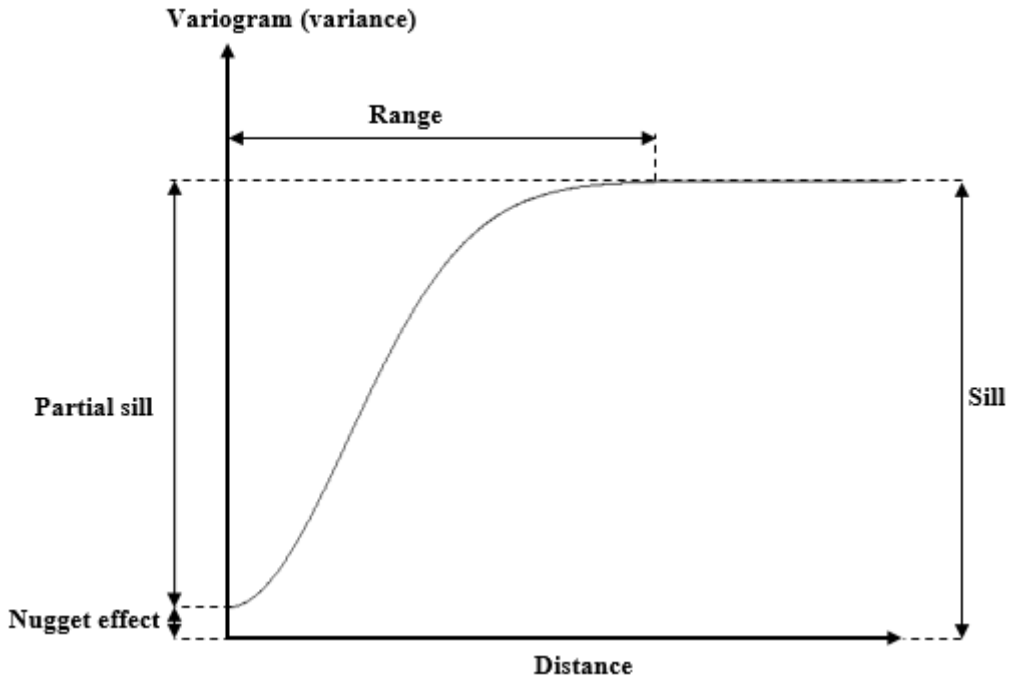

Figure 13. A theoretical variogram of Gaussian type and its characteristics.

Table 7 shows the parameters for the variogram models for Equation 3.5 and Equation 3.6. The models for these equation are given in Figure 14. The sill values in the models were chosen based on the data variance.

Table 7. Parameters for the variogram models.

Parameter	**Value from using Equation 3.5**	**Value from using Equation 3.6**
Nugget effect [m/d]	0.005	0.01
Sill (contribution) [m/d]	0.155	0.14
Type	Gaussian	Gaussian
Range [m]	16200	18000
Angle	0°	0°

Presence of a nugget effect in the variogram models (Table 7) indicates there is discontinuity in K_h in the LPB aquifer. This discontinuity is probably related to sedimentary heterogeneity in the aquifer and/or measurement error.

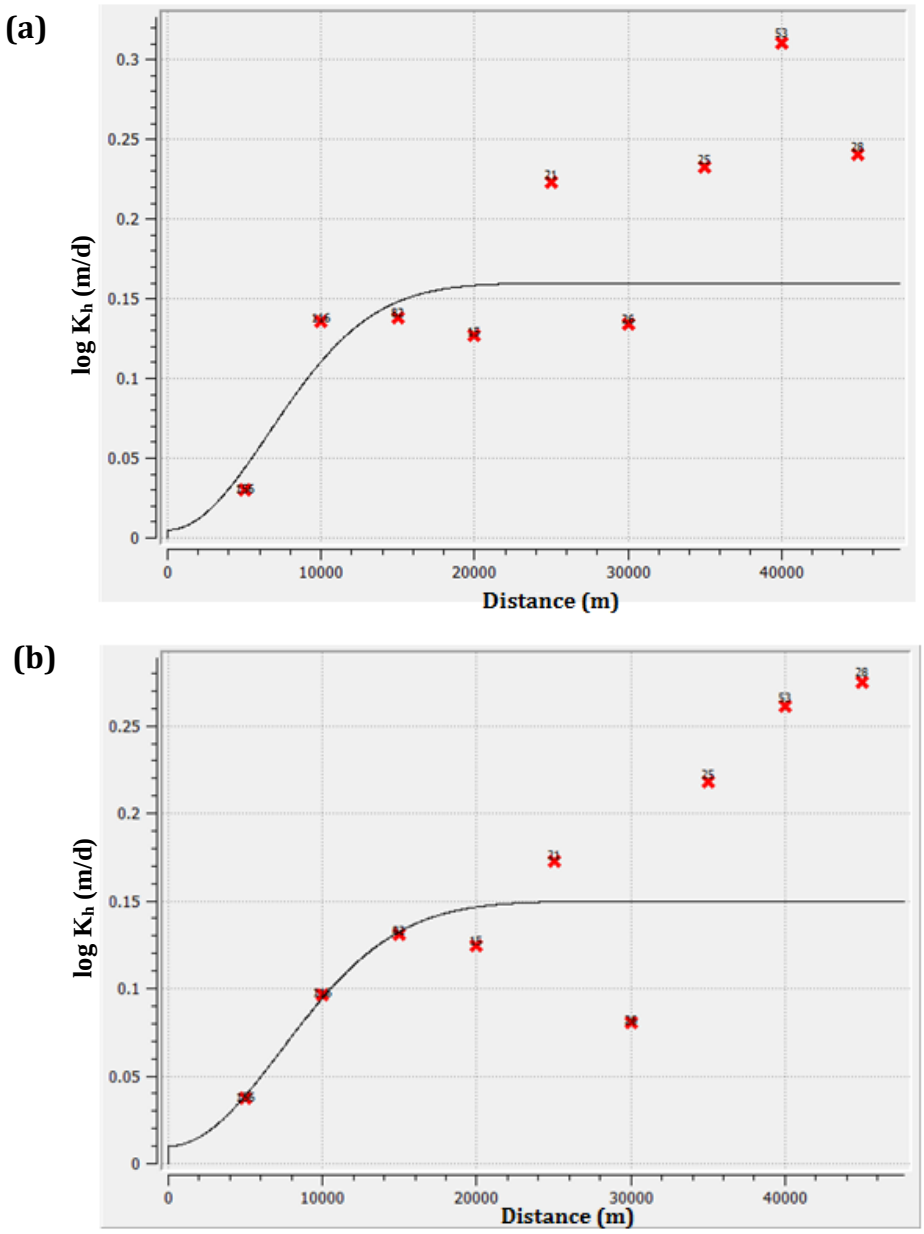

Figure 14. Variogram models for the depth-dependent K_h distribution in the LPB aquifer by using, (a) Equation 3.5 (b) Equation 3.6.

The final K_h values for the entire LPB aquifer were arranged into multiplier arrays by using the spreadsheet. The multiplier files are integrated into the current DAP model and the HK_LPB parameter is introduced (the scaling factor for the multiplier arrays). As the results of using the two equations (Equation 3.5 and Equation 3.6) and the two kriging algorithms (Simple Kriging and Ordinary Kriging), four multiplier files containing K_h values for the entire LPB aquifer were created. All files were used in the analysis for comparison purpose.

Figure 15 gives a summary of the major tasks executed in the integration of LPB pumping tests data into the current DAP model after establishing Equation 3.5 and Equation 3.6.

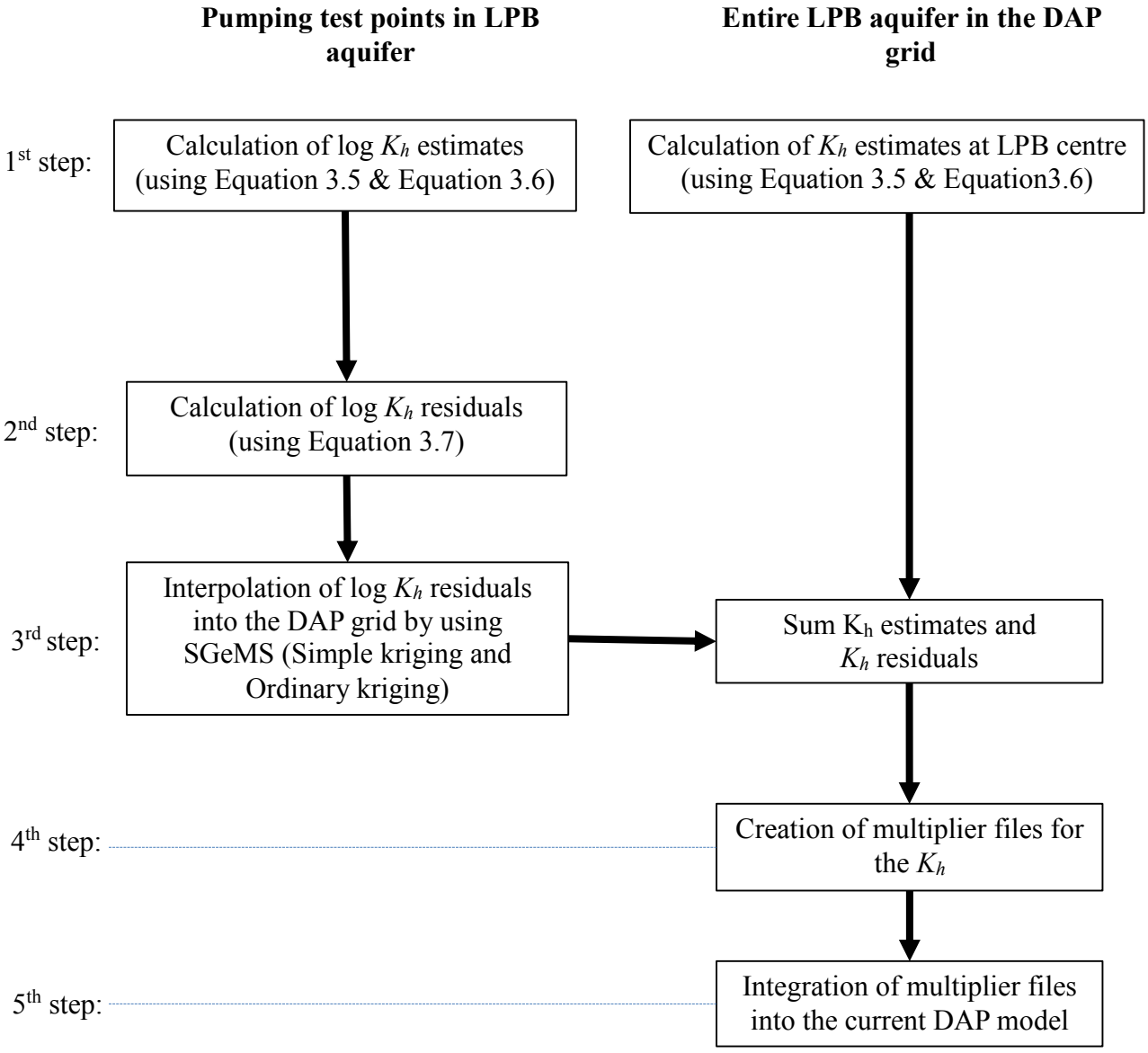

Figure 15. Flowchart showing major steps in the integration of LPB pumping tests data into the current DAP model after obtaining Equation 3.5 and Equation 3.6.

After incorporating all necessary changes in the current DAP model, from here on, the model is referred as the updated DAP model.

3.5 Sensitivity analysis and calibration of the updated DAP model

The universal automated calibration program UCODE 2005 developed by Poeter et al. (2005) was used to perform sensitivity analysis and calibration of the updated DAP model. The program was run by using ModelMate, a graphical user interface designed to facilitate model analysis by software applications that invoke model simulations as external processes (Banta, 2011). The optimisation method used by UCODE 2005 consists of finding the model parameter values that minimize a misfit criterion, in this case the sum of squared residuals based on observed groundwater levels. Sensitivity analysis for the model parameters was done prior to model calibration in order to identify the parameters influence the objective function value most, and also to identify parameters which are difficult to optimize, which are the non-sensitive parameters. The sensitivity analysis was interpreted using the composite scaled sensitivities. According to Ely (2006), composite scaled sensitivities indicate the information content of all the observations for the estimation of a parameter. The composite scaled sensitivity for the j_{th} parameter (css_j) is calculated as (Hill, 1998):

$$\boldsymbol{css_j} = \sqrt{\frac{\left[\sum_{i=1}^{ND} (ss_{ij})^2\right]_{\underline{b}}}{ND}} \tag{3.12}$$

where

$$\boldsymbol{ss_{ij}} = \sum_{k=1}^{ND} \left[\left(\frac{\partial y'_k}{\partial b_j}\right) \boldsymbol{b_j}\sqrt{\boldsymbol{\omega_{ik}}}\right] \tag{3.13}$$

and

i is the observation,

ND is the number of observations being used in the regression,

y'_i is a simulated value,

b_j is the j_{th} estimated parameter,

$\frac{\partial y'_k}{\partial b_j}$ is the sensitivity of the simulated value with respect to the j_{th} parameter evaluated at $\underline{b}$,

$\underline{b}$ is a vector which contains the parameter values at which the sensitivities are evaluated,

ω_{ik} is the weight of the i_{th} observation.

In order to have good starting values for the automated calibration procedures in this study, manual calibrations through trial-and-error for the updated DAP model alternatives were performed in advance.

Furthermore, after the automatic calibration of the updated DAP model analysis on the dimensionless scaled sensitivity was performed. In this study emphasis was given on the piezometers which show high values of weighted residuals. Dimensionless scaled sensitivities (dss_{ij}) compare the importance of different observations to the estimation of a single parameter or the importance of different parameters to the calculation of a simulated value. In both cases, greater absolute values are associated with greater importance. A positive value of the dss means that an increase in parameter value will invoke an increase in the simulated heads and vice versa. (Hill, 1998). The dimensionless scaled sensitivity (dss_{ij}) is calculated as (Hill, 1998):

$$\boldsymbol{dss_{ij}} = \left(\frac{\partial y'_i}{\partial b_j}\right) \boldsymbol{b_j}\sqrt{\boldsymbol{\omega_{ii}}} \tag{3.14}$$

where

i is the observation, y'_i is a simulated value, b_j is the j_{th} estimated parameter,

$\frac{\partial y'_i}{\partial b_j}$ is the sensitivity of the simulated value with respect to the j_{th} parameter evaluated at $\underline{b}$,

$\underline{b}$ is a vector which contains the parameter values at which the sensitivities are evaluated,

ω_{ii} is the weight of the i_{th} observation.

4 Results and discussion

4.1 Air permeameter-based measurements

The TinyPerm II air permeameter values for the members of the Oligocene aquifer from Essen-1 core slabs lie between 2 mD and 13,623 mD. These values correspond to the saturated hydraulic conductivity (K_s) values of 3.0 x 10^{-5} m/d and 2.01 m/d respectively, with an average value of 0.23 m/d (Table 15 in Appendix 1). The K_s distribution for these data has a variance of 0.11 $(m/d)^2$ and a standard deviation of 0.33 m/d (Table 15 in Appendix 1). While for core slabs from Herenthout-1, the values lie between 151 mD and 27,817 mD corresponding to 6.6 x 10^{-3} m/d and 5.0 m/d respectively, with an average value of 0.45 m/d (Table 16 in Appendix 1). The K_s

distribution here has a variance of 0.25 $(m/d)^2$ and a standard deviation of 0.50 m/d (Table 16 in Appendix 1). For the summary of K_s values for each member measured from the core slabs of the investigated two boreholes, see Table 8.

Table 8. Summary of K_s for each member of Oligocene found in Essen-1 and Herenthout-1[N is the number of K_a measurements per member].

Member	**Borehole**	**N**	**K_s (m/d)**			**variance K_s $(m/d)^2$**	**standard deviation K_s (m/d)**
			Minimum	**Maximum**	**Mean**		
Belsele-Waas	**Herenthout-1**	23	6.6×10^{-3}	0.3	0.09	0.01	0.08
	Essen-1	187	3.0×10^{-5}	1.4	0.11	0.05	0.22
Ruisbroek	**Herenthout-1**	94	0.11	5.0	0.53	0.27	0.52
	Essen-1	56	0.08	2.0	0.69	0.19	0.43
Wintham	**Essen-1**	121	9.7×10^{-4}	1.4	0.21	0.05	0.22
Watervliet	**Essen-1**	29	3.4×10^{-3}	1.6	0.14	0.08	0.29

From Table 8 and Figure 16, the maximum K_s value for the Ruisbroek and Watervliet member are 5.0 m/d and 1.6 m/d respectively. However by analysing all raw K_s data (Figure 17), these values are noticed and considered as an outlier compared to other values for the same member. These outliers are attributed to the measurement error. Therefore the possible maximum K_s value for the Ruisbroek and Watervliet member are 2.0 m/d and 0.2 m/d respectively.

By considering members of the same formation, the Ruisbroek, Wintham and Watervliet, which all belong to the Zelzate formation, it can be noticed in Figure 17 (b) that the mean K_s values for these members decrease with increase in depth hence confirming the assumption of depth-dependency of the hydraulic conductivity in the Oligocene aquifer. In this case the hydraulic conductivity depth-dependency is mainly due to differences in lithology.

The hydraulic conductivity depth-dependency due to compaction in the Ruisbroek member cannot be easily noticed as there is only five metres difference between top and bottom of the Ruisbroek member (Figure 17).

Figure 16 shows the graphical presentation of K_s data ranges together with the number of measurements (n) for each member of Oligocene aquifer found in Herenthout-1 and Essen-1 core slabs. Figure 17 shows the distributions of all raw K_s data for the measured members.

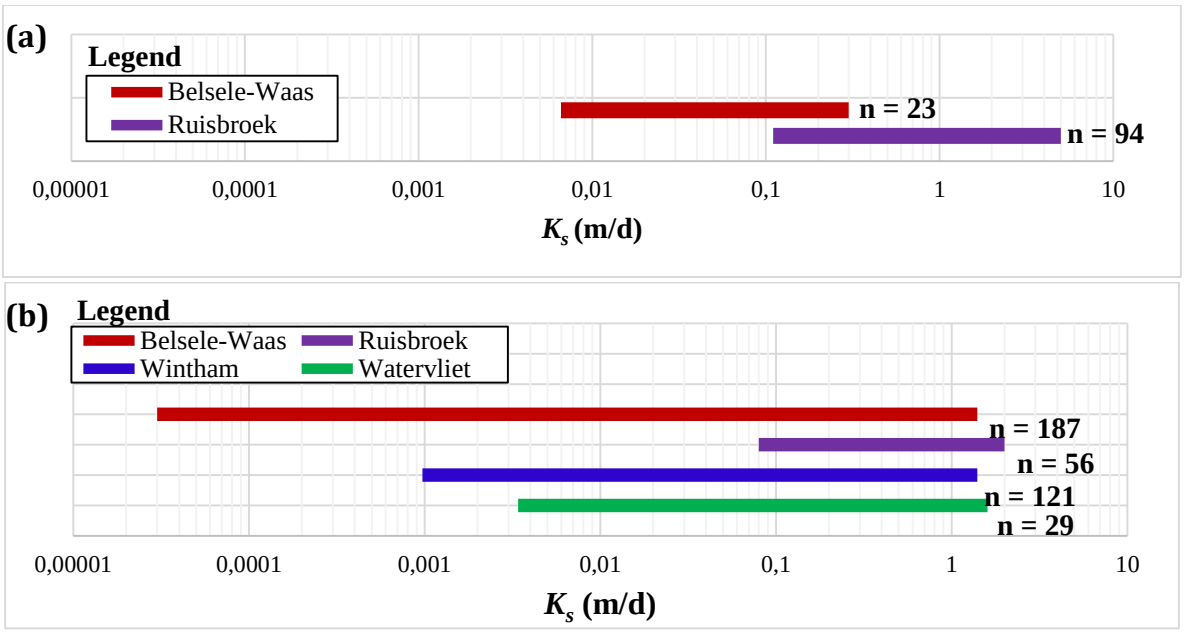

Figure 16. Saturated hydraulic conductivity (K_s) measurement ranges for the Oligocene members from (a) Herenthout-1, and (b) Essen-1 core slabs, together with the number of measurements (n).

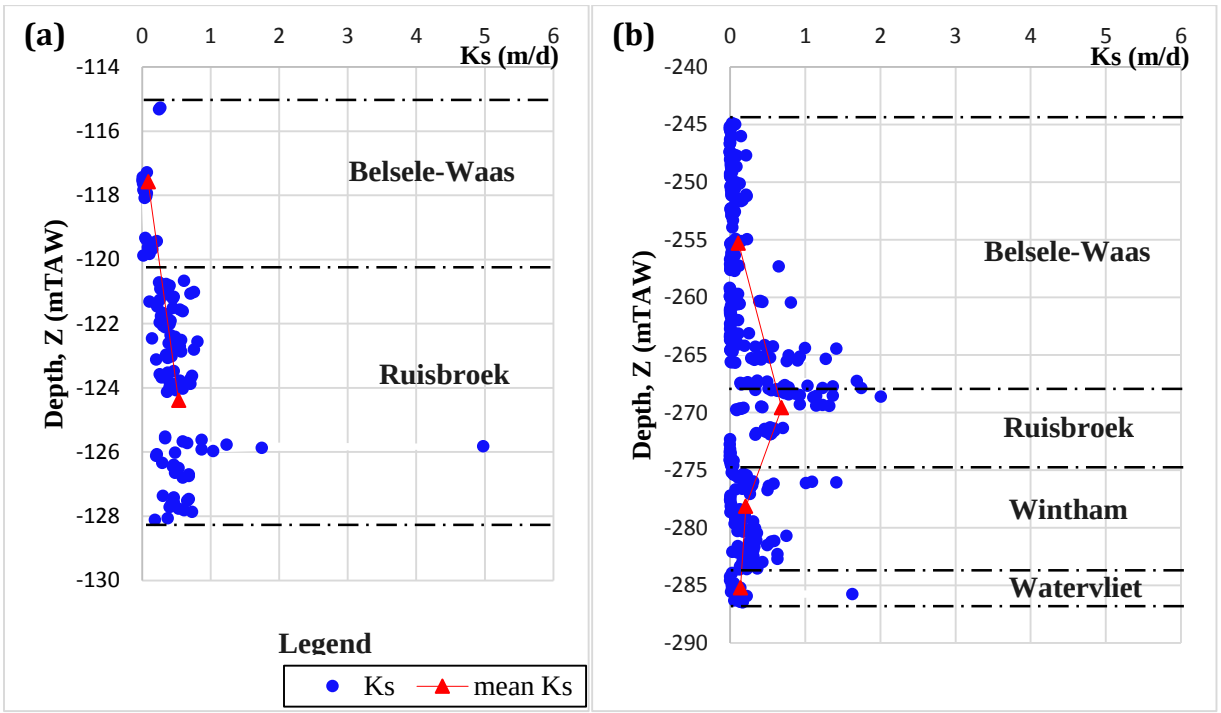

Figure 17. Overview of all raw K_s data for the members of Oligocene aquifer found in (a) Herenthout-1, and (b) Essen-1 core slabs.

4.2 Pumping test data

A total of 20 hydraulic conductivity data from pumping test performed in different locations of the Oligocene aquifer are available (Table 17 in Appendix 2). Data values for this aquifer range from 0.0026 m/d to 3.5 m/d with an average value of 0.45 m/d. This data set has a variance of 0.73 and a standard deviation of 0.86. For the Ledo-Paniselian-Brusselian aquifer, there a total of 47 hydraulic conductivity data from different locations (Table 18 in Appendix 2). Here the values range from 0.19 m/d to 75.0 m/d with an average value of 13.10 m/d, and have a variance and a standard deviation of 184.15 and 13.57 respectively.

By comparing these two aquifer systems, on average, the Ledo-Paniselian-Brusselian aquifer is approximately 30 times more permeable than the Oligocene aquifer. Since there is the higher conductivity for the LPB aquifer, people will preferably pump from this aquifer and not from the Oligocene aquifer. Also, because of the low transmissivity of the Oligocene aquifer, pumping effects in this aquifer are likely to remain local, while for the LPB aquifer (which has a higher transmissivity), there are regional effects of pumping. Therefore the LPB aquifer is regarded as the most important part in the current DAP model to be further investigated.

4.3 Comparison of air permeameter measurements versus pumping test data

The Oligocene aquifer is the only aquifer below the Boom Clay to be characterised by the air permeameter measurements in this study (section 3.1), for which a comparison with the pumping test data can be made. Values of air permeameter-based hydraulic conductivity estimates vary between 0.00003 m/d and 5.0 m/d with average values ranging from 0.09 m/d to 0.69 m/d (Table 8 in section 4.1). Pumping test values range from 0.0026 m/d to 3.5 m/d with the average value of 0.45 m/d (section 4.2). This shows that air permeameter measurements have a high variability and slightly higher values compared to the pumping test data. Small-scale measurements by the air permeameter display a lot of variability on the core samples due to sedimentary heterogeneity of the aquifer. This is not the case in pumping tests where there is a much larger measurement volume, showing less variability than in small-scale measurements hence giving values that are averages of permeabilities of the entire measured volume. Furthermore, the high values of air permeameter measurements may be due to the expansion of the sediment after being brought to

the surface. This is caused by the release of the in-situ stress, which causes the soil sample to swell and increases its hydraulic conductivity. Larger-scale measurements like pump tests also tend to give larger hydraulic conductivity values than smaller-scale measurements (Rogiers et al., 2010).

4.4 Up-scaled air permeameter-based hydraulic conductivity

The up-scaled air permeameter-based hydraulic conductivity values for the Oligocene aquifer (Table 9) range from 0.03 – 0.6 m/d for K_h, and from 0.003 – 0.4 m/d for K_v. Now the up-scaled values of K_h are within the range of pumping test data (0.0026 – 3.5 m/d) (section 4.2). It is probably a consequence of the sediment expansion in the core slabs and the large support volume of the pumping tests. That is, they match, but it might be a coincidence, and we should be careful in using the air permeameter data directly in the model. Since the up-scaled air permeameter-based K_h values are within the range of pumping test data, therefore pumping test data are used to set the reasonable lower and upper values of the hydraulic conductivity parameter for the Oligocene aquifer. A start value for this parameter is arbitrarily chosen to be 0.003.

Based on the up-scaled hydraulic conductivities, vertical anisotropy values for the Oligocene lie between 1.5 and 10.5 aquifer (Table 9). By assuming that $K_h - K_v$ ratio is minimally affected by the sediment expansion, the current assumption of isotropic hydraulic conductivities for this aquifer is updated to be anisotropic hydraulic conductivities. The range 1.5 – 10.5 is used to updates the current DAP model by setting the reasonable lower and upper values for the VANI_OB_sand parameter. A start value for this parameter was arbitrarily chosen as 2.

Table 9. Up-scaled air permeameter-based hydraulic conductivities for members of the Oligocene aquifer.

Member	**Borehole**	**K_h (m/d)**	**K_v (m/d)**	**K_h/K_v**	**K_{geom} (m/d)**		**Overall K_h/K_v**
					K_{h_geom}	**K_{v_geom}**	
Belsele-Waas	**Herenthout-1**	0.074	0.031	2.4	0.03	0.003	10
	Essen-1	0.011	0.0003	37			
Ruisbroek	**Herenthout-1**	0.534	0.403	1.3	0.6	0.4	1.5
	Essen-1	0.686	0.401	1.7			
Wintham	**Essen-1**	0.21	0.02	10.5			
Watervliet	**Essen-1**	0.14	0.03	4.7			

The up-scaled values support the depth-dependency relationships for hydraulic conductivities in the Zelzate formation based on the Ruisbroek, Wintham, and Watervliet members (Figure 18 & Figure 19). The relationships are approximated by using Equation 4.1 and Equation 4.2 for K_h and K_v respectively. There is a large uncertainty for these equations since they use only three points (Figure 18 & Figure 19). Therefore additional data should be gathered to improve the equations.

$$K_h = 8.08\ x\ 10^{10} e^{0.0953d} \tag{4.1}$$

$$K_v = 3.73\ x\ 10^{19} e^{0.172d} \tag{4.2}$$

where d is the depth below the reference surface expressed in metre, and K_h is in m/d.

Despite having low R^2 compared to the linear relationship, Equation 4.2 is considered because it is more realistic (Figure 19). The linear function is unrealistic because it contradicts the data value of 0.02 m/d at – 285 mTAW by giving a value of 0 m/d at – 283 mTAW. This is because K_v has a log-normal distribution. So it can be said that hydraulic conductivities in the Zelzate formation exponentially decrease with the increase in depth. In this case, the decrease of hydraulic conductivities with depth can mainly be due to differences in lithology.

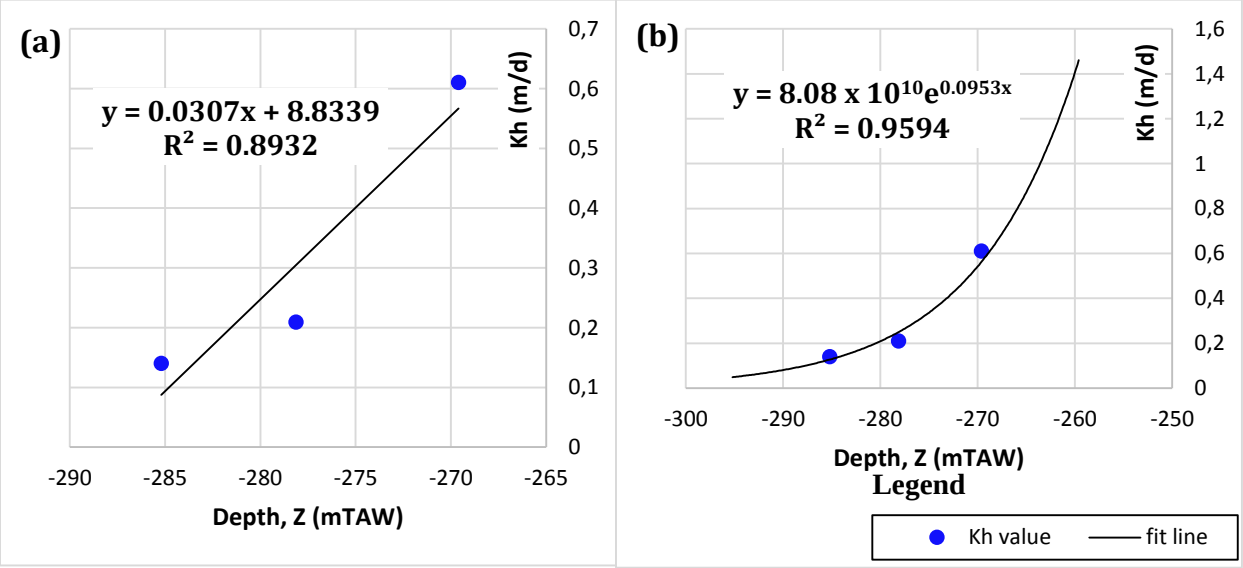

Figure 18. Relationships between K_h and depth for the Zelzate formation, (a) Linear relationship (b) Exponential relationship.

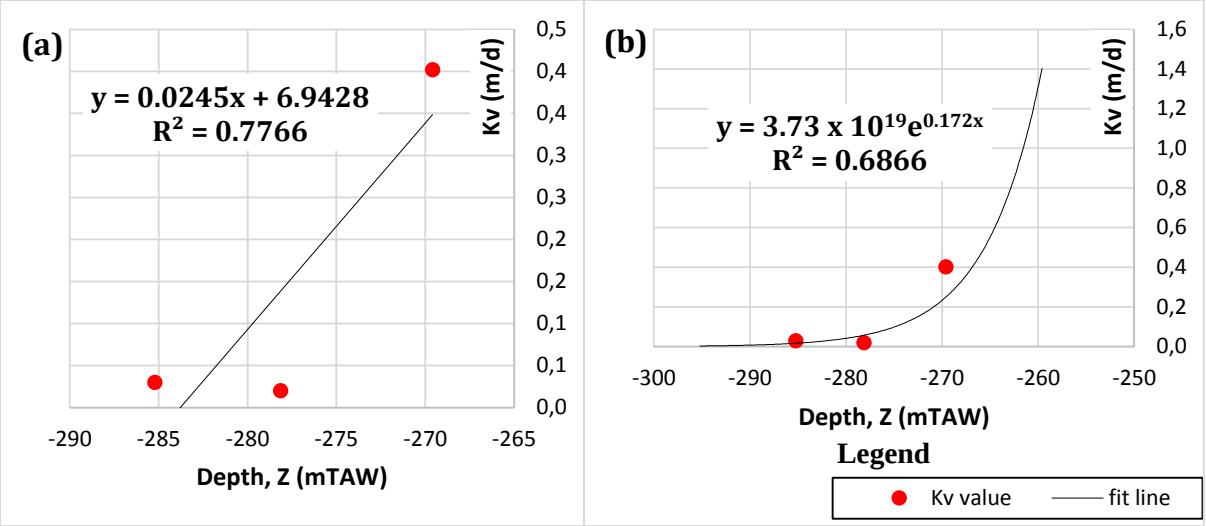

Figure 19. Relationships between K_v and depth for the Zelzate formation, (a) Linear relationship (b) Exponential relationship.

Based on the location of the Herenthout-1 and Essen-1, the up-scaled values of K_h and K_v for the Belsele-Waas member increase with the increase in depth (Figure 20). This member become more permeable as the depth increase due to changes in lithology. At a lower depth its main lithology is clay while at a higher depth the lithology is mainly composed of sand (section 3.1).

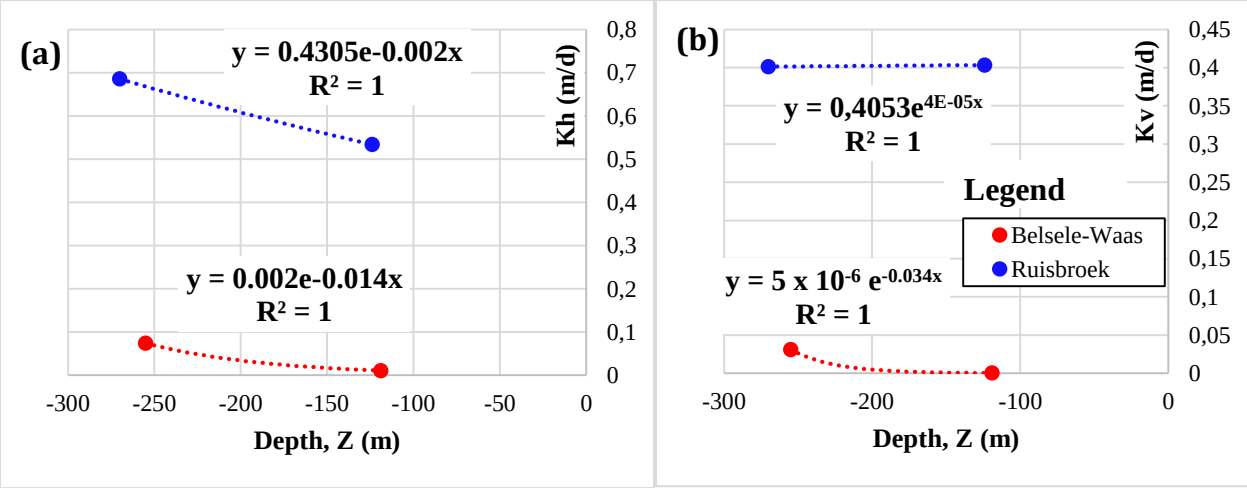

Figure 20. Analysis of hydraulic conductivity depth-dependency for the Belsele-Waas and the Ruisbroek member based on the location of the Herenthout-1 and Essen-1, (a) K_h depth-dependency analysis (b) K_v depth-dependency analysis.

Figure 20(a) shows that the up-scaled K_h values for the Ruisbroek member increase with the increase in depth. This is probably related to differences in the geological structure and/or changes in the lithology composition. Figure 20(b) shows that there is no a significant decrease in K_v due to compaction for the Ruisbroek member based on the up-scaled values from the Herenthout-1 and Essen-1. Here there is no significant changes probably due to its small thickness (5 m). There is a large uncertainty in these relations (Figure 20) since they use only two points, additional data should be gathered.

4.5 Interpolated maps of hydraulic conductivity

The interpolated maps showing the log K_h distribution in the LPB aquifer in reference to the DAP model extent are shown in Figure 21 and Figure 22. The maps were produced based on the log K_h values present in the multiplier files created for the model updates (section 3.4). The maps show that the values of log K_h are decreasing towards the north-east. The lower values of log K_h relate to the lower values of K_h, and vice versa. The K_h values are decreasing towards the north-east due to the increase in depth. This display the K_h depth-dependency (section 3.4), as the LPB aquifer dips towards the north-east (section 2.3). Figure 21 has lower values of log K_h towards the north-east compared to Figure 22. This implies that as the depth increase Equation 3.5 gives lower values of K_h compared to Equation 3.6. There are only small differences between the simple kriging and ordinary kriging versions.

The distribution of the log K_h values for the LPB aquifer in the current DAP model is shown in Figure 23. Results show that the current DAP model (Figure 23) has lower values of log K_h compared to the interpolated maps (Figure 21& Figure 22). This indicates that the current DAP model has lower values of calibrated K_h in the LPB aquifer compared to the initials K_h values used for the model updates. Differences in K_h distribution densities (Figure 24) is another reason for differences in K_h distribution between the interpolated maps and the current K_h distribution map.

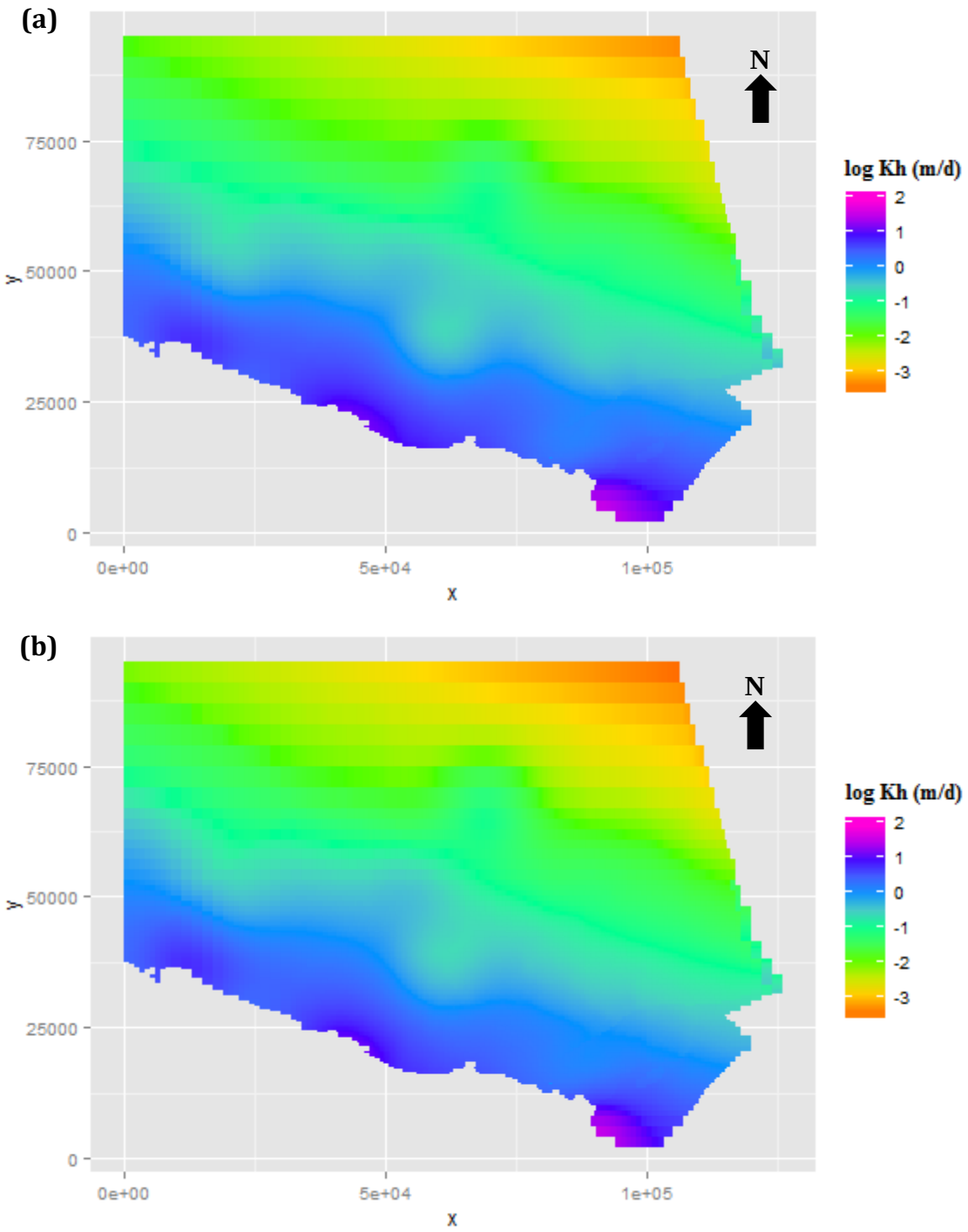

Figure 21. Interpolated maps of the log K_h in LPB aquifer using Equation 3.5 and, (a) Simple Kriging estimation (b) Ordinary Kriging estimation.

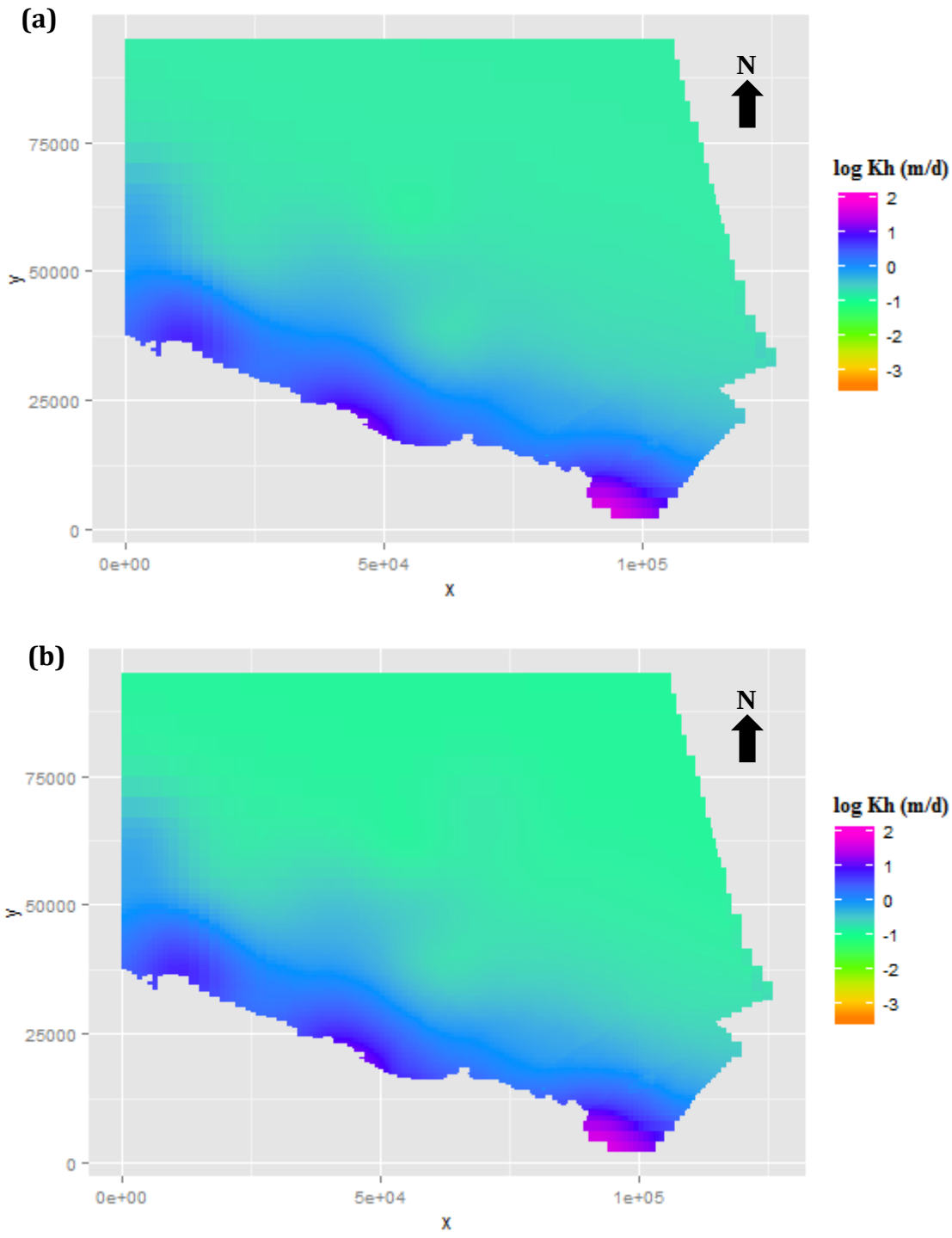

Figure 22. Interpolated maps of the log K_h in LPB aquifer using Equation 3.6 and, (a) Simple Kriging estimation (b) Ordinary Kriging estimation.

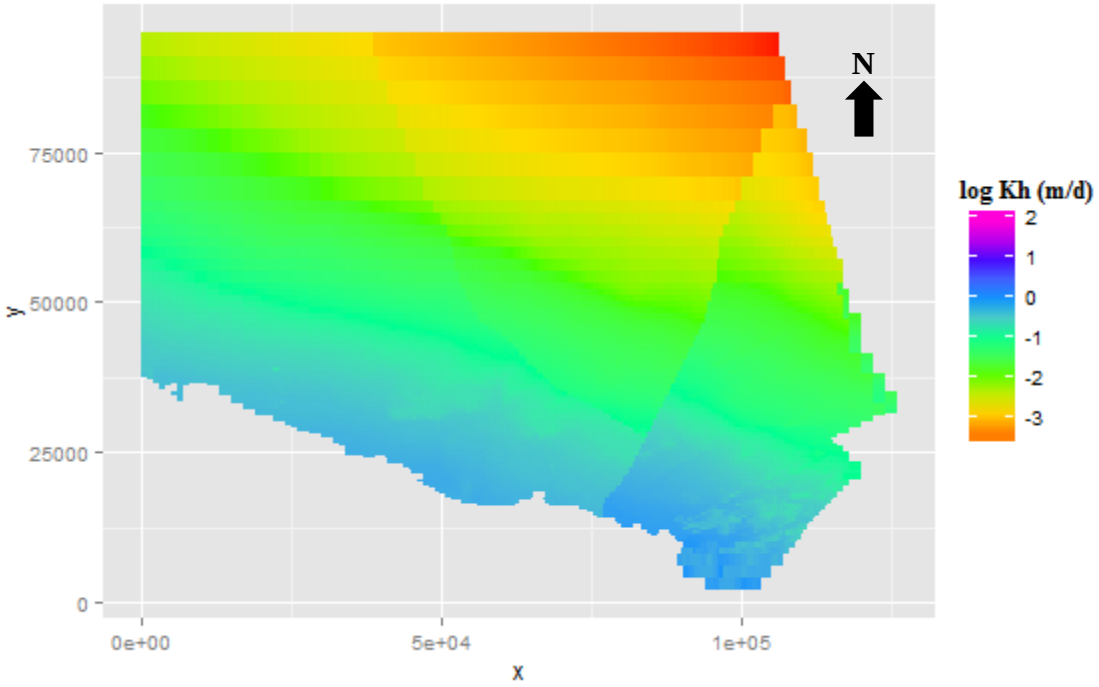

Figure 23. Map of the log K_h distribution in the LPB aquifer used in the current DAP model.

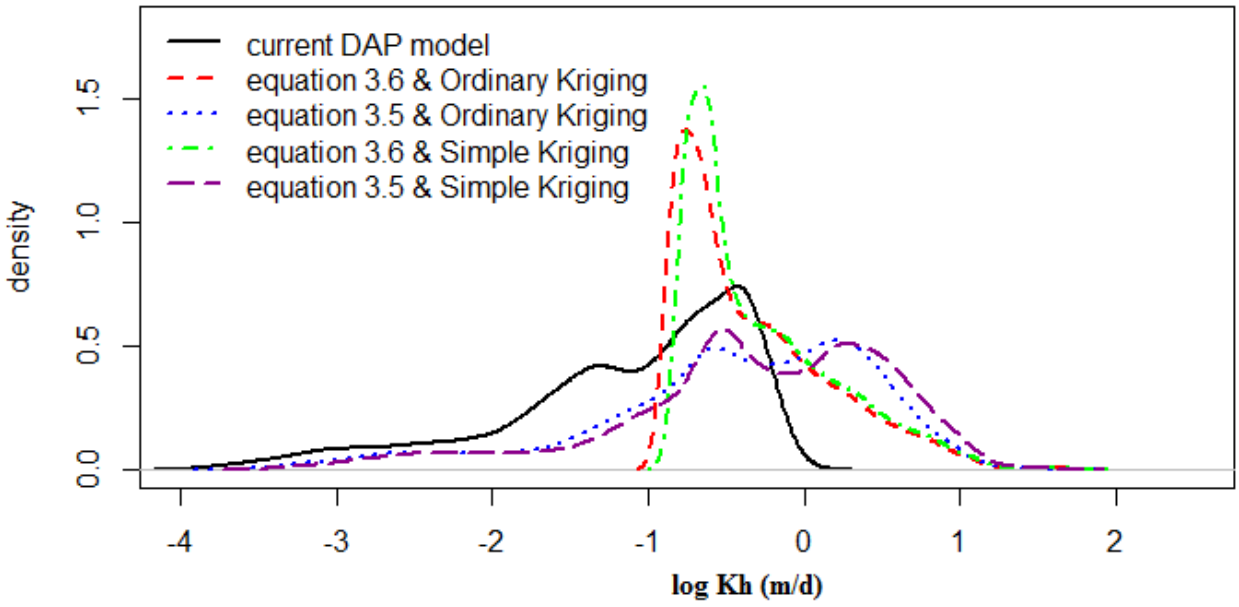

Figure 24. Density plots of the log K_h distribution in the LPB aquifer for different cases.

4.6 Updated DAP model

In the updated DAP model, four parameters of the current DAP model (HK1_LPB, HK2_LPB, HK3_LPB and KD_LPB) have been replaced by one new parameter (HK_LPB) (section 3.4). Also some of the parameter names of the current DAP model have been renamed. For clarity, all parameter names used in the updated DAP model are given in Table 10.

Table 10. Parameter name and corresponding hydrostratigraphic unit in the updated DAP model. New names are given in bold and their old names beside inside the square bracket [ ]. The explanation of the symbols used in the parameter name is given below the table.

Parameter name	**Hydrostratigraphic unit**	**Material type**
HK_mio	Miocene	sand
VANI_mio		
HK_BmBoer	Boom – Boeretang	clay
VANI_BmBoer		
HK_BmPuTe	Boom – Putte Boom – Terhagen	clay
VANI_BmPuTe		
KD_Bm		
HK_Bmbw	Boom – Belsele Waas / Bilzen – Berg	clay/sand
VANI_Bmbw		
HK_orup [HK_OB_sand]	Borgloon Ruisbroek Neerrepen Bassevelde Buisputten Onderdaele	sand
VANI_orup [VANI_OB_sand]		
KD_orup [KD_OB_sand]		
HK_UrAs [HK_OB_clay]	Watervliet Onderdijke Zomergem Ursel Asse	clay
VANI_UrAs [VANI_OB_clay]		
KD_Klei [KD_OB_clay]		
HK_LPB (scaling factor)	Ledo-Paniselian-Brusselian	sand
VANI_LPB		
SS_sand (scaling factor)	All sandy units	sand
SS_Klei	All clayey units	clay
Well_mlt	-	-

HK: hydraulic conductivity; VANI: vertical anisotropy; KD: depth-dependence parameter; SS: specific storage; WELL_MLT: well multiplication factor

Four alternatives of the updated DAP model were obtained based on the four multiplier files created in section 3.4. Table 11 shows start values and sum squared weighted residuals for the non-calibrated updated DAP model alternatives. The sum of squared weighted residuals for the current DAP model is 1392 m^2 (Table 5).

Table 11. Start values and sum squared weighted residuals for the non-calibrated updated DAP model alternatives [SK = Simple Kriging, OK = Ordinary Kriging].

Parameter name	**Starting value**
HK_mio [m/d]	1×10^{-5}
HK_UrAs [m/d]	4.52×10^{-6}
HK_LPB (scaling factor) [-]	1
HK_BmBoer [m/d]	3.6×10^{-6}
HK_BmPuTe [m/d]	1.6×10^{-6}
HK_Bmbw [m/d]	1.6×10^{-4}
HK_orup [m/d]	0.003
VANI_mio [-]	2×10^{-6}
VANI_BmPuTe [-]	2.9
VANI_BmBo [-]	6.4
VANI_Bmbw [-]	84
VANI_orup [-]	2
VANI_UrAs [-]	0.546
VANI_ LPB [-]	1
SS_Klei [1/m]	3.2×10^{-5}
SS_sand (scaling factor) [-]	0.03893
Well_mlt [-]	1
KD_Klei [1/m]	0.004488
KD_Bm [1/m]	1×10^{-4}
KD_orup [1/m]	0.001
Fit statistics	
Updated DAP model alterative	**Sum squared weighted residuals [m^2]**
Equation 3.5 and SK	55607
Equation 3.5 and OK	45055
Equation 3.6 and SK	31420
Equation 3.6 and OK	27686

Manually calibrated values for the updated DAP model alternatives are given in Table 12. The results show that the model using Equation 3.5 and ordinary kriging performs better than the rest. There is only small difference between the simple kriging and ordinary kriging versions when using Equation 3.6. The manually calibrated values (Table 12) were used as starting values for the automated calibration of each model alternative.

Table 12. Manually calibrated values for the updated DAP model alternatives [SK = Simple Kriging, OK = Ordinary Kriging].

Parameter name	**Equation 3.5 and SK value**	**Equation 3.5 and OK value**	**Equation 3.6 and SK value**	**Equation 3.6 and OK value**
HK_mio [m/d]	1×10^{-5}	1×10^{-5}	1.5×10^{-4}	1.5×10^{-4}
HK_UrAs [m/d]	4.52×10^{-6}	4.52×10^{-6}	4.7×10^{-6}	4.7×10^{-6}
HK_LPB (scaling factor) [-]	0.1577	0.1577	0.24	0.24
HK_BmBoer [m/d]	4×10^{-6}	4×10^{-6}	1.4×10^{-2}	1.4×10^{-2}
HK_BmPuTe [m/d]	1.6×10^{-6}	1.6×10^{-6}	1.6×10^{-6}	1.6×10^{-6}
HK_Bmbw [m/d]	5×10^{-5}	5×10^{-5}	5×10^{-5}	5×10^{-5}
HK_orup [m/d]	0.003	0.003	0.003	0.003
VANI_mio [-]	1×10^{-6}	1×10^{-6}	1×10^{-6}	1×10^{-6}
VANI_BmPuTe [-]	2.2	2.2	2.2	2.2
VANI_BmBo [-]	1.5	1.5	1.5	1.5
VANI_Bmbw [-]	110	110	110	110
VANI_orup [-]	1.5	1.5	1.5	1.5
VANI_UrAs [-]	1	1	1	1
VANI_ LPB [-]	1	1	1	1
SS_Klei [1/m]	3×10^{-5}	3×10^{-5}	3×10^{-5}	3×10^{-5}
SS_sand (scaling factor) [-]	0.2	0.2	0.2	0.2
Well_mlt [-]	1	1	1	1
KD_Klei [1/m]	0.0045	0.0045	0.0045	0.0045
KD_Bm [1/m]	5×10^{-5}	5×10^{-5}	5×10^{-5}	5×10^{-5}
KD_orup [1/m]	8.08×10^{-4}	8.08×10^{-4}	8×10^{-4}	8×10^{-4}
Sum squared weighted residuals [m^2]	4041	2799	4972	5660

Figure 25 shows the composite scaled sensitivities for the starting parameter values of the updated DAP model using Equation 3.5 and ordinary kriging. Figure 25 shows that the most sensitive parameters are: WELL_MLT, KD_Klei, HK_LPB, SS_Klei, VANI_UrAs and HK_UrAs. The least sensitive ones are: VANI_Mio, VANI_LPB, HK_Mio, KD_Bm, VANI_orup, VANI_BmBo, HK_BmBoer and KD_orup. This shows that the groundwater levels at the piezometers located in the aquifers below the Boom Clay are mainly influenced by the hydraulic conductivity of the LPB aquifer and the hydraulic conductivity of the clayey part of the Oligocene and Bartoon Formations. To solve the problem of parameter insensitivity, all least and low sensitive parameters were fixed during the automatic calibration process.

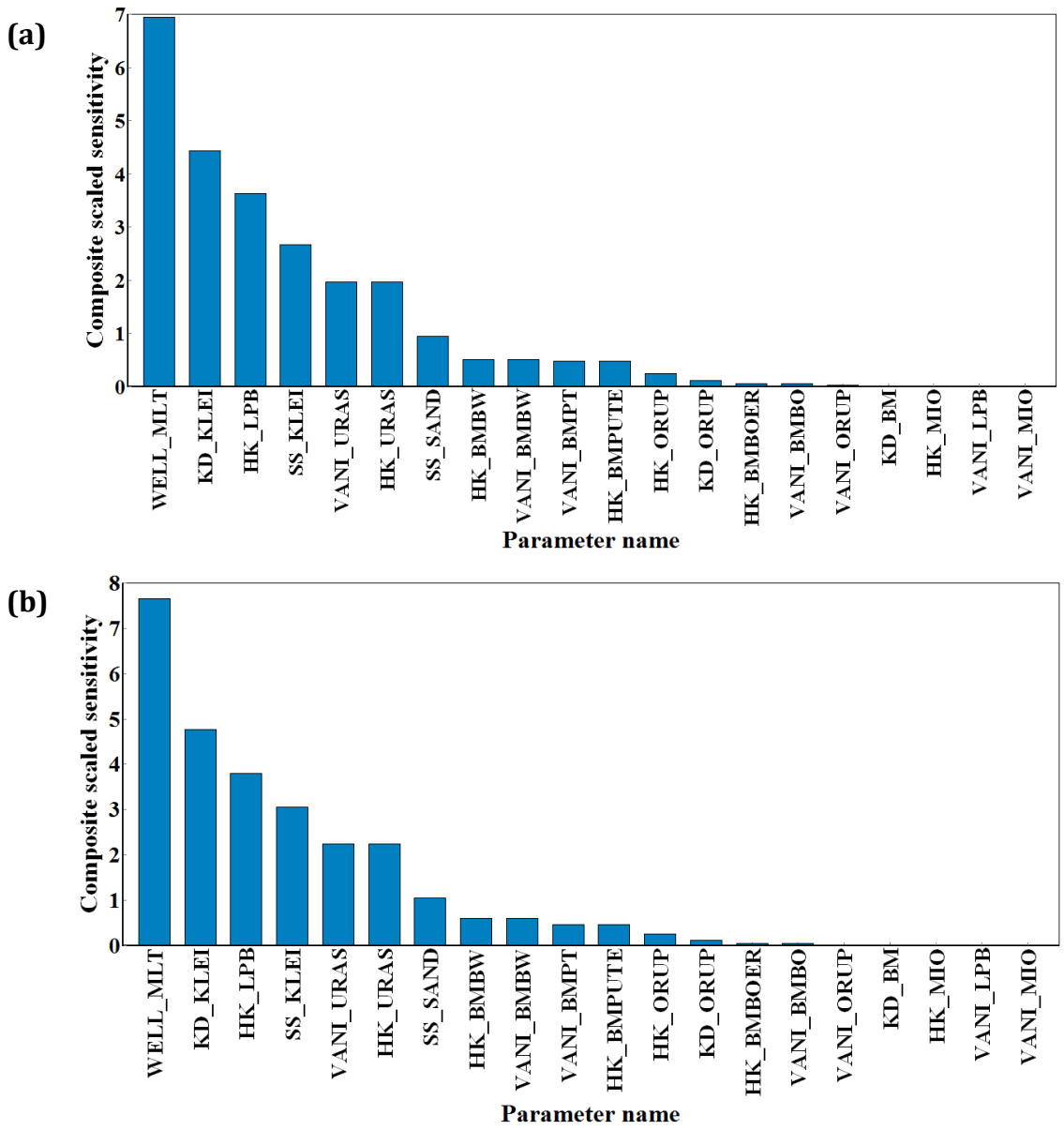

Figure 25. Composite scaled sensitivities of the updated DAP model starting parameters using Equation 3.5 and, (a) Simple Kriging estimation (b) Ordinary Kriging estimation.

Table 13 shows parameter correlation matrix for parameter pairs whose correlation are greater than 0.90 for the updated DAP model using Equation 3.5 and ordinary kriging estimation. The parameter correlation matrix indicates the level of correlation between parameters. Parameter pairs with high correlations are indicative of parameter values that cannot be uniquely estimated with the observations used in the regression (Hill, 1998). To solve the problem of high

correlation between the parameters in Table 13, the WELL_MLT parameter was excluded from the automatic calibration process by being fixed.

Table 13. Parameter correlation matrix showing parameter pairs whose correlation values are greater than 0.90 for starting values of the updated DAP model using Equation 3.5 and ordinary kriging.

	HK_LPB	HK_orup	SS_Klei	SS_sand	HK_BmBoer	HK_BmPuTe	HK_Bmbw	WELL_MLT	VANI_BmBo	VANI_BmPuTe	VANI_Bmbw	VANI_orup	VANI_LPB
HK_LPB	1	1	1	1	.	.	.	1	.	.	.	.	.
HK_orup		1	1	1	.	.	.	1	.	.	.	.	.
SS_Klei			1	1	.	.	.	1	.	.	.	.	.
SS_sand				1	.	.	.	1	.	.	.	.	.
HK_BmBoer					1	.	.	.	0.99	.	.	.	.
HK_BmPuTe						1	.	.	.	0.98	.	.	.
HK_Bmbw							1	.	.	.	0.92	.	.
WELL_MLT								1	.	.	.	.	.
VANI_BmBo									1	.	.	.	.
VANI_BmPuTe										1	.	.	.
VANI_Bmbw											1	.	-0.89
VANI_orup												1	.
VANI_LPB													1

Table 14 shows automatically calibrated values for the updated DAP model alternatives. Results show that models using Equation 3.5 perform better than those using Equation 3.6. There are only small differences between the simple kriging and ordinary kriging versions for the same equation.

The updated DAP model by using Equation 3.5 and simple kriging estimation gives a lowest sum of squared weighted residuals of 1685 m^2 (Table 14). The current DAP model has sum of squared weighted residuals of 1392 m^2 (Table 5). The updated DAP model performs slightly worse than the current DAP model, but similar.

Table 14. Automatically calibrated values for the updated DAP model alternatives [SK = Simple Kriging, OK = Ordinary Kriging].

Parameter name	**Equation 3.5 and SK value**	**Equation 3.5 and OK value**	**Equation 3.6 and SK value**	**Equation 3.6 and OK value**
HK_mio [m/d]	5×10^{-4}	1.1×10^{-5}	1.5×10^{-4}	1×10^{-5}
HK_UrAs [m/d]	5.325×10^{-6}	4.476×10^{-6}	8.278×10^{-6}	3.969×10^{-6}
HK_LPB (scaling factor) [-]	0.1317	0.163	0.2248	0.2736
HK_BmBoer [m/d]	1.5×10^{-6}	3.184×10^{-6}	1.4×10^{-2}	4×10^{-6}
HK_BmPuTe [m/d]	2.902×10^{-6}	2.117×10^{-6}	1.6×10^{-6}	1.6×10^{-6}
HK_Bmbw [m/d]	6.999×10^{-5}	8.522×10^{-5}	5×10^{-5}	5×10^{-5}
HK_orup [m/d]	4.561×10^{-3}	6.345×10^{-3}	5.624×10^{-3}	8.624×10^{-3}
VANI_mio [-]	2.9×10^{-6}	1×10^{-6}	1×10^{-6}	1×10^{-6}
VANI_BmPuTe [-]	2.193	1.798	2.2	2.2
VANI_BmBo [-]	2.276	1.5	1.5	1.5
VANI_Bmbw [-]	87.64	99.98	29.53	110
VANI_orup [-]	1.5	1.5	1.5	1.5
VANI_UrAs [-]	1	1	1	1
VANI_ LPB [-]	1.9	1	1	1
SS_Klei [1/m]	2.887×10^{-5}	3.332×10^{-5}	3×10^{-5}	1.292×10^{-5}
SS_sand (scaling factor) [-]	0.1336	0.1454	0.2	0.8191
Well_mlt [-]	1	1	1	1
KD_Klei [1/m]	4.214×10^{-3}	4.51×10^{-3}	4.5×10^{-3}	4.282×10^{-3}
KD_Bm [1/m]	4.55×10^{-4}	5.464×10^{-4}	5×10^{-5}	5×10^{-5}
KD_orup [1/m]	6.217×10^{-4}	1×10^{-3}	7.798×10^{-4}	1×10^{-3}
Fit statistics				
Sum squared weighted residuals [m^2]	1685	1786	3389	3300
Mean residual (ME) [m]	0.023	0.29	1.11	0.571
R^2 (measured vs. simulated)	0.95	0.97	0.84	0.83

The composite scaled sensitivities for the automatically calibrated parameter values (Figure 26) provide a similar picture as the css values of the initial parameters. Results still show that the groundwater levels at the piezometers located in the aquifers below the Boom Clay are mainly influenced by the hydraulic conductivity of the LPB aquifer and the hydraulic conductivity of the clayey part of the Oligocene and Bartoon Formations.

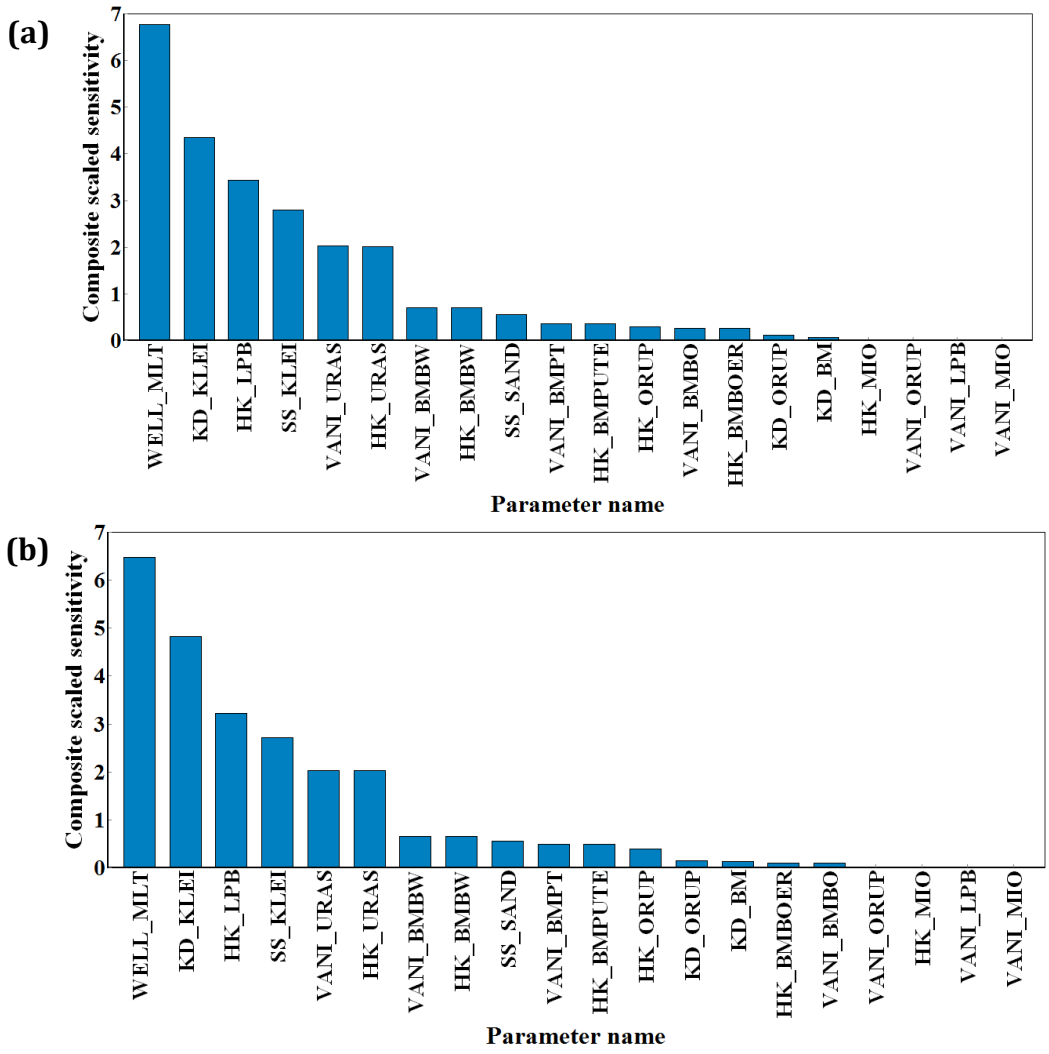

Figure 26. Composite scaled sensitivities of the automatically calibrated parameters of the updated DAP model using Equation 3.5 and, (a) Simple Kriging estimation (b) Ordinary Kriging estimation.

The plot of observed values against simulated groundwater levels (Figure 27) shows that along the simulated value axis the highest weighted residuals are found around head values of -10 m. Here most values are from SCK_18 piezometer and few from VMM_80208 piezometer. The SCK_18 piezometer series mainly overestimate the heads by about 1 – 7.8 m. This is due to its proximity to a pumping well with a large uncertainty on the well data. The higher residuals are also found around head values of 0 m and 13m for the SCK_51 and SCK_20d piezometer respectively. The heads are underestimated by about 4 – 5 m and 3.5 m at the SCK_51 and SCK_20d piezometer respectively.

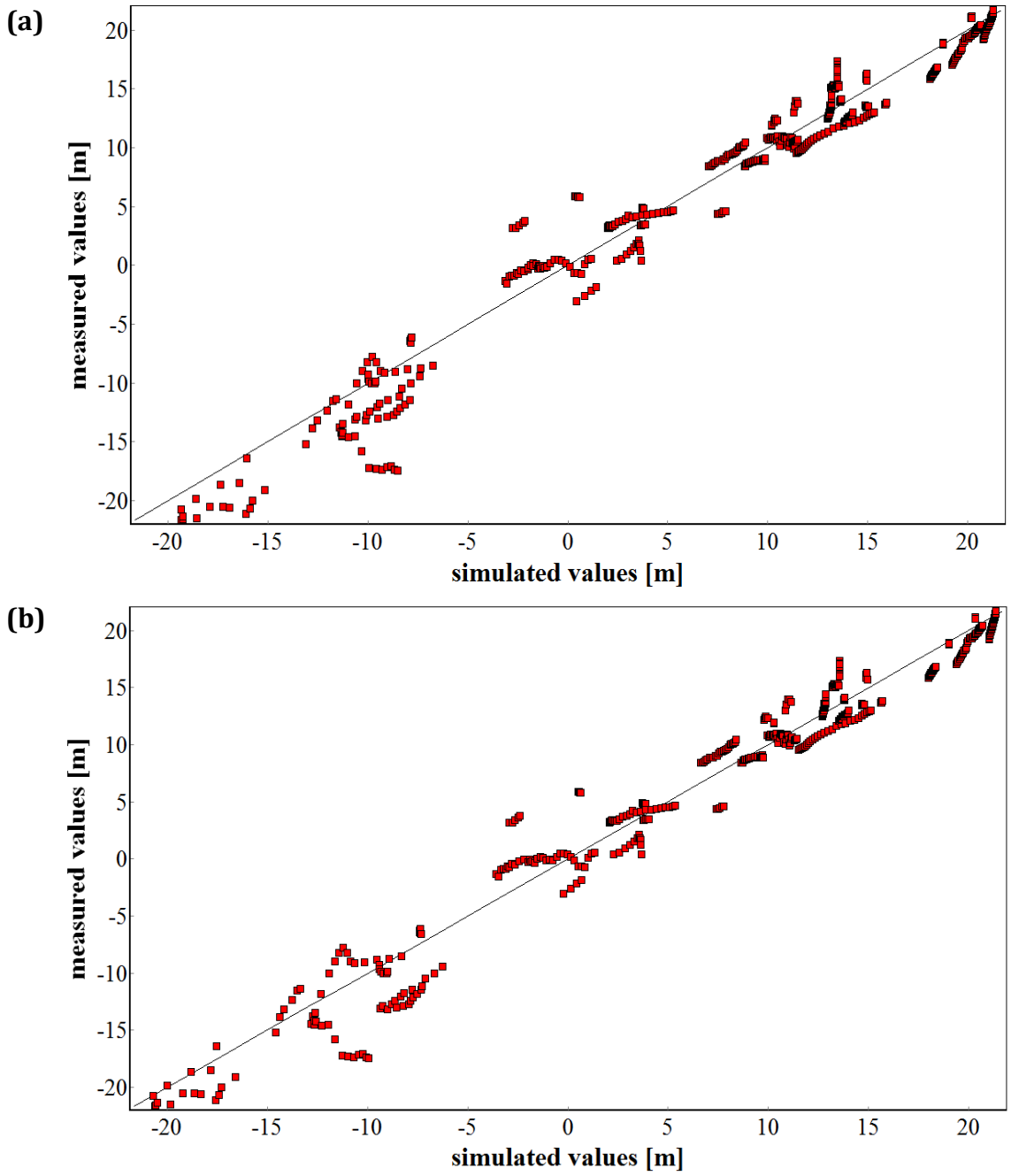

Figure 27. Measured versus simulated groundwater level values using the automatically estimated parameters of the updated DAP model using Equation 3.5 and , (a) Simple Kriging estimation (b) Ordinary Kriging estimation.

The analysis on the dimensionless scaled sensitivities (dss) was done on the SCK_51, SCK_18 and SCK_20d piezometers due to their higher weighted residuals. Figure 28 shows the averaged values of dss for the calibrated parameters of the updated DAP model using Equation 3.5 and

ordinary kriging method. A positive value of the dss means that an increase in parameter value will invoke an increase in the simulated heads and vice versa. In both cases, greater absolute values are associated with greater importance. The results show that the WELL_MLT, HK_LPB and SS_Klei are the most important parameters to the simulated heads at the SCK_51 and SCK_18 piezometers. For the SCK_20d piezometer the model parameters are less important to the simulated heads.

For the SCK_51 and SCK_18 piezometers the dss are all positive for the HK_LPB and SS_Klei parameters and all negative for the WELL_MLT parameter. This means that an increase in HK_LPB and/or SS_Klei will invoke an increase in the simulated heads. The increase in the simulated heads indicates a slower response to the pumping. When the SS_Klei increases more groundwater can be stored in the aquifer causing a rise in the piezometric heads. An increase in WELL_MLT will result in lower simulated heads.

Despite the heads being underestimated by about 3.5 m at the SCK_20d piezometer, the model parameters are less important to the simulated heads. This indicates that there are still conceptual issues to resolve in the Oligocene aquifer as observed in the current DAP model (Vandersteen et al., 2012) and in the previous version of the model (Gedeon and Wemaere, 2009).

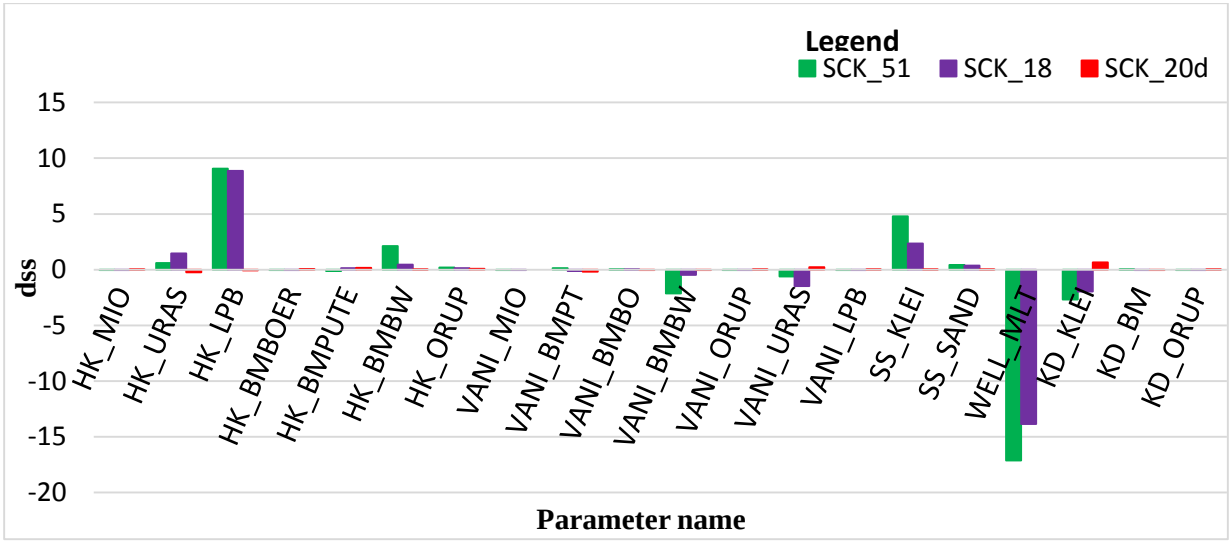

Figure 28. Averaged values of dimensionless scaled sensitivities for the calibrated parameters of the updated DAP model using Equation 3.5 and ordinary kriging method on the SCK_51, SCK_18 and SCK_20d piezometers.

5 Conclusions and Recommendations

The assumption of depth-dependency for the hydraulic conductivity in the Oligocene aquifer has been confirmed by air permeameter-based K_s data, and the mathematical equations for Kh and Kv depth-dependency for the Zelzate formation have been established based on the upscaled values of the Ruisbroek, Wintham, and Watervliet members. Based on the up-scaled air permeameter-based hydraulic conductivities for the Oligocene aquifer, the vertical anisotropy values for this aquifer are greater than 1. This updates the current assumption of isotropic hydraulic conductivities to anisotropic hydraulic conductivities for this aquifer.

Pumping test data show that on average the Ledo-Paniselian-Brusselian aquifer is approximately 30 times more permeable than the Oligocene aquifer. The average horizontal hydraulic conductivity value for this aquifer is 13.10 m/d.

The updated DAP model still underestimates the heads around the SCK_20d and SCK_51 piezometers. Moreover the current DAP model overestimates the heads around the SCK_18 piezometer. To solve this problem in-depth investigation of the area surrounding these piezometers should be performed.

Integration of the air permeameter-based data from the Oligocene and Bartoon Formations system and pumping test data from the Oligocene and LPB aquifers into the current DAP model have increased the model confidence as the model parameterization in the updated DAP model is more data-based on realistic. However, in-depth further investigations on the LPB aquifer and the clayey part of the Oligocene and Bartoon Formations system is of significance importance for continuing improving the updated DAP model performance.

The similar performance of the updated and current DAP models indicates that accounting for available hydraulic conductivity data in the large-scale model is possible. Therefore, this should be performed as much as possible for the other aquifer units as well, because the conceptual model uncertainty decreases by incorporating more data in the model.

As accounting for hydraulic conductivity data is not improving the model considerably, we should start looking at the uncertainty of the pumping data, and accounting for that uncertainty in the model. Adjusting the well multiplication factor would be a first step. As depth-dependency is clearly present for some of the units, it should be considered for all units in the model.

6 References

Anderman, E.R. & Hill, M.C., 2000. MODFLOW-2000, the U.S. Geological Survey modular ground-water model – Documentation of the Hydrogeologic-Unit Flow (HUF) package. U.S. Geological Survey Open-File Report 00-342, 89p.

Anderman, E.R. & Hill, M.C., 2003. MODFLOW-2000, the U.S. Geological Survey modular ground-water model – Three additions to the Hydrogeologic-Unit Flow (HUF) Package – Alternative storage for the uppermost active cells (SYTP parameter type), flows in hydrogeologic units, and the hydraulic–conductivity depth-dependence (KDEP) capability: U.S. Geological Survey Open-File Report 03-347, 36p.

Banta, E.R., 2011, ModelMate; A graphical user interface for model analysis: U.S. Geological Survey Techniques and Methods, book 6, chapter E4, 31 p.

Deutsch, C.V. & Journel, A.G., 1998. GSLIB Geostatistical Software Library and User's Guide. Oxford University Press, New York.

El-Rawy, M., 2013. Calibration of Hydraulic Conductivities in Groundwater Flow Models using the Double Constraint Method and the Kalman Filter. PhD Thesis, Vrije Universiteit Brussel. Retrieved from http://twws6.vub.ac.be/hydr/download/MustafaElRawy.pdf on 22-10-2013

Ely, D.M., 2006. Analysis of Sensitivity of Simulated Recharge to Selected Parameters for Seven Watersheds Modeled Using the Precipitation-Runoff Modeling System. U.S. Geological Survey Scientific Investigations Report 2006-5041, 21 p.

Gedeon, M. & Wemaere, I., 2003. Updated regional hydrogeological model for the Mol site (the north-eastern Belgium model). SCK•CEN-R-3751.

Gedeon M. & Wemaere I., 2009. Transient model of the confined aquifers located below the Boom Clay. Regional Hydrogeological Model for the Mol Site. SCK•CEN-ER-72, 87p.

Goggin, D.J., Chandles, M.A., Kocurec, G. & Lake, L.W., 1988. Patterns of permeability in eolian deposits: Page Sandstone (Jurassic), NE Arizona. SPE Formation Evaluation, 3, 297-306.

Harbaugh, A.W., 2005. MODFLOW-2005, the U.S. Geological Survey modular ground-water model – the Ground-Water Flow Process: U.S. Geological Survey Techniques and Methods 6-A16.

Harding ESE Inc., 2001. Final Report. Hydrogeologic Investigation of the Salinas Valley Basin in the Vicinity of Fort Ord and Marina Salinas Valley, California. Retrieved from http://www.mcwra.co.monterey.ca.us/Agency_data/Hydrogeologic%20Reports/Salinas%20Basin%20Ft%20Ord%20Marina/SV_BASIN_FT_ORD_MARIN.HTM on 26-4-2014.

Hill, M.C., 1998. Methods and guidelines for effective model calibration. U.S. Geological Survey. Water-resources investigations report 98-4005, Denver, Colorado.

Huysmans, M. & Dassargues, A., 2009. Application of multiple-point geostatistics on modeling groundwater flow and transport in a cross-bedded aquifer (Belgium). Hydrogeology Journal, 17(8), 1901-1911. doi: 10.1007/s10040-009-0495-2

Huysmans, M., Peeters, L., Moermans, G. & Dassargues, A., 2008. Relating small-scale sedimentary structures and permeability in a cross-bedded aquifer. Journal of Hydrology, 361 (1-2), 41-51. doi: 10.1016/j.jhydrol.2008.07.047

Jensen, J.L., Glasbey, C.A. & Corbett, P.W.M., 1994. On the interaction of geology, measurement, and statistical-analysis of small-scale permeability measurements. Terra Nova, 6(4), 397–403.

Labat, S., 2011. Overview and analysis of 30 years piezometric observations in north-east Belgium. Mol, Belgium: SCK•CEN -ER-163, 69 p.

Loll, P., Moldrup, P., Schjønning, P. & Riley, H., 1999. Predicting saturated hydraulic conductivity from air permeability: Application in stochastic water infiltration modeling. Water Resources Research, 35(8), 2387–2400.

Meyus, Y., Batelaan, O. & De Smedt, F., 2000, Concept Vlaams Grondwater Model (VGM), technisch concept van het VGM, Deelrapport I: Hydrogeologische Codering van de ondergrond van Vlaanderen (HCOV)

Mukherjee, S., 2011. Hydrostratigraphy. YES Bulletin, Vol. 1, 2011. ISSN 2222-7458.

New England Research & Vindum Engineering, 2013. TinyPerm II Portable Air Permeameter, User's Manual. Retrieved from http://www.vindum.com/TinyPermManual.pdf on 5-10-2013.

Poeter, E.P., Hill, M.C., Banta, E.R., Mehl, S. & Christensen, S., 2005. UCODE_2005 and six other computer codes for universal sensitivity analysis, calibration and uncertainty evaluation: U.S. Geological Survey Techniques and Methods, book. 6, chapter A11, 283 p.

Possemiers, M., Huysmans, M., Peeters L., Batelaan, O. & Dassargues, A., 2012. Relationship between sedimentary features and permeability at different scales in the Brussels Sands. Geologica Belgica, 15(3), 156-164**.**

Potums, L., 2014. Gedetailleerde karakterisatie van boorkernen uit de diepe aquifers rond de Boomse klei, met behulp van een luchtpermeameter. Bachelor thesis. KU Leuven

Remy, N., Boucher, A. & Wu, J., 2009. Applied Geostatistics with SGeMS. A User's Guide. Cambridge, Cambridge University Press, 284 p.

Rogiers, B., Beerten, K., Smeekens, T. & Mallants, D., 2011. Air permeability measurements on Neogene and Quaternary sediments from the Campine area: using outcrop analogues for determining hydrodynamic aquifer properties. Mol, Belgium: SCK•CEN ER-177, 23 p.

Rogiers, B., Beerten, K., Smeekens, T., Mallants, D., Gedeon, M., Huysmans, M., Batelaan, O. & Dassargues, A., 2013a. Derivation of flow and transport parameters from outcropping sediments of the Neogene aquifer, Belgium. Geologica Belgica, 16 (3), 129-147.

Rogiers, B., Beerten, K., Smeekens, T., Mallants, D., Gedeon, M., Huysmans, M., Batelaan, O. & Dassargues, A., 2013b. The usefulness of outcrop analogue air permeameter measurements for analyzing aquifer heterogeneity: quantifying outcrop hydraulic conductivity and its spatial variability. Hydrological Processes. doi: 10.1002/hyp.10007

Rogiers, B., Beerten, K., Smeekens, T., Mallants, D., Gedeon, M., Huysmans, M., Batelaan, O. & Dassargues, A., 2013c. The usefulness of outcrop analogue air permeameter measurements for analyzing aquifer heterogeneity: testing outcrop hydrogeological parameters with independent borehole data. Hydrology and Earth System Sciences. doi: 10.5194/hess-17-5155-2013

Rogiers, B., Schiltz, M., Beerten, K., Gedeon, M., Mallants, D., Batelaan, O., Dassargues, A. & Huysmans, M., 2010. Groundwater model parameter identification using a combination of cone-penetration tests and borehole data. IAHR international groundwater symposium (p.19).Valencia.

Rogiers, B., Winters, P., Huysmans, M., Beerten, K., Mallants, D., Gedeon, M., Batelaan, O. & Dassargues, A., 2014. High resolution hydraulic conductivity logging of borehole cores using air permeability measurements. Hydrogeology Journal, accepted.

Sakata, S., Ashida, F. & Zako, M., 2004. An efficient algorithm for Kriging approximation and optimization with large-scale sampling data. Computer Methods in Applied Mechanics and Engineering. 193 (3-5), 385-404. doi: 10.1016/j.cma.2003.10.006

Van der Gun, J., 1979. Schatting van de elastische bergingscoëfficiënt van zandige watervoerende paketten. Jaarverslag 1979, TNO dienst waterverkenning, Delft, 51-61.

Vandersteen, K. & Gedeon, M., 2013. A hydrogeological study of the confined aquifers below the Boom Clay in NE-Belgium: combining a piezometric analysis with groundwater modelling. Geophysical Research Abstract. Vol. 15, EGU General Assembly 2013, Vienna, 7-12 April 2013.

Vandersteen, K., Gedeon, M. & Beerten, K., 2014. A synthesis of hydraulic conductivity measurements of the subsurface in Northeastern Belgium. Geologica Belgica, 17 (3-4), 196-210

Vandersteen, K., Gedeon, M. & Leterme, B., 2013. Hydrogeology of North-East Belgium. Status report 2012. Mol, Belgium: SCK•CEN ER-236, 209 p.

Vandersteen, K., Gedeon, M. & Rogiers, B., 2012. Transient model of the confined aquifers below the Boom Clay: 2011 update. Mol, Belgium: SCK•CEN ER-199, 132 p.

Wen, X.-H. & Gómez-Hernández, J.J., 1996. Upscaling hydraulic conductivities in heterogeneous media: an overview. Journal of Hydrology, 183, ix-xxxii. doi: 10.1016/S0022-1694(96)80030-8

Winters, P., 2012. Haalbaarheidsstudie voor de gedetailleerde opmeting van de hydraulische conductiviteit op boorkernen, met behulp van een luchtpermeameter. Bachelor thesis. KU Leuven.

7 Appendices

7.1 Appendix 1

Table 15. Air permeameter measurements from Essen-1 core slabs.

Core #	distance from core bottom (m)	Depth, Z (m)	Tinyperm value	Hydrostratigraphic unit	Operator	k_a (mD)	K_s (m/d)	K_s (m/s)
116	0.75	-244.9	10.71	Boom (Belsele-Waas)	George	491	0.0296	3.42E-07
116	0.65	-245	10.46	Boom (Belsele-Waas)	George	976	0.0707	8.18E-07
116	0.6	-245.05	10.55	Boom (Belsele-Waas)	George	762	0.0517	5.98E-07
116	0.45	-245.2	11.63	Boom (Belsele-Waas)	George	39	0.0012	1.38E-08
116	0.25	-245.4	12.06	Boom (Belsele-Waas)	George	12	0.0003	3.09E-09
116	0.2	-245.45	11.2	Boom (Belsele-Waas)	George	128	0.0054	6.20E-08
117	0.05	-245.6	11.14	Boom (Belsele-Waas)	George	151	0.0066	7.64E-08
117	0.75	-245.99	10.79	Boom (Belsele-Waas)	George	394	0.0224	2.59E-07
117	0.7	-246.04	10.25	Boom (Belsele-Waas)	George	1737	0.1471	1.70E-06
117	0.55	-246.19	11	Boom (Belsele-Waas)	George	222	0.0108	1.24E-07
117	0.4	-246.34	11.16	Boom (Belsele-Waas)	George	143	0.0062	7.13E-08
117	0.15	-246.59	11.4	Boom (Belsele-Waas)	George	74	0.0027	3.09E-08
117	0.1	-246.64	11.29	Boom (Belsele-Waas)	George	100	0.0039	4.53E-08
117	0.05	-246.69	11.53	Boom (Belsele-Waas)	George	52	0.0017	1.96E-08
118	0.45	-247.33	12.7	Boom (Belsele-Waas)	George	2	0.0000	3.32E-10
118	0.4	-247.38	12.1	Boom (Belsele-Waas)	George	11	0.0002	2.69E-09
118	0.35	-247.43	11.64	Boom (Belsele-Waas)	George	38	0.0012	1.34E-08
118	0.25	-247.53	11.4	Boom (Belsele-Waas)	George	74	0.0027	3.09E-08
118	0.2	-247.58	10.97	Boom (Belsele-Waas)	George	241	0.0119	1.38E-07
118	0.15	-247.63	10.5	Boom (Belsele-Waas)	George	875	0.0615	7.12E-07
118	0.1	-247.68	10.14	Boom (Belsele-Waas)	George	2350	0.2158	2.50E-06
118	0.05	-247.73	10.38	Boom (Belsele-Waas)	George	1216	0.0935	1.08E-06
119	0.8	-247.96	10.69	Boom (Belsele-Waas)	George	519	0.0317	3.67E-07
119	0.75	-248.01	11.12	Boom (Belsele-Waas)	George	159	0.0071	8.19E-08
119	0.7	-248.06	11.24	Boom (Belsele-Waas)	George	115	0.0047	5.39E-08
119	0.6	-248.16	10.82	Boom (Belsele-Waas)	George	363	0.0201	2.33E-07
119	0.5	-248.26	10.72	Boom (Belsele-Waas)	George	478	0.0286	3.31E-07
119	0.45	-248.31	10.9	Boom (Belsele-Waas)	George	292	0.0152	1.76E-07
119	0.35	-248.41	10.68	Boom (Belsele-Waas)	George	534	0.0328	3.80E-07
119	0.25	-248.51	10.98	Boom (Belsele-Waas)	George	234	0.0115	1.33E-07
119	0.2	-248.56	10.65	Boom (Belsele-Waas)	George	579	0.0365	4.22E-07
119	0.15	-248.61	10.78	Boom (Belsele-Waas)	George	405	0.0232	2.68E-07
119	0.1	-248.66	10.4	Boom (Belsele-Waas)	George	1151	0.0872	1.01E-06
119	0.05	-248.71	10.84	Boom (Belsele-Waas)	George	344	0.0188	2.17E-07
120	0.75	-249.02	10.82	Boom (Belsele-Waas)	George	363	0.0201	2.33E-07
120	0.7	-249.07	10.79	Boom (Belsele-Waas)	George	394	0.0224	2.59E-07
120	0.6	-249.17	10.69	Boom (Belsele-Waas)	George	519	0.0317	3.67E-07
120	0.55	-249.22	10.99	Boom (Belsele-Waas)	George	228	0.0111	1.29E-07
120	0.5	-249.27	11.21	Boom (Belsele-Waas)	George	124	0.0052	5.99E-08
120	0.3	-249.47	11.32	Boom (Belsele-Waas)	George	92	0.0035	4.08E-08
120	0.2	-249.57	11.08	Boom (Belsele-Waas)	George	178	0.0081	9.42E-08
120	0.15	-249.62	10.84	Boom (Belsele-Waas)	George	344	0.0188	2.17E-07
121	0.7	-250.03	10.42	Boom (Belsele-Waas)	George	1089	0.0813	9.41E-07
121	0.65	-250.08	10.59	Boom (Belsele-Waas)	George	683	0.0449	5.20E-07

121	0.6	-250.13	10.28	Boom (Belsele-Waas)	George	1600	0.1325	1.53E-06
121	0.5	-250.23	10.37	Boom (Belsele-Waas)	George	1250	0.0968	1.12E-06
121	0.4	-250.33	10.88	Boom (Belsele-Waas)	George	308	0.0163	1.89E-07
121	0.35	-250.38	11.04	Boom (Belsele-Waas)	George	199	0.0094	1.08E-07
121	0.3	-250.43	10.66	Boom (Belsele-Waas)	George	564	0.0352	4.07E-07
121	0.2	-250.53	10.45	Boom (Belsele-Waas)	George	1003	0.0732	8.47E-07
121	0.15	-250.58	10.68	Boom (Belsele-Waas)	George	534	0.0328	3.80E-07
121	0.1	-250.63	10.66	Boom (Belsele-Waas)	George	564	0.0352	4.07E-07
121	0.05	-250.68	10.84	Boom (Belsele-Waas)	George	344	0.0188	2.17E-07
122	0.8	-250.97	10.8	Boom (Belsele-Waas)	George	384	0.0216	2.50E-07
122	0.7	-251.07	10.59	Boom (Belsele-Waas)	George	683	0.0449	5.20E-07
122	0.65	-251.12	10.14	Boom (Belsele-Waas)	George	2350	0.2158	2.50E-06
122	0.6	-251.17	10.79	Boom (Belsele-Waas)	George	394	0.0224	2.59E-07
122	0.55	-251.22	10.13	Boom (Belsele-Waas)	George	2416	0.2235	2.59E-06
122	0.5	-251.27	10.45	Boom (Belsele-Waas)	George	1003	0.0732	8.47E-07
122	0.4	-251.37	10.5	Boom (Belsele-Waas)	George	875	0.0615	7.12E-07
122	0.25	-251.52	10.35	Boom (Belsele-Waas)	George	1320	0.1038	1.20E-06
122	0.2	-251.57	10.21	Boom (Belsele-Waas)	George	1939	0.1691	1.96E-06
122	0.1	-251.67	10.25	Boom (Belsele-Waas)	George	1737	0.1471	1.70E-06
123	0.7	-252.28	10.85	Boom (Belsele-Waas)	George	335	0.0181	2.10E-07
123	0.65	-252.33	11.04	Boom (Belsele-Waas)	George	199	0.0094	1.08E-07
123	0.6	-252.38	10.56	Boom (Belsele-Waas)	George	742	0.0499	5.77E-07
123	0.55	-252.43	10.87	Boom (Belsele-Waas)	George	317	0.0169	1.96E-07
123	0.5	-252.48	10.86	Boom (Belsele-Waas)	George	325	0.0175	2.03E-07
123	0.45	-252.53	10.87	Boom (Belsele-Waas)	George	317	0.0169	1.96E-07
123	0.4	-252.58	10.48	Boom (Belsele-Waas)	George	924	0.0659	7.63E-07
123	0.3	-252.68	10.53	Boom (Belsele-Waas)	George	805	0.0554	6.41E-07
123	0.2	-252.78	10.68	Boom (Belsele-Waas)	George	534	0.0328	3.80E-07
123	0.1	-252.88	10.79	Boom (Belsele-Waas)	George	394	0.0224	2.59E-07
123	0.05	-252.93	10.77	Boom (Belsele-Waas)	George	417	0.0240	2.78E-07
124	0.65	-253.34	10.62	Boom (Belsele-Waas)	George	629	0.0405	4.68E-07
124	0.05	-253.94	10.67	Boom (Belsele-Waas)	George	548	0.0340	3.93E-07
125	0.85	-254.93	10.43	Boom (Belsele-Waas)	George	1060	0.0785	9.09E-07
125	0.8	-254.98	10.12	Boom (Belsele-Waas)	George	2483	0.2314	2.68E-06
125	0.65	-255.13	10.24	Boom (Belsele-Waas)	George	1786	0.1523	1.76E-06
125	0.6	-255.18	10.63	Boom (Belsele-Waas)	George	612	0.0391	4.52E-07
125	0.5	-255.28	10.82	Boom (Belsele-Waas)	George	363	0.0201	2.33E-07
125	0.45	-255.33	11.07	Boom (Belsele-Waas)	George	183	0.0084	9.75E-08
125	0.4	-255.38	11.15	Boom (Belsele-Waas)	George	147	0.0064	7.38E-08
125	0.25	-255.53	10.62	Boom (Belsele-Waas)	George	629	0.0405	4.68E-07
125	0.15	-255.63	10.64	Boom (Belsele-Waas)	George	595	0.0377	4.37E-07
125	0.1	-255.68	10.74	Boom (Belsele-Waas)	George	452	0.0266	3.08E-07
125	0.05	-255.73	10.64	Boom (Belsele-Waas)	George	595	0.0377	4.37E-07
127	0.7	-256.06	10.57	Boom (Belsele-Waas)	George	722	0.0482	5.58E-07
127	0.6	-256.16	10.79	Boom (Belsele-Waas)	George	394	0.0224	2.59E-07
127	0.4	-256.36	10.47	Boom (Belsele-Waas)	George	950	0.0683	7.90E-07
127	0.35	-256.41	10.7	Boom (Belsele-Waas)	George	505	0.0306	3.54E-07
127	0.3	-256.46	10.76	Boom (Belsele-Waas)	George	428	0.0248	2.87E-07
127	0.25	-256.51	10.85	Boom (Belsele-Waas)	George	335	0.0181	2.10E-07
127	0.1	-256.66	10.57	Boom (Belsele-Waas)	George	722	0.0482	5.58E-07
127	0.05	-256.71	11.29	Boom (Belsele-Waas)	George	100	0.0039	4.53E-08
128	0.8	-256.98	10.76	Boom (Belsele-Waas)	Lisa	428	0.0269	3.12E-07
128	0.65	-257.13	11.38	Boom (Belsele-Waas)	Lisa	78	0.0027	3.14E-08

128	0.6	-257.18	10.94	Boom (Belsele-Waas)	Lisa	261	0.0138	1.60E-07
128	0.55	-257.23	11.11	Boom (Belsele-Waas)	Lisa	164	0.0074	8.52E-08
128	0.5	-257.28	10.35	Boom (Belsele-Waas)	Lisa	1320	0.1229	1.42E-06
128	0.45	-257.33	9.9	Boom (Belsele-Waas)	Lisa	4542	0.6510	7.53E-06
128	0.4	-257.38	10.85	Boom (Belsele-Waas)	Lisa	335	0.0193	2.23E-07
128	0.35	-257.43	10.71	Boom (Belsele-Waas)	Lisa	491	0.0324	3.75E-07
128	0.3	-257.48	10.88	Boom (Belsele-Waas)	Lisa	308	0.0173	2.00E-07
128	0.25	-257.53	11.11	Boom (Belsele-Waas)	Lisa	164	0.0074	8.52E-08
128	0.2	-257.58	11.06	Boom (Belsele-Waas)	Lisa	188	0.0089	1.03E-07
128	0.15	-257.63	11.06	Boom (Belsele-Waas)	Lisa	188	0.0089	1.03E-07
128	0.05	-257.73	10.53	Boom (Belsele-Waas)	Lisa	805	0.0631	7.31E-07
130	0.6	-259.18	11.74	Boom (Belsele-Waas)	George	29	0.0008	9.43E-09
130	0.5	-259.28	11.16	Boom (Belsele-Waas)	George	143	0.0062	7.13E-08
130	0.4	-259.38	11.41	Boom (Belsele-Waas)	George	72	0.0026	2.98E-08
130	0.1	-259.68	10.5	Boom (Belsele-Waas)	George	875	0.0615	7.12E-07
130	0.05	-259.73	10.33	Boom (Belsele-Waas)	George	1395	0.1113	1.29E-06
131	0.85	-259.92	11.8	Boom (Belsele-Waas)	George	25	0.0007	7.65E-09
131	0.8	-259.97	11.31	Boom (Belsele-Waas)	George	95	0.0036	4.22E-08
131	0.75	-260.02	10.73	Boom (Belsele-Waas)	George	465	0.0276	3.19E-07
131	0.7	-260.07	10.56	Boom (Belsele-Waas)	George	742	0.0499	5.77E-07
131	0.65	-260.12	10.92	Boom (Belsele-Waas)	George	276	0.0142	1.65E-07
131	0.6	-260.17	10.5	Boom (Belsele-Waas)	George	875	0.0615	7.12E-07
131	0.55	-260.22	10.61	Boom (Belsele-Waas)	George	647	0.0419	4.85E-07
131	0.5	-260.27	10.46	Boom (Belsele-Waas)	George	976	0.0707	8.18E-07
131	0.45	-260.32	9.96	Boom (Belsele-Waas)	George	3852	0.4043	4.68E-06
131	0.4	-260.37	9.97	Boom (Belsele-Waas)	George	3748	0.3904	4.52E-06
131	0.35	-260.42	9.94	Boom (Belsele-Waas)	George	4070	0.4335	5.02E-06
131	0.3	-260.47	9.76	Boom (Belsele-Waas)	George	6672	0.8120	9.40E-06
131	0.25	-260.52	10.3	Boom (Belsele-Waas)	George	1515	0.1235	1.43E-06
131	0.2	-260.57	10.28	Boom (Belsele-Waas)	George	1600	0.1325	1.53E-06
131	0.15	-260.62	10.32	Boom (Belsele-Waas)	George	1434	0.1152	1.33E-06
131	0.1	-260.67	10.46	Boom (Belsele-Waas)	George	976	0.0707	8.18E-07
131	0.05	-260.72	10.87	Boom (Belsele-Waas)	George	317	0.0169	1.96E-07
132	0.75	-261.02	11.19	Boom (Belsele-Waas)	George	132	0.0055	6.42E-08
132	0.65	-261.12	11.18	Boom (Belsele-Waas)	George	135	0.0057	6.65E-08
132	0.55	-261.22	11.32	Boom (Belsele-Waas)	George	92	0.0035	4.08E-08
132	0.45	-261.32	11.1	Boom (Belsele-Waas)	George	168	0.0076	8.78E-08
132	0.4	-261.37	11.21	Boom (Belsele-Waas)	George	124	0.0052	5.99E-08
132	0.3	-261.47	10.86	Boom (Belsele-Waas)	George	325	0.0175	2.03E-07
132	0.25	-261.52	10.93	Boom (Belsele-Waas)	George	269	0.0137	1.59E-07
132	0.2	-261.57	10.97	Boom (Belsele-Waas)	George	241	0.0119	1.38E-07
132	0.05	-261.72	10.86	Boom (Belsele-Waas)	George	325	0.0175	2.03E-07
133	0.8	-261.99	10.33	Boom (Belsele-Waas)	George	1395	0.1113	1.29E-06
133	0.7	-262.09	10.59	Boom (Belsele-Waas)	George	683	0.0449	5.20E-07
133	0.6	-262.19	10.84	Boom (Belsele-Waas)	George	344	0.0188	2.17E-07
133	0.5	-262.29	11.31	Boom (Belsele-Waas)	George	95	0.0036	4.22E-08
133	0.35	-262.44	11.13	Boom (Belsele-Waas)	George	155	0.0068	7.91E-08
134	0.05	-262.74	11.23	Boom (Belsele-Waas)	George	118	0.0048	5.58E-08
134	0.7	-263.07	10.55	Boom (Belsele-Waas)	George	762	0.0517	5.98E-07
134	0.65	-263.12	10.09	Boom (Belsele-Waas)	George	2696	0.2569	2.97E-06
134	0.6	-263.17	10.32	Boom (Belsele-Waas)	George	1434	0.1152	1.33E-06
134	0.55	-263.22	10.85	Boom (Belsele-Waas)	George	335	0.0181	2.10E-07
134	0.5	-263.27	11.2	Boom (Belsele-Waas)	George	128	0.0054	6.20E-08

134	0.45	-263.32	10.93	Boom (Belsele-Waas)	George	269	0.0137	1.59E-07
134	0.4	-263.37	11.04	Boom (Belsele-Waas)	George	199	0.0094	1.08E-07
134	0.35	-263.42	11.34	Boom (Belsele-Waas)	George	87	0.0033	3.80E-08
134	0.3	-263.47	11.33	Boom (Belsele-Waas)	George	90	0.0034	3.94E-08
134	0.2	-263.57	10.95	Boom (Belsele-Waas)	George	254	0.0128	1.48E-07
134	0.15	-263.62	10.92	Boom (Belsele-Waas)	George	276	0.0142	1.65E-07
134	0.1	-263.67	11.12	Boom (Belsele-Waas)	George	159	0.0071	8.19E-08
134	0.05	-263.72	11.33	Boom (Belsele-Waas)	George	90	0.0034	3.94E-08
135	0.75	-264.01	10.35	Boom (Belsele-Waas)	George	1320	0.1038	1.20E-06
135	0.7	-264.06	10.34	Boom (Belsele-Waas)	George	1357	0.1074	1.24E-06
135	0.65	-264.11	10.33	Boom (Belsele-Waas)	George	1395	0.1113	1.29E-06
135	0.6	-264.16	9.92	Boom (Belsele-Waas)	George	4300	0.4648	5.38E-06
135	0.55	-264.21	10.17	Boom (Belsele-Waas)	George	2164	0.1944	2.25E-06
135	0.5	-264.26	9.86	Boom (Belsele-Waas)	George	5070	0.5729	6.63E-06
135	0.45	-264.31	10.01	Boom (Belsele-Waas)	George	3358	0.3396	3.93E-06
135	0.4	-264.36	9.9	Boom (Belsele-Waas)	George	4542	0.4984	5.77E-06
135	0.35	-264.41	9.7	Boom (Belsele-Waas)	George	7866	1.0010	1.16E-05
135	0.3	-264.46	9.6	Boom (Belsele-Waas)	George	10352	1.4186	1.64E-05
135	0.25	-264.51	10.86	Boom (Belsele-Waas)	George	325	0.0175	2.03E-07
135	0.2	-264.56	11.01	Boom (Belsele-Waas)	George	216	0.0104	1.20E-07
135	0.15	-264.61	11.03	Boom (Belsele-Waas)	George	204	0.0097	1.12E-07
135	0.1	-264.66	10.96	Boom (Belsele-Waas)	George	247	0.0124	1.43E-07
135	0.05	-264.71	10.63	Boom (Belsele-Waas)	George	612	0.0391	4.52E-07
136	0.7	-265.05	9.77	Boom (Belsele-Waas)	George	6491	0.7842	9.08E-06
136	0.65	-265.1	9.98	Boom (Belsele-Waas)	George	3647	0.3770	4.36E-06
136	0.6	-265.15	9.72	Boom (Belsele-Waas)	George	7446	0.9335	1.08E-05
136	0.55	-265.2	9.93	Boom (Belsele-Waas)	George	4183	0.4489	5.20E-06
136	0.5	-265.25	9.88	Boom (Belsele-Waas)	George	4799	0.5343	6.18E-06
136	0.45	-265.3	10.06	Boom (Belsele-Waas)	George	2927	0.2853	3.30E-06
136	0.4	-265.35	9.63	Boom (Belsele-Waas)	George	9533	1.2777	1.48E-05
136	0.35	-265.4	9.95	Boom (Belsele-Waas)	George	3960	0.4186	4.85E-06
136	0.3	-265.45	10.02	Boom (Belsele-Waas)	George	3267	0.3279	3.80E-06
136	0.25	-265.5	9.73	Boom (Belsele-Waas)	George	7244	0.9015	1.04E-05
136	0.2	-265.55	9.78	Boom (Belsele-Waas)	George	6315	0.7573	8.77E-06
136	0.15	-265.6	10.99	Boom (Belsele-Waas)	George	228	0.0111	1.29E-07
136	0.1	-265.65	10.83	Boom (Belsele-Waas)	George	353	0.0195	2.25E-07
136	0.05	-265.7	10.46	Boom (Belsele-Waas)	George	976	0.0707	8.18E-07
138	0.7	-267.23	9.99	Zelzate (Ruisbroek)	George	3548	0.3641	4.21E-06
138	0.65	-267.28	9.55	Zelzate (Ruisbroek)	George	11875	1.6888	1.95E-05
138	0.6	-267.33	9.9	Zelzate (Ruisbroek)	George	4542	0.4984	5.77E-06
138	0.55	-267.38	10.11	Zelzate (Ruisbroek)	George	2552	0.2396	2.77E-06
138	0.5	-267.43	10.26	Zelzate (Ruisbroek)	George	1690	0.1420	1.64E-06
138	0.45	-267.48	10.21	Zelzate (Ruisbroek)	George	1939	0.1691	1.96E-06
138	0.4	-267.53	10	Zelzate (Ruisbroek)	George	3452	0.3516	4.07E-06
138	0.35	-267.58	10.24	Zelzate (Ruisbroek)	George	1786	0.1523	1.76E-06
138	0.3	-267.63	9.79	Zelzate (Ruisbroek)	George	6144	0.7313	8.46E-06
138	0.25	-267.68	9.69	Zelzate (Ruisbroek)	George	8085	1.0365	1.20E-05
138	0.2	-267.73	9.61	Zelzate (Ruisbroek)	George	10072	1.3700	1.59E-05
138	0.15	-267.78	9.8	Zelzate (Ruisbroek)	George	5978	0.7063	8.17E-06
138	0.1	-267.83	9.77	Zelzate (Ruisbroek)	George	6491	0.7842	9.08E-06
138	0.05	-267.88	9.64	Zelzate (Ruisbroek)	George	9275	1.2339	1.43E-05
139	0.85	-267.89	9.54	Zelzate (Ruisbroek)	George	12206	1.7488	2.02E-05
139	0.8	-267.94	9.89	Zelzate (Ruisbroek)	George	4669	0.5160	5.97E-06

139	0.75	-267.99	9.84	Zelzate (Ruisbroek)	George	5356	0.6143	7.11E-06
139	0.7	-268.04	10.01	Zelzate (Ruisbroek)	George	3358	0.3396	3.93E-06
139	0.65	-268.09	9.87	Zelzate (Ruisbroek)	George	4932	0.5533	6.40E-06
139	0.6	-268.14	9.83	Zelzate (Ruisbroek)	George	5505	0.6361	7.36E-06
139	0.55	-268.19	9.77	Zelzate (Ruisbroek)	George	6491	0.7842	9.08E-06
139	0.5	-268.24	9.8	Zelzate (Ruisbroek)	George	5978	0.7063	8.17E-06
139	0.45	-268.29	9.78	Zelzate (Ruisbroek)	George	6315	0.7573	8.77E-06
139	0.4	-268.34	9.79	Zelzate (Ruisbroek)	George	6144	0.7313	8.46E-06
139	0.35	-268.39	9.74	Zelzate (Ruisbroek)	George	7048	0.8707	1.01E-05
139	0.3	-268.44	9.77	Zelzate (Ruisbroek)	George	6491	0.7842	9.08E-06
139	0.25	-268.49	9.72	Zelzate (Ruisbroek)	George	7446	0.9335	1.08E-05
139	0.2	-268.54	9.61	Zelzate (Ruisbroek)	George	10072	1.3700	1.59E-05
139	0.15	-268.59	9.66	Zelzate (Ruisbroek)	George	8780	1.1508	1.33E-05
139	0.1	-268.64	9.5	Zelzate (Ruisbroek)	George	13623	2.0105	2.33E-05
139	0.05	-268.69	9.67	Zelzate (Ruisbroek)	George	8542	1.1114	1.29E-05
140	0.55	-269.3	9.72	Zelzate (Ruisbroek)	George	7446	0.9335	1.08E-05
140	0.5	-269.35	9.64	Zelzate (Ruisbroek)	George	9275	1.2339	1.43E-05
140	0.45	-269.4	9.66	Zelzate (Ruisbroek)	George	8780	1.1508	1.33E-05
140	0.4	-269.45	9.62	Zelzate (Ruisbroek)	George	9799	1.3230	1.53E-05
140	0.35	-269.5	9.95	Zelzate (Ruisbroek)	George	3960	0.4186	4.85E-06
140	0.3	-269.55	9.94	Zelzate (Ruisbroek)	George	4070	0.4335	5.02E-06
140	0.25	-269.6	10.19	Zelzate (Ruisbroek)	George	2049	0.1813	2.10E-06
140	0.2	-269.65	10.28	Zelzate (Ruisbroek)	George	1600	0.1325	1.53E-06
140	0.15	-269.7	10.24	Zelzate (Ruisbroek)	George	1786	0.1523	1.76E-06
140	0.1	-269.75	10.41	Zelzate (Ruisbroek)	George	1120	0.0842	9.74E-07
140	0.05	-269.8	10.38	Zelzate (Ruisbroek)	George	1216	0.0935	1.08E-06
143	0.7	-271.3	9.88	Zelzate (Ruisbroek)	George	4799	0.5343	6.18E-06
143	0.65	-271.35	9.8	Zelzate (Ruisbroek)	George	5978	0.7063	8.17E-06
143	0.6	-271.4	9.85	Zelzate (Ruisbroek)	George	5211	0.5933	6.87E-06
143	0.55	-271.45	9.92	Zelzate (Ruisbroek)	George	4300	0.4648	5.38E-06
143	0.5	-271.5	9.92	Zelzate (Ruisbroek)	George	4300	0.4648	5.38E-06
143	0.45	-271.55	9.92	Zelzate (Ruisbroek)	George	4300	0.4648	5.38E-06
143	0.4	-271.6	9.85	Zelzate (Ruisbroek)	George	5211	0.5933	6.87E-06
143	0.35	-271.65	9.88	Zelzate (Ruisbroek)	George	4799	0.5343	6.18E-06
143	0.3	-271.7	9.91	Zelzate (Ruisbroek)	George	4419	0.4813	5.57E-06
143	0.25	-271.75	9.87	Zelzate (Ruisbroek)	George	4932	0.5533	6.40E-06
143	0.2	-271.8	10	Zelzate (Ruisbroek)	George	3452	0.3516	4.07E-06
143	0.15	-271.85	9.87	Zelzate (Ruisbroek)	George	4932	0.5533	6.40E-06
143	0.1	-271.9	9.88	Zelzate (Ruisbroek)	George	4799	0.5343	6.18E-06
143	0.05	-271.95	10.01	Zelzate (Ruisbroek)	George	3358	0.3396	3.93E-06
144	0.55	-272.33	11.28	Zelzate (Wintham)	George	103	0.0041	4.69E-08
144	0.1	-272.78	11.69	Zelzate (Wintham)	George	33	0.0010	1.12E-08
145	0.7	-273.18	11.21	Zelzate (Wintham)	George	124	0.0052	5.99E-08
145	0.45	-273.43	11.49	Zelzate (Wintham)	George	58	0.0019	2.25E-08
145	0.35	-273.53	10.98	Zelzate (Wintham)	George	234	0.0115	1.33E-07
145	0.1	-273.78	11.53	Zelzate (Wintham)	George	52	0.0017	1.96E-08
145	0.05	-273.83	11.12	Zelzate (Wintham)	George	159	0.0071	8.19E-08
146	0.6	-274.1	11.49	Zelzate (Wintham)	George	58	0.0019	2.25E-08
146	0.55	-274.15	11.53	Zelzate (Wintham)	George	52	0.0017	1.96E-08
146	0.5	-274.2	10.56	Zelzate (Wintham)	George	742	0.0499	5.77E-07
146	0.45	-274.25	10.68	Zelzate (Wintham)	George	534	0.0328	3.80E-07
146	0.4	-274.3	10.71	Zelzate (Wintham)	George	491	0.0296	3.42E-07
146	0.35	-274.35	10.77	Zelzate (Wintham)	George	417	0.0240	2.78E-07

146	0.3	-274.4	10.87	Zelzate (Wintham)	George	317	0.0169	1.96E-07
146	0.25	-274.45	10.85	Zelzate (Wintham)	George	335	0.0181	2.10E-07
146	0.2	-274.5	10.99	Zelzate (Wintham)	George	228	0.0111	1.29E-07
146	0.15	-274.55	10.76	Zelzate (Wintham)	George	428	0.0248	2.87E-07
146	0.1	-274.6	10.57	Zelzate (Wintham)	George	722	0.0482	5.58E-07
146	0.05	-274.65	10.82	Zelzate (Wintham)	George	363	0.0201	2.33E-07
147	0.6	-275.17	10.68	Zelzate (Wintham)	George	534	0.0328	3.80E-07
147	0.55	-275.22	10.75	Zelzate (Wintham)	George	440	0.0257	2.98E-07
147	0.5	-275.27	10.62	Zelzate (Wintham)	George	629	0.0405	4.68E-07
147	0.45	-275.32	10.19	Zelzate (Wintham)	George	2049	0.1813	2.10E-06
147	0.4	-275.37	10.56	Zelzate (Wintham)	George	742	0.0499	5.77E-07
147	0.35	-275.42	10.54	Zelzate (Wintham)	George	784	0.0535	6.19E-07
147	0.3	-275.47	10.13	Zelzate (Wintham)	George	2416	0.2235	2.59E-06
147	0.25	-275.52	10.26	Zelzate (Wintham)	George	1690	0.1420	1.64E-06
147	0.2	-275.57	10.17	Zelzate (Wintham)	George	2164	0.1944	2.25E-06
147	0.15	-275.62	10.3	Zelzate (Wintham)	George	1515	0.1235	1.43E-06
147	0.1	-275.67	10.33	Zelzate (Wintham)	George	1395	0.1113	1.29E-06
147	0.05	-275.72	10.16	Zelzate (Wintham)	George	2225	0.2013	2.33E-06
148	0.8	-275.98	10.1	Zelzate (Wintham)	Lisa	2623	0.3103	3.59E-06
148	0.75	-276.03	9.76	Zelzate (Wintham)	Lisa	6672	1.0934	1.27E-05
148	0.7	-276.08	9.69	Zelzate (Wintham)	Lisa	8085	1.4170	1.64E-05
148	0.65	-276.13	9.78	Zelzate (Wintham)	Lisa	6315	1.0153	1.18E-05
148	0.6	-276.18	9.93	Zelzate (Wintham)	Lisa	4183	0.5825	6.74E-06
148	0.55	-276.23	10.21	Zelzate (Wintham)	Lisa	1939	0.2065	2.39E-06
148	0.5	-276.28	10.12	Zelzate (Wintham)	Lisa	2483	0.2882	3.34E-06
148	0.45	-276.33	10.11	Zelzate (Wintham)	Lisa	2552	0.2991	3.46E-06
148	0.4	-276.38	9.96	Zelzate (Wintham)	Lisa	3852	0.5213	6.03E-06
148	0.35	-276.43	10.18	Zelzate (Wintham)	Lisa	2106	0.2308	2.67E-06
148	0.3	-276.48	10.26	Zelzate (Wintham)	Lisa	1690	0.1716	1.99E-06
148	0.25	-276.53	10.13	Zelzate (Wintham)	Lisa	2416	0.2777	3.21E-06
148	0.15	-276.63	10.27	Zelzate (Wintham)	Lisa	1645	0.1653	1.91E-06
148	0.1	-276.68	10.48	Zelzate (Wintham)	Lisa	924	0.0760	8.79E-07
148	0.05	-276.73	9.97	Zelzate (Wintham)	Lisa	3748	0.5023	5.81E-06
149	0.7	-277.07	10.14	Zelzate (Wintham)	Lisa	2350	0.2676	3.10E-06
149	0.55	-277.22	11.06	Zelzate (Wintham)	Lisa	188	0.0089	1.03E-07
149	0.4	-277.37	11.06	Zelzate (Wintham)	Lisa	188	0.0089	1.03E-07
149	0.2	-277.57	11.33	Zelzate (Wintham)	Lisa	90	0.0033	3.77E-08
150	0.05	-277.72	11.12	Zelzate (Wintham)	Lisa	159	0.0071	8.21E-08
150	0.7	-278.02	10.84	Zelzate (Wintham)	Lisa	344	0.0200	2.32E-07
150	0.6	-278.12	10.98	Zelzate (Wintham)	Lisa	234	0.0119	1.38E-07
150	0.45	-278.27	10.77	Zelzate (Wintham)	Lisa	417	0.0259	3.00E-07
150	0.4	-278.32	10.72	Zelzate (Wintham)	Lisa	478	0.0312	3.61E-07
150	0.3	-278.42	10.33	Zelzate (Wintham)	Lisa	1395	0.1324	1.53E-06
150	0.05	-278.67	11.04	Zelzate (Wintham)	Lisa	199	0.0095	1.10E-07
151	0.8	-278.91	10.22	Zelzate (Wintham)	Lisa	1887	0.1990	2.30E-06
151	0.75	-278.96	10.46	Zelzate (Wintham)	Lisa	976	0.0818	9.47E-07
151	0.7	-279.01	10.37	Zelzate (Wintham)	Lisa	1250	0.1142	1.32E-06
151	0.65	-279.06	10.24	Zelzate (Wintham)	Lisa	1786	0.1848	2.14E-06
151	0.6	-279.11	10.32	Zelzate (Wintham)	Lisa	1434	0.1374	1.59E-06
151	0.55	-279.16	10.26	Zelzate (Wintham)	Lisa	1690	0.1716	1.99E-06
151	0.5	-279.21	10.5	Zelzate (Wintham)	Lisa	875	0.0705	8.16E-07
151	0.45	-279.26	10.38	Zelzate (Wintham)	Lisa	1216	0.1100	1.27E-06
151	0.4	-279.31	10.33	Zelzate (Wintham)	Lisa	1395	0.1324	1.53E-06

151	0.35	-279.36	10.34	Zelzate (Wintham)	Lisa	1357	0.1276	1.48E-06
151	0.3	-279.41	10.41	Zelzate (Wintham)	Lisa	1120	0.0984	1.14E-06
151	0.25	-279.46	10.1	Zelzate (Wintham)	Lisa	2623	0.3103	3.59E-06
151	0.2	-279.51	10.29	Zelzate (Wintham)	Lisa	1557	0.1535	1.78E-06
151	0.15	-279.56	10.47	Zelzate (Wintham)	Lisa	950	0.0788	9.12E-07
151	0.1	-279.61	10.4	Zelzate (Wintham)	Lisa	1151	0.1022	1.18E-06
151	0.05	-279.66	10.52	Zelzate (Wintham)	Lisa	828	0.0655	7.58E-07
152	0.7	-280.05	10.08	Zelzate (Wintham)	Lisa	2771	0.3342	3.87E-06
152	0.65	-280.1	10.12	Zelzate (Wintham)	Lisa	2483	0.2882	3.34E-06
152	0.6	-280.15	10.15	Zelzate (Wintham)	Lisa	2286	0.2579	2.98E-06
152	0.55	-280.2	10.21	Zelzate (Wintham)	Lisa	1939	0.2065	2.39E-06
152	0.5	-280.25	10.14	Zelzate (Wintham)	Lisa	2350	0.2676	3.10E-06
152	0.45	-280.3	10.4	Zelzate (Wintham)	Lisa	1151	0.1022	1.18E-06
152	0.4	-280.35	10.25	Zelzate (Wintham)	Lisa	1737	0.1781	2.06E-06
152	0.35	-280.4	10.09	Zelzate (Wintham)	Lisa	2696	0.3221	3.73E-06
152	0.3	-280.45	10.06	Zelzate (Wintham)	Lisa	2927	0.3599	4.17E-06
152	0.25	-280.5	10.13	Zelzate (Wintham)	Lisa	2416	0.2777	3.21E-06
152	0.2	-280.55	10.12	Zelzate (Wintham)	Lisa	2483	0.2882	3.34E-06
152	0.15	-280.6	10.11	Zelzate (Wintham)	Lisa	2552	0.2991	3.46E-06
152	0.1	-280.65	10.11	Zelzate (Wintham)	Lisa	2552	0.2991	3.46E-06
152	0.05	-280.7	9.86	Zelzate (Wintham)	Lisa	5070	0.7549	8.74E-06
153	0.65	-281.11	10	Zelzate (Wintham)	George	3452	0.3516	4.07E-06
153	0.6	-281.16	9.85	Zelzate (Wintham)	George	5211	0.5933	6.87E-06
153	0.55	-281.21	9.87	Zelzate (Wintham)	George	4932	0.5533	6.40E-06
153	0.5	-281.26	10.09	Zelzate (Wintham)	George	2696	0.2569	2.97E-06
153	0.45	-281.31	10.03	Zelzate (Wintham)	George	3179	0.3167	3.67E-06
153	0.25	-281.51	9.9	Zelzate (Wintham)	George	4542	0.4984	5.77E-06
153	0.15	-281.61	10.34	Zelzate (Wintham)	George	1357	0.1074	1.24E-06
153	0.1	-281.66	10.02	Zelzate (Wintham)	George	3267	0.3279	3.80E-06
153	0.05	-282.7	9.83	Zelzate (Wintham)	George	5505	0.6361	7.36E-06
154	0.8	-281.95	10.03	Zelzate (Wintham)	George	3179	0.3167	3.67E-06
154	0.75	-282	10.11	Zelzate (Wintham)	George	2552	0.2396	2.77E-06
154	0.7	-282.05	10.14	Zelzate (Wintham)	George	2350	0.2158	2.50E-06
154	0.65	-282.1	10.67	Zelzate (Wintham)	George	548	0.0340	3.93E-07
154	0.6	-282.15	10.35	Zelzate (Wintham)	George	1320	0.1038	1.20E-06
154	0.55	-282.2	10.23	Zelzate (Wintham)	George	1836	0.1577	1.82E-06
154	0.5	-282.25	10.19	Zelzate (Wintham)	George	2049	0.1813	2.10E-06
154	0.45	-282.3	9.83	Zelzate (Wintham)	George	5505	0.6361	7.36E-06
154	0.4	-282.35	10.12	Zelzate (Wintham)	George	2483	0.2314	2.68E-06
154	0.35	-282.4	10.08	Zelzate (Wintham)	George	2771	0.2660	3.08E-06
154	0.25	-282.5	10.03	Zelzate (Wintham)	George	3179	0.3167	3.67E-06
154	0.1	-282.65	10.16	Zelzate (Wintham)	George	2225	0.2013	2.33E-06
154	0.05	-282.7	10.2	Zelzate (Wintham)	George	1993	0.1751	2.03E-06
155	0.75	-282.99	9.94	Zelzate (Wintham)	George	4070	0.4335	5.02E-06
155	0.7	-283.04	10	Zelzate (Wintham)	George	3452	0.3516	4.07E-06
155	0.65	-283.09	10.22	Zelzate (Wintham)	George	1887	0.1633	1.89E-06
155	0.6	-283.14	10.11	Zelzate (Wintham)	George	2552	0.2396	2.77E-06
155	0.55	-283.19	10.08	Zelzate (Wintham)	George	2771	0.2660	3.08E-06
155	0.5	-283.24	10.03	Zelzate (Wintham)	George	3179	0.3167	3.67E-06
155	0.4	-283.34	10.27	Zelzate (Wintham)	George	1645	0.1372	1.59E-06
155	0.25	-283.49	10.17	Zelzate (Wintham)	George	2164	0.1944	2.25E-06
155	0.2	-283.54	9.99	Zelzate (Wintham)	George	3548	0.3641	4.21E-06
155	0.15	-283.59	10.13	Zelzate (Wintham)	George	2416	0.2235	2.59E-06

156	0.1	-283.64	10.29	Zelzate (Wintham)	George	1557	0.1279	1.48E-06
156	0.7	-283.93	10.71	Zelzate (Wintham)	George	491	0.0296	3.42E-07
156	0.4	-284.23	11.17	Zelzate (Watervliet)	George	139	0.0059	6.88E-08
156	0.05	-284.58	11.33	Zelzate (Watervliet)	George	90	0.0034	3.94E-08
157	0.8	-284.82	10.54	Zelzate (Watervliet)	George	784	0.0535	6.19E-07
157	0.7	-284.92	10.71	Zelzate (Watervliet)	George	491	0.0296	3.42E-07
157	0.65	-284.97	10.62	Zelzate (Watervliet)	George	629	0.0405	4.68E-07
157	0.6	-285.02	10.72	Zelzate (Watervliet)	George	478	0.0286	3.31E-07
157	0.55	-285.07	10.72	Zelzate (Watervliet)	George	478	0.0286	3.31E-07
157	0.5	-285.12	10.63	Zelzate (Watervliet)	George	612	0.0391	4.52E-07
157	0.45	-285.17	10.63	Zelzate (Watervliet)	George	612	0.0391	4.52E-07
157	0.4	-285.22	10.26	Zelzate (Watervliet)	George	1690	0.1420	1.64E-06
157	0.35	-285.27	10.7	Zelzate (Watervliet)	George	505	0.0306	3.54E-07
157	0.3	-285.32	10.33	Zelzate (Watervliet)	George	1395	0.1113	1.29E-06
157	0.2	-285.42	10.66	Zelzate (Watervliet)	George	564	0.0352	4.07E-07
157	0.15	-285.47	10.57	Zelzate (Watervliet)	George	722	0.0482	5.58E-07
157	0.05	-285.57	10.87	Zelzate (Watervliet)	George	317	0.0169	1.96E-07
158	0.75	-285.78	9.56	Zelzate (Watervliet)	George	11554	1.6310	1.89E-05
158	0.7	-285.83	10.44	Zelzate (Watervliet)	George	1031	0.0758	8.77E-07
158	0.6	-285.93	10.13	Zelzate (Watervliet)	George	2416	0.2235	2.59E-06
158	0.55	-285.98	10.36	Zelzate (Watervliet)	George	1285	0.1002	1.16E-06
158	0.5	-286.03	10.22	Zelzate (Watervliet)	George	1887	0.1633	1.89E-06
158	0.45	-286.08	10.3	Zelzate (Watervliet)	George	1515	0.1235	1.43E-06
158	0.4	-286.13	10.26	Zelzate (Watervliet)	George	1690	0.1420	1.64E-06
158	0.35	-286.18	10.22	Zelzate (Watervliet)	George	1887	0.1633	1.89E-06
158	0.3	-286.23	10.22	Zelzate (Watervliet)	George	1887	0.1633	1.89E-06
158	0.25	-286.28	10.4	Zelzate (Watervliet)	George	1151	0.0872	1.01E-06
158	0.2	-286.33	10.52	Zelzate (Watervliet)	George	828	0.0574	6.64E-07
158	0.15	-286.38	10.2	Zelzate (Watervliet)	George	1993	0.1751	2.03E-06
158	0.1	-286.43	10.27	Zelzate (Watervliet)	George	1645	0.1372	1.59E-06
158	0.05	-286.48	10.21	Zelzate (Watervliet)	George	1939	0.1691	1.96E-06

Table 16. Air permeameter measurements from Herenthout-1 core slabs.

Core #	**distance from core bottom (m)**	**Depth, Z (m)**	**Tinyperm value**	**Hydrostratigraphic unit**	**Operator**	**k_a (mD)**	**K_s (m/d)**	**K_s (m/s)**
1	0.1	-115.28	10.08	Boom (Belsele-Waas)	Lisa	2771	0.2660	3.08E-06
1	0.05	-115.33	10.1	Boom (Belsele-Waas)	Lisa	2623	0.2481	2.87E-06
4	0.85	-117.29	10.46	Boom (Belsele-Waas)	Lisa	976	0.0707	8.18E-07
4	0.7	-117.44	11.04	Boom (Belsele-Waas)	Lisa	199	0.0094	1.08E-07
4	0.6	-117.54	11.14	Boom (Belsele-Waas)	Lisa	151	0.0066	7.64E-08
4	0.5	-117.64	10.87	Boom (Belsele-Waas)	Lisa	317	0.0169	1.96E-07
4	0.4	-117.74	10.67	Boom (Belsele-Waas)	Lisa	548	0.0340	3.93E-07
4	0.3	-117.84	10.84	Boom (Belsele-Waas)	Lisa	344	0.0188	2.17E-07
4	0.25	-117.89	10.66	Boom (Belsele-Waas)	Lisa	564	0.0352	4.07E-07
4	0.2	-117.94	10.45	Boom (Belsele-Waas)	Lisa	1003	0.0732	8.47E-07
4	0.1	-118.04	10.49	Boom (Belsele-Waas)	Lisa	899	0.0637	7.37E-07
4	0.05	-118.09	10.63	Boom (Belsele-Waas)	Lisa	612	0.0391	4.52E-07
6	0.85	-119.33	10.56	Boom (Belsele-Waas)	Lisa	742	0.0499	5.77E-07
6	0.8	-119.38	10.5	Boom (Belsele-Waas)	Lisa	875	0.0615	7.12E-07
6	0.75	-119.43	10.14	Boom (Belsele-Waas)	Lisa	2350	0.2158	2.50E-06

6	0.7	-119.48	10.21	Boom (Belsele-Waas)	Lisa	1939	0.1691	1.96E-06
6	0.65	-119.53	10.25	Boom (Belsele-Waas)	Lisa	1737	0.1471	1.70E-06
6	0.6	-119.58	10.34	Boom (Belsele-Waas)	Lisa	1357	0.1074	1.24E-06
6	0.55	-119.63	10.41	Boom (Belsele-Waas)	Lisa	1120	0.0842	9.74E-07
6	0.5	-119.68	10.24	Boom (Belsele-Waas)	Lisa	1786	0.1523	1.76E-06
6	0.35	-119.83	10.33	Boom (Belsele-Waas)	Lisa	1395	0.1113	1.29E-06
6	0.3	-119.88	10.84	Boom (Belsele-Waas)	Lisa	344	0.0188	2.17E-07
7	0.7	-120.67	9.84	Zelzate (Ruisbroek)	Lisa	5356	0.6143	7.11E-06
7	0.65	-120.72	10.1	Zelzate (Ruisbroek)	Lisa	2623	0.2481	2.87E-06
7	0.6	-120.77	10	Zelzate (Ruisbroek)	Lisa	3452	0.3516	4.07E-06
7	0.55	-120.82	9.96	Zelzate (Ruisbroek)	Lisa	3852	0.4043	4.68E-06
7	0.5	-120.87	9.97	Zelzate (Ruisbroek)	Lisa	3748	0.3904	4.52E-06
7	0.45	-120.92	10.08	Zelzate (Ruisbroek)	Lisa	2771	0.2660	3.08E-06
7	0.4	-120.97	10.05	Zelzate (Ruisbroek)	Lisa	3009	0.2954	3.42E-06
7	0.35	-121.02	9.78	Zelzate (Ruisbroek)	Lisa	6315	0.7573	8.77E-06
7	0.3	-121.07	9.8	Zelzate (Ruisbroek)	Lisa	5978	0.7063	8.17E-06
7	0.25	-121.12	9.96	Zelzate (Ruisbroek)	Lisa	3852	0.4043	4.68E-06
7	0.2	-121.17	9.92	Zelzate (Ruisbroek)	Lisa	4300	0.4648	5.38E-06
7	0.15	-121.22	9.93	Zelzate (Ruisbroek)	Lisa	4183	0.4489	5.20E-06
7	0.1	-121.27	10.09	Zelzate (Ruisbroek)	Lisa	2696	0.2569	2.97E-06
7	0.05	-121.32	10.33	Zelzate (Ruisbroek)	Lisa	1395	0.1113	1.29E-06
8	0.7	-121.47	10.13	Zelzate (Ruisbroek)	Lisa	2416	0.2235	2.59E-06
8	0.65	-121.52	9.93	Zelzate (Ruisbroek)	Lisa	4183	0.4489	5.20E-06
8	0.6	-121.57	9.87	Zelzate (Ruisbroek)	Lisa	4932	0.5533	6.40E-06
8	0.55	-121.62	9.85	Zelzate (Ruisbroek)	Lisa	5211	0.5933	6.87E-06
8	0.5	-121.67	10.05	Zelzate (Ruisbroek)	Lisa	3009	0.2954	3.42E-06
8	0.45	-121.72	10	Zelzate (Ruisbroek)	Lisa	3452	0.3516	4.07E-06
8	0.4	-121.77	10.07	Zelzate (Ruisbroek)	Lisa	2848	0.2755	3.19E-06
8	0.35	-121.82	9.99	Zelzate (Ruisbroek)	Lisa	3548	0.3641	4.21E-06
8	0.3	-121.87	10.04	Zelzate (Ruisbroek)	Lisa	3093	0.3059	3.54E-06
8	0.25	-121.92	9.95	Zelzate (Ruisbroek)	Lisa	3960	0.4186	4.85E-06
8	0.2	-121.97	10.09	Zelzate (Ruisbroek)	Lisa	2696	0.2569	2.97E-06
8	0.15	-122.02	9.96	Zelzate (Ruisbroek)	Lisa	3852	0.4043	4.68E-06
8	0.1	-122.07	10.04	Zelzate (Ruisbroek)	Lisa	3093	0.3059	3.54E-06
8	0.05	-122.12	10.01	Zelzate (Ruisbroek)	Lisa	3358	0.3396	3.93E-06
9	0.8	-122.37	9.95	Zelzate (Ruisbroek)	Lisa	3960	0.4186	4.85E-06
9	0.75	-122.42	9.91	Zelzate (Ruisbroek)	Lisa	4419	0.4813	5.57E-06
9	0.7	-122.47	10.25	Zelzate (Ruisbroek)	Lisa	1737	0.1471	1.70E-06
9	0.65	-122.52	9.86	Zelzate (Ruisbroek)	Lisa	5070	0.5729	6.63E-06
9	0.6	-122.57	9.76	Zelzate (Ruisbroek)	Lisa	6672	0.8120	9.40E-06
9	0.55	-122.62	9.97	Zelzate (Ruisbroek)	Lisa	3748	0.3904	4.52E-06
9	0.5	-122.67	9.93	Zelzate (Ruisbroek)	Lisa	4183	0.4489	5.20E-06
9	0.45	-122.72	9.87	Zelzate (Ruisbroek)	Lisa	4932	0.5533	6.40E-06
9	0.4	-122.77	9.93	Zelzate (Ruisbroek)	Lisa	4183	0.4489	5.20E-06
9	0.35	-122.82	9.78	Zelzate (Ruisbroek)	Lisa	6315	0.7573	8.77E-06
9	0.3	-122.87	9.86	Zelzate (Ruisbroek)	Lisa	5070	0.5729	6.63E-06
9	0.25	-122.92	9.95	Zelzate (Ruisbroek)	Lisa	3960	0.4186	4.85E-06
9	0.2	-122.97	10	Zelzate (Ruisbroek)	Lisa	3452	0.3516	4.07E-06
9	0.15	-123.02	9.94	Zelzate (Ruisbroek)	Lisa	4070	0.4335	5.02E-06
9	0.1	-123.07	9.98	Zelzate (Ruisbroek)	Lisa	3647	0.3770	4.36E-06
9	0.05	-123.12	10.15	Zelzate (Ruisbroek)	Lisa	2286	0.2084	2.41E-06
10	0.7	-123.48	9.92	Zelzate (Ruisbroek)	Lisa	4300	0.4648	5.38E-06
10	0.65	-123.53	9.98	Zelzate (Ruisbroek)	Lisa	3647	0.3770	4.36E-06

10	0.6	-123.58	10.09	Zelzate (Ruisbroek)	Lisa	2696	0.2569	2.97E-06
10	0.55	-123.63	9.79	Zelzate (Ruisbroek)	Lisa	6144	0.7313	8.46E-06
10	0.5	-123.68	10.06	Zelzate (Ruisbroek)	Lisa	2927	0.2853	3.30E-06
10	0.45	-123.73	9.8	Zelzate (Ruisbroek)	Lisa	5978	0.7063	8.17E-06
10	0.4	-123.78	9.87	Zelzate (Ruisbroek)	Lisa	4932	0.5533	6.40E-06
10	0.35	-123.83	9.96	Zelzate (Ruisbroek)	Lisa	3852	0.4043	4.68E-06
10	0.3	-123.88	9.8	Zelzate (Ruisbroek)	Lisa	5978	0.7063	8.17E-06
10	0.25	-123.93	9.88	Zelzate (Ruisbroek)	Lisa	4799	0.5343	6.18E-06
10	0.2	-123.98	9.96	Zelzate (Ruisbroek)	Lisa	3852	0.4043	4.68E-06
10	0.15	-124.03	9.85	Zelzate (Ruisbroek)	Lisa	5211	0.5933	6.87E-06
10	0.1	-124.08	9.9	Zelzate (Ruisbroek)	Lisa	4542	0.4984	5.77E-06
10	0.05	-124.13	9.99	Zelzate (Ruisbroek)	Lisa	3548	0.3641	4.21E-06
12	0.65	-125.53	10.01	Zelzate (Ruisbroek)	Lisa	3358	0.3396	3.93E-06
12	0.6	-125.58	10.01	Zelzate (Ruisbroek)	Lisa	3358	0.3396	3.93E-06
12	0.55	-125.63	9.74	Zelzate (Ruisbroek)	Lisa	7048	0.8707	1.01E-05
12	0.5	-125.68	9.85	Zelzate (Ruisbroek)	Lisa	5211	0.5933	6.87E-06
12	0.45	-125.73	9.82	Zelzate (Ruisbroek)	Lisa	5658	0.6587	7.62E-06
12	0.4	-125.78	9.64	Zelzate (Ruisbroek)	Lisa	9275	1.2339	1.43E-05
12	0.35	-125.83	9.24	Zelzate (Ruisbroek)	Lisa	27817	4.9780	5.76E-05
12	0.3	-125.88	9.54	Zelzate (Ruisbroek)	Lisa	12206	1.7488	2.02E-05
12	0.25	-125.93	9.74	Zelzate (Ruisbroek)	Lisa	7048	0.8707	1.01E-05
12	0.2	-125.98	9.69	Zelzate (Ruisbroek)	Lisa	8085	1.0365	1.20E-05
12	0.15	-126.03	9.91	Zelzate (Ruisbroek)	Lisa	4419	0.4813	5.57E-06
12	0.1	-126.08	10.14	Zelzate (Ruisbroek)	Lisa	2350	0.2158	2.50E-06
12	0.05	-126.13	10.15	Zelzate (Ruisbroek)	Lisa	2286	0.2084	2.41E-06
13	0.8	-126.35	10.05	Zelzate (Ruisbroek)	Lisa	3009	0.2954	3.42E-06
13	0.75	-126.4	9.92	Zelzate (Ruisbroek)	Lisa	4300	0.4648	5.38E-06
13	0.7	-126.45	9.93	Zelzate (Ruisbroek)	Lisa	4183	0.4489	5.20E-06
13	0.65	-126.5	9.88	Zelzate (Ruisbroek)	Lisa	4799	0.5343	6.18E-06
13	0.6	-126.55	9.91	Zelzate (Ruisbroek)	Lisa	4419	0.4813	5.57E-06
13	0.55	-126.6	9.9	Zelzate (Ruisbroek)	Lisa	4542	0.4984	5.77E-06
13	0.5	-126.65	9.91	Zelzate (Ruisbroek)	Lisa	4419	0.4813	5.57E-06
13	0.45	-126.7	9.81	Zelzate (Ruisbroek)	Lisa	5816	0.6821	7.89E-06
13	0.4	-126.75	9.81	Zelzate (Ruisbroek)	Lisa	5816	0.6821	7.89E-06
13	0.35	-126.8	9.85	Zelzate (Ruisbroek)	Lisa	5211	0.5933	6.87E-06
14	0.8	-127.37	10.04	Zelzate (Ruisbroek)	Lisa	3093	0.3059	3.54E-06
14	0.75	-127.42	9.92	Zelzate (Ruisbroek)	Lisa	4300	0.4648	5.38E-06
14	0.7	-127.47	9.81	Zelzate (Ruisbroek)	Lisa	5816	0.6821	7.89E-06
14	0.65	-127.52	9.82	Zelzate (Ruisbroek)	Lisa	5658	0.6587	7.62E-06
14	0.6	-127.57	9.92	Zelzate (Ruisbroek)	Lisa	4300	0.4648	5.38E-06
14	0.55	-127.62	9.94	Zelzate (Ruisbroek)	Lisa	4070	0.4335	5.02E-06
14	0.5	-127.67	9.92	Zelzate (Ruisbroek)	Lisa	4300	0.4648	5.38E-06
14	0.45	-127.72	9.96	Zelzate (Ruisbroek)	Lisa	3852	0.4043	4.68E-06
14	0.4	-127.77	9.88	Zelzate (Ruisbroek)	Lisa	4799	0.5343	6.18E-06
14	0.35	-127.82	9.84	Zelzate (Ruisbroek)	Lisa	5356	0.6143	7.11E-06
14	0.3	-127.87	9.79	Zelzate (Ruisbroek)	Lisa	6144	0.7313	8.46E-06
14	0.1	-128.07	9.98	Zelzate (Ruisbroek)	Lisa	3647	0.3770	4.36E-06
14	0.05	-128.12	10.18	Zelzate (Ruisbroek)	Lisa	2106	0.1877	2.17E-06

Summary: Minimum K_s = 0.0066 m/d, Maximum K_s = 5.0 m/d, Average K_s = 0.45 m/d

Variance K_s = 0.25 $(m/d)^2$, Standard deviation K_s = 0.50 m/d

7.2 Appendix 2

Table 17. Pumping test data for the Oligocene aquifer (SCK•CEN data).

SN	Coordinates		mean K_h (m/d)
	X	Y	
1	125538.9	228349.9	1.097742
2	129557.3	218823.9	0.475238
3	135118	203528	2.071232**
4	142221	224446	0.00596
5	144287	219656	0.015661**
6	156663	238672	0.148819
7	160165	227770	0.14
8	173321	214841	0.002592
9	175304	202909	0.008417
10	175725	236845	0.11
11	175805	225892	0.00864
12	185001	207740	0.644452**
13	190553	221424	0.003456
14	197390	222680	0.009487**
15	198380	211750	0.45
16	200078	235542	0.01
17	208980	208200	0.045789**
18	209640	215490	0.06964**
19	212425	217790	0.127236**
20	234804	174541	3.5

Summary: Minimum K_h = 0.0026 m/d, Maximum K_h = 3.5 m/d, Average K_h = 0.45 m/d

Variance = 0.73, Standard deviation = 0.86

** Geometric mean value

Table 18. Pumping test data for the Ledo-Paniselian-Brusselian aquifer (SCK•CEN data).

SN	Coordinates		Depth, Z (mTAW)	Mean K_h (m/d)	Mean_log_K_h
	X	Y			
1	67062	209521	-23.8558	1.471069285**	0.167633128
2	77442	200314	-11.5391	3.081081081	0.488703127
3	77475	200356	-11.6395	6.108825598**	0.785957727
4	87900	204200	-53.8782	2.112070365**	0.324708383
5	89789.24	232132	-160	1.04375	0.018596488
6	94740	211620	-107.403	3.228571429	0.509010399
7	100761	207271	-92.3309	4.821630036**	0.683193884
8	106806.1	220792.1	-160	0.398484848	-0.399588187
9	108900	192850	-24.0447	1.874902559**	0.272978702
10	117580	178550	38.49447	0.822727273	-0.084744106
11	129260	189960	-24.5106	13.7	1.136720567
12	129557.3	218823.9	-201.826	0.4075	-0.389872387
13	142221	224446	-290.827	0.186	-0.730487056
14	144287	219656	-256.383	0.258	-0.588380294
15	147560	206260	-144.531	0.2	-0.698970004
16	156663	238672	-404.359	0.185674741**	-0.731247174
17	158154	162156	53.98065	74.9952	1.875033468

18	164585	169959	21.20764	14.6016	1.164400447
19	164608	169971	21.14244	16.5024	1.21754711
20	164680	169994	20.98455	16.7616	1.224315472
21	164715	170031	20.86624	19.872	1.298241578
22	164758	170060	20.75457	19.872	1.298241578
23	166490	171618	10.91527	25.2288	1.401896594
24	166514	171637	10.94036	18.4896	1.266927516
25	166547	171661	10.97296	19.008	1.278936423
26	166549	171739	10.89073	12.8736	1.109700011
27	166606	171706	11.01346	10.2816	1.012060704
28	166693	171771	11.02054	18.0576	1.256660029
29	166720	171792	11.00605	15.984	1.203685471
30	166759	171822	10.97432	14.6016	1.164400447
31	167475	172013	12.18299	16.0704	1.206026687
32	167516	172037	12.16927	17.28	1.237543738
33	168750	184250	-23.3532	1.656218439**	0.219117615
34	168925	184088	-57.5609	2.9376	0.46799266
35	169876	172390	15.76213	19.1808	1.282866717
36	169930	172477	11.88896	21.6864	1.336187464
37	169945	172493	11.84815	19.1808	1.282866717
38	170574	172590	11.81146	30.0672	1.478092986
39	170613	183675	-58.5165	2.3328	0.367877507
40	170628	172585	11.65756	32.9184	1.517438718
41	171212	177845	-27.0563	6.244997998**	0.795532304
42	172197	182594	-54.7989	1.728	0.237543738
43	172293	178112	-24.3231	15.33333333	1.185636577
44	175304	202909	-193.236	0.27353465**	-0.562987651
45	176306	175957	-3.42207	29.376	1.46799266
46	176359	175956	-3.38897	32.832	1.516297339
47	176408	175954	-3.38065	29.376	1.46799266
	Summary: Minimum K_h = 0.19 m/d, Maximum K_h = 75.0 m/d, Average K_h = 13.10 m/d Variance = 184.15, Standard deviation = 13.57 ** Geometric mean value				

Table 19. Slug test data for the Ledo-Paniselian-Brusselian aquifer (SCK data).

X	Y	Depth, Z (mTAW)	K_h (m/d)	log K_h
173321	214841	-298.954544	0.07776	-1.10924
175725	236845	-496.768135	0.25000	-0.60206
175805	225892	-395.246803	0.34560	-0.46143
190553	221424	-405.258989	0.43200	-0.36452